HIGHLY EFFICIENT NEW METHODS OF CHANNEL ESTIMATION FOR
OFDM SYSTEMS

A THESIS SUBMITTED TO
THE GRADUATE SCHOOL OF NATURAL AND APPLIED SCIENCES
OF
MIDDLE EAST TECHNICAL UNIVERSITY

BY

SELVA MURATOĞLU ÇÜRÜK

IN PARTIAL FULLFILLMENT OF THE REQUIREMENTS
FOR
THE DEGREE OF DOCTOR OF PHILOSOPHY
IN
ELECTRICAL AND ELECTRONICS ENGINEERING

FEBRUARY 2008

Approval of the thesis:

HIGHLY EFFICIENT NEW METHODS OF CHANNEL ESTIMATION FOR OFDM SYSTEMS

submitted by **SELVA MURATOĞLU ÇÜRÜK** in partial fulfillment of the requirements for the degree of **Doctor of Philosophy in Electrical and Electronics Engineering Department, Middle East Technical University** by,

Prof. Dr. Canan Özgen   _____
Dean, Graduate School of **Natural and Applied Sciences**

Prof. Dr. İsmet Erkmen   _____
Head of Department, **Electrical and Electronics Engineering**

Prof. Dr. Yalçın Tanık   _____
Supervisor, **Electrical and Electronics Engineering Dept., METU**

Examining Committee Members:

Prof. Dr. Mehmet Şafak   _____
Electrical and Electronics Engineering Dept., HU

Prof. Dr. Yalçın Tanık   _____
Electrical and Electronics Engineering Dept., METU

Assoc. Prof. Dr. Melek Yücel   _____
Electrical and Electronics Engineering Dept., METU

Asst. Prof. Dr. Ali Özgür Yılmaz   _____
Electrical and Electronics Engineering Dept., METU

Asst. Prof. Dr. Elif Uysal Bıyıkoğlu   _____
Electrical and Electronics Engineering Dept., METU

Date: <u>05.02.2008</u>

I hereby declare that all information in this document has been obtained and presented in accordance with academic rules and ethical conduct. I also declare that, as required by these rules and conduct, I have fully cited and referenced all material and results that are not original to this work.

Name, Last name   : Selva Muratoğlu Çürük

Signature   :

ABSTRACT

HIGHLY EFFICIENT NEW METHODS OF CHANNEL ESTIMATION FOR OFDM SYSTEMS

Çürük, Selva Muratoğlu

Ph. D., Department of Electrical and Electronics Engineering

Supervisor: Prof. Dr. Yalçın Tanık

In the first part, the topic of average channel capacity for Orthogonal Frequency Division Multiplexing (OFDM) under Rayleigh, Rician, Nakagami-m, Hoyt, Weibull and Lognormal fading is addressed. With the assumption that channel state information is known, we deal with a lower bound for the capacity and find closed computable forms for Rician fading without diversity and with Maximum Ratio Combining diversity at the receiver. Approximate expressions are also provided for the capacity lower bound in the case of high Signal to Noise Ratio.

This thesis presents two simplified Maximum A Posteriori (MAP) channel estimators to be used in OFDM systems under frequency selective slowly varying Rayleigh fading. Both estimators use parametric models, where the first model assumes exponential frequency domain correlation while the second model is based on the assumption of exponential power delay profile. Expressions for the mean square error of estimations are derived and the relation between the correlation of subchannel taps and error variance is investigated. Dependencies of

the proposed estimators' performances on the model parameter and noise variance estimation errors are analyzed. We also provide approximations on the estimators' algorithms in order to make the estimators practical. Finally, we investigate SER performance of the simplified MAP estimator based on exponential power delay profile assumption used for OFDM systems with QPSK modulation. The results indicate that the proposed estimator performance is always better than that of the ML estimator, and as the subchannel correlation increases the performance comes closer to that of perfectly estimated channel case.

Keywords: Orthogonal Frequency Division Multiplexing, Channel Capacity, MAP Channel Estimator, MSE, SER.

ÖZ

OFDM SİSTEMLERİNDE KANAL KESTİRİMİ İÇİN ÇOK ETKİN YENİ METODLAR

Çürük, Selva Muratoğlu

Doktora, Elektrik Elektronik Mühendisliği Bölümü

Tez Yöneticisi: Prof. Dr. Yalçın Tanık

Şubat 2008, 144 sayfa

Bu tezin ilk bölümünde Rayleigh, Rician, Nakagami-m, Hoyt, Weibull ve Lognormal sönümlü kanallarında Dikgen Sıklık Bölümlü Çoğullama (OFDM)'nın ortalama kanal kapasitesi konusu incelenmiştir. Durum bilgisinin bilindiği varsayılarak, kanal kapasitesi için bir alt sınırla ilgilenilmiş, ve Rician sönümlemeli kanallar için çeşitlemesiz ve almaçta Maksimum Oran Birleşimi çeşitlemesi uygulandığı durumda kapalı hesaplanır formlar bulunmuştur. Ayrıca sinyal gürültü oranı yüksek olduğunda, kapasite alt sınırı için yaklaşık ifadeler de verilmiştir.

Bu tezde, frekans seçici zamanla yavaş değişen Rayleigh kanallarda kullanılacak OFDM sistemleri için basitleştirilmiş iki tane MAP kestirici sunulmuştur. İki kestirici de parametric modele dayanmaktadır, öyleki ilk model frekans bölgesi ilintisinin üstel olduğunu varsayarken, ikinci model güç gecikme profilinin üstel olduğu varsayımına dayanmaktadır. Kestiricilerin başarımını değerlendirmek amacıyla ortalama karesel hata ifadeleri bulunmuş ve altkanallar arasındaki ilinti

ile hata değişintileri arasındaki ilişki incelenmiştir. Önerilen kestiricilerinin başarımlarının gürültü değişintisi ve model parametresi hatasına olan bağımlılıkları da incelenmiştir. Ayrıca, kesticileri pratikleştirmek amacıyla algoritmaları sadeleştirilmiştir. Son olarak, Dördün Faz Kaydırmalı Kiplenimli (QPSK) OFDM sistemlerinde kullanılan üstel güç gecikme spektrumuna dayanan basitleştirilmiş MAP kestiricisinin Simge Hata Oranı (SER) başarımı incelenmiştir. Sonuçlar, önerilen kestiricinin her zaman ML kestiriciye göre daha iyi olduğunu göstermiştir. Altkanallar arasındaki ilinti arttıkça, kestirici başarımı kanalın tam bilindiği duruma yaklaşmaktadır.

Anahtar Kelimeler: Dikgen Frekans Bölüşümlü Çoğullama, Kanal Kapasitesi, MAP Kanal Kestiricisi, MSE, SER.

To my daughter Öykü

ACKNOWLEDGEMENTS

I would like to express my sincere gratitude to my supervisor Prof. Dr. Yalçın Tanık for his criticism and insight throughout my research. I would also like to express my gratitude to the committee members, Prof. Dr. Mehmet Şafak and Assist. Prof. Dr. Ali Özgür Yılmaz, for their helpful comments during the progress of my study.

I would like to express my appreciations to my friends for all the emotional support, camaraderie and entertainment they provided. Throughout this long way, their supports were priceless.

Special thanks are due to my parents, my sisters and my brother, who provided a persistent inspiration for my journey in this life, formed part of my vision and supported me with the necessary motivation to complete this study. I am very grateful for their loves and consistent supports during this period.

No part of this manuscript would see the day of light, without the support of my endless love, Sebahattin, who encouraged me to have a Ph.D. degree and helped me get through the difficult times. One of the best experiences that we lived through in this period was the birth of our daughter Öykü, who provided an additional and joyful dimension to our life mission. My husband and my daughter have lost a lot due to my research far away. Without their encouragement and understanding it would have been impossible for me to finish this work.

I dedicated this thesis to my daughter Öykü, whom innocent, smiling face keeps me energetic.

TABLE OF CONTENTS

LIST OF TABLES

LIST OF FIGURES

FIGURES

xvii

LIST OF ABBREVIATIONS

ADC   : Analog to Digital Converter

ADSL   : Asymmetric Digital Subscriber Loop

ATM   : Asynchronous Transfer Mode

AWGN   : Additive White Gaussian Noise

BER   : Bit Error Ratio

COST   : European Cooperation in the Field of Scientific and Technical Research.

DAB   : Digital Audio Broadcasting

DAC   : Digital to Analog Converter

DDCE   : Decision Directed Channel Estimation

DFT   : Discrete Fourier Transform

DVB   : Digital Video Broadcasting

DVB-T: Digital Video Broadcasting Terrestrial

ETSI   : European Telecommunications Standards Institute

FDM   : Frequency Division Multiplexing

FDMA   : Frequency Division Multiple Access

FFT   : Fast Fourier Transform

HDSL   : High-bit-rate Digital Subscriber Loop

HIPERLAN   : High Performance Radio Local Area Network

IFFT   : Inverse Fast Fourier Transform

IDFT   : Inverse Discrete Fourier Transform

IEEE   : Institution of Electrical and Electronics Engineers

ISI   : Intersymbol Interference

LOS   : Line of Sight

MAP   : Maximum A Posteriori

MCM   : Multicarrier Modulation

MIMO   : Multiple Input Multiple Output

ML   : Maximum Likelihood

MMSE   : Minimum Mean Square Error

MRC   : Maximum Ratio Combining

MSE   : Mean Square Error

OFDM   : Orthogonal Frequency Division Multiplexing

PSK   : Phase Shift Keying

RF   : Radio Frequency

QAM   : Quadrature Amplitude Modulation

SER   : Symbol Error Rate

SMAP-efdc   : Simplified MAP Estimator with Exponential Frequency Domain Correlation assumption

SMAP-epdp   : Simplified MAP Estimator with Exponential Power Delay Profile assumption

SNR   : Signal to Noise Ratio

WLAN   : Wireless Local Area Networks

WSSUS   : Wide Sense Stationary Uncorrelated Scattering

CHAPTER 1

INTRODUCTION

1.1 Background

The proliferating demand for reliable and effective transmission of information through various communication media has flourished many interesting research areas over the past decades. These led to a rapid growth in the fields of wired and wireless communications and to substantial advances in digital transmission techniques. Multicarrier Modulation (MCM) is the principle of transmitting data by dividing the input stream into several parallel bit streams, each of which has a much lower bit rate, and by using these substreams to modulate several carriers. The first systems using MCM were military high frequency radio links in 1960s 0, [2]. Starting from the early 1990s, multicarrier systems have taken considerable attention for their numerous advantages over the conventional single carrier schemes.

Orthogonal Frequency Division Multiplexing (OFDM), a special form of MCM with densely spaced subcarriers and overlapping spectra, was patented in 1970 0. Instead of using steep bandpass filters that completely separated the spectrum of subcarriers, as it was common practice in older Frequency Division Multiplexing systems, OFDM waveforms are chosen that mutually orthogonality is ensured even though subcarrier spectra may overlap. OFDM is popular for high-data-rate wireless communication systems due to its features such as multipath immunity, bandwidth efficiency and resistance to narrowband interference. The use of

Discrete Fourier Transform (DFT) in modulation and demodulation of OFDM systems was first proposed by Weinstein and Ebert in 1971 0. For a relatively long time, since implementation aspects such as the complexity of real time Fourier transform and the linearity required in radio frequency power amplifiers appeared prohibitive, the practicality of the concept seemed to be limited. Today, many of the problems associated with OFDM have become solvable and MCM has become a part of several international standards [3-5], including Asymmetric Digital Subscriber Loop (ADSL) and High-bit-rate Digital Subscriber Loop (HDSL), Digital Audio Broadcasting (DAB), Digital Video Broadcasting (DVB) and several wireless local area networks (WLAN) standards like IEEE 802.11a, 802.16 and ETSI HIPERLAN type II, for spectrally efficient very high data rate wireless services.

Capacity analysis of multipath fading channels is an important and fundamental issue in the design and study of wireless communication systems due both to the scarce radio spectrum available and to the rapidly growing demand for wireless services. Indeed, the performance limit of any coding and modulation technique is dictated by the channel capacity bound. Accordingly, there have been many papers dealing with the instantaneous channel capacity of various fading channels, in the past decade [1, 2, 6-16]. Moreover, studies that present average channel capacity for Rayleigh fading channels [1, 2, 15, 16], Nakagami-m fading channels [7] and Hoyt fading channels [8] have been published. Some of these studies have dealt with multiple input multiple output (MIMO) systems, and the performance of OFDM has been studied. In 0, the capacity bounds and performance of adaptive loading OFDM under frequency selective Rayleigh fading channel conditions have been investigated, assuming that the channel state information is available to the transmitter. The average capacity with ideal maximum ratio combining (MRC) diversity at the receiver is also evaluated. We aim to expand the results obtained in 0, which are for Rayleigh fading, to other channel models, especially for Rician channels, since studies have shown that indoor fading is often expected to be Rician distributed.

In this thesis, the topic of average channel capacity for OFDM under Rayleigh, Rician, Nakagami-m, Nakagami-q, Weibull and Lognormal fading is extensively addressed. The performance of OFDM under Rician fading, with MRC diversity at the receiver is also investigated. Following the investigation and comparison, we deal with a lower bound given in 0 for the sake of simple computable and handy forms. Finally, we reach a closed form expression for the Rician fading channel. Approximate expressions for the average capacity are also provided for high Signal to Noise Ratio (SNR) case.

In wireless systems, the transmitted signals are subject to the effects of multipath channels, caused by the remote terrestrial objects and the inhomogenities in the physical medium. These effects will degrade system performance and need to be kept to a minimum. Therefore, channel estimation is a demanding task for coherent detection in order to reduce the channel impairments and detect the transmitted symbols coherently. Dispersion estimation is necessary for many wireless communication systems, but it is particularly crucial for OFDM based wireless communication systems. Because, although OFDM signaling is proven to be an efficient way to overcome the effects of fading channel and multipath, it is very sensitive to carrier frequency and phase offset. Basic assumption that subcarriers are orthogonal within an OFDM symbol is valid only if perfect synchronization is established. Channel estimation is an integral part of the synchronization process and performance of the synchronization unit, in particular the accurate estimation of the frequency offset and timing error, is of crucial influence on the overall OFDM system performance.

There have been many papers dealing with channel estimation for OFDM systems under fading [17-31], which are based on Maximum Likelihood (ML) or Maximum A-Posteriori (MAP) techniques. The ML based estimators have acceptable complexity, but since they ignore the correlation between subchannels they suffer from a high mean-square error (MSE), especially if the system operates with low SNR. In contrast, the MAP estimators which use a priori channel information have good performance but higher complexity.

3

In OFDM systems, the frequency domain channel coefficients at different subcarriers are typically highly correlated. If the correlation between the subchannel coefficients is well estimated, MAP estimation procedure can be performed optimally. However, in practical systems, such knowledge is not precisely available at design time. Because the correlation depends upon the power delay profile of the channel impulse response, which is a function of the wireless environment in which the system will operate. Additionally, the subcarrier phases inevitably fluctuate from packet to packet. Therefore, the phases must be estimated dynamically and MAP estimation procedure is an excellent candidate for the purpose.

Some modifications to MAP estimator for simplifying the computations have been presented in the literature [27-31]. In [27], the authors introduce a low complexity approximation to the frequency-based linear minimum mean square error (MMSE) estimator that uses the theory of optimal rank reduction. To reduce the implementation complexity, [29] considers the use of a channel estimation filter whose tap coefficient is real-valued and symmetrically weighted. In the work published in [31], a low-complexity windowed Discrete Fourier Transform (DFT) based MMSE channel estimators is presented. However, we believe that there is still work to be done to develop an estimator with good performance and acceptable complexity. Therefore, we have developed a simplified MAP estimator [28], which yields the channel estimates under fading conditions using a parametric correlation model. A block estimates this parameter from the channel coefficients and feeds it to the MAP estimator.

The performance of the estimators is another task that should follow, for the sake of the completeness. All coherent receivers assume exact channel information. In practical situations, however, the estimator will experience estimation errors, which leads to detector performance degradation. The error variances of the channel coefficients are good indicators of the resultant performance of the receiver. Hence, we have determined the error variances of the estimates. We have

also analyzed the sensitivity of the proposed estimator to the correlation parameter estimation error and SNR estimation error.

The performance degradation due to the channel estimation error may be analyzed by investigating bit error ratio (BER). There have been various works interested in BER performances of OFDM systems for different channel estimation methods [3], [32-38]. Probability of error expressions for various modulation schemes under Rician channel fading are given in [3]. Another method for analytical calculation of BER is given in [32], which presents a systematic approach for evaluating the BER performance of OFDM receivers in Rayleigh fading when pilot aided channel estimate is used. Using these references, BER expressions for the proposed simplified MAP estimator are found.

1.2 Outline

The rest of this thesis consists of five main chapters. Chapter 2 is devoted to channel capacity for OFDM systems under fading. In Chapter 3, after reviewing multipath channels and OFDM transmission systems, channel estimation methods, namely, ML and MAP estimators, and their MSE and BER performances are briefly discussed. Chapter 4 is devoted to the proposal of two simplified MAP estimators. Following a description of these estimators, we present the MSE performances and sensitivities to model parameters and SNR estimation errors. Real channel simulations and results related to the MSE and BER performances are given in Chapter 5. Finally, in Chapter 6, we draw our conclusions and discuss some possible future research directions in accordance with the study performed throughout this study.

CHAPTER 2

CHANNEL CAPACITY

In this chapter, the topic of channel capacity for OFDM systems under Rayleigh, Rician, Nakagami-m, Hoyt, Weibull and Lognormal fading is addressed in some detail. We assume that perfect channel estimates are available to the transmitter through an ideal feedback channel. The performance of OFDM under Rician fading, with MRC diversity at the receiver is also investigated.

2.1 Channel Capacity

2.1.1 Average Capacity of Single Carrier Systems

In order to assess the performance of any kind of coding and modulation technique, the ultimate reference is the channel capacity bound. The capacity of an ideal bandlimitted additive white Gaussian noise (AWGN) channel is given by the well known result due to Shannon [39]:

$$C = W \log_2 \left(1 + \frac{P_R}{N_0 W} \right), \tag{2.1}$$

where N_0 is the noise power per Hertz, W is the transmission bandwidth and P_R is the average received power. The channel capacity in a fading channel has to be calculated in an average sense. If the transmission time is long enough to reveal

the longterm ergodic properties of the channel, a capacity in the Shannon sense exists and is given by the *ergodic capacity*. The instantaneous capacity is [1]:

$$C_i = W \log_2\left(1 + \frac{P_R\gamma}{N_0 W}\right),$$ (2.2)

where γ is the instantaneous power gain of the channel for a specific instant. Since γ has a certain distribution $p(\gamma)$ under fading channel, the average value of capacity (ergodic capacity) is expressed as:

$$C_{av} = \int_0^\infty W \log_2\left(1 + \frac{P_R\gamma}{N_0 W}\right) p(\gamma)\,d\gamma.$$ (2.3)

The ergodic capacity indicates the average over the fading environment. Note that if the transmission time is not long enough to reveal the long-term ergodic properties of the fading channel, the concept of *outage capacity* is evoked, in which the capacity is viewed as a random variable, because it depends on the instantaneous random channel parameters. Thus, the system has no Shannon capacity in the strict sense.

The integral of average channel capacity given in (2.3) is easily evaluated for Rayleigh channel, where we can get the following expression for the average channel capacity [1]:

$$C_{av\_rayleigh} = \frac{W}{\ln 2} e^{\frac{1}{\gamma_a}} Ei\left(\frac{1}{\gamma_a}\right),$$ (2.4)

where $\gamma_a = \dfrac{P_R\bar{\gamma}}{N_0 W}$ and $Ei(x) = \displaystyle\int_x^\infty \frac{e^{-u}}{u}\,du$.

2.1.2 Average Capacity of OFDM Systems

We assume that the channel is frequency selective for the whole band, but is nearly flat for subbands. Hence, the total bandwidth of the OFDM signal, W, is much greater than the coherence bandwidth of the channel (B_c), while subcarrier bandwidth is small compared to B_c. We further assume that channel fading is independent on each subcarrier. For a given set of channel gains at subcarrier frequencies, the capacity maximization problem can be stated as [1]:

$$\text{Maximize} \quad C = \Delta f \log_2\left(\prod_{i=1}^{N}\left(1 + \frac{P_i \gamma_i}{N_0 \Delta f}\right)\right),$$

$$\text{subject to} \quad \sum_{i=1}^{N} P_i = P_R \quad P_i \geq 0, \quad i:1..N$$

(2.5)

where Δf is the subcarrier bandwidth, N is the number of subcarriers, P_i is the power assigned to the ith subcarrier, γ_i is the instantaneous SNR at i^{th} subcarrier frequency. For the ease of notation, it is assumed that instantaneous SNR's, γ_i's are grouped in decreasing order, hence γ_1 is the maximum gain and γ_N is the minimum gain (or the largest attenuation). As given in [1], the above problem can be solved and we get the following optimal power distribution:

$$P_i = \frac{P_R}{D} + N_0 \Delta f \left(\frac{1}{D}\sum_{j=1}^{D}\frac{1}{\gamma_j} - \frac{1}{\gamma_i}\right), \qquad 1 \leq i \leq D$$

$$P_i = 0, \qquad\qquad\qquad\qquad D+1 \leq i \leq N$$

(2.6)

where the number $D+1$ is the minimum index in the set $\{1/\gamma_i\}$, which satisfies

$$\frac{1}{\gamma_i} > \frac{P_R}{N_0 \Delta f (i-1)} + \frac{1}{i-1}\sum_{j=1}^{i-1}\frac{1}{\gamma_j}.$$

(2.7)

The resultant maximum capacity value is:

$$C_{max} = \Delta f \sum_{i=1}^{D} \log_2 \left(\frac{\gamma_i}{D} \left(\frac{P_R}{N_0 \Delta f} + \sum_{j=1}^{D} \frac{1}{\gamma_j} \right) \right). \tag{2.8}$$

When the result is averaged over the joint probability density function (pdf) of γ_i's, which are independent and identically distributed (distributed according to the channel pdf with the same average power), we can get the average capacity of OFDM system for any chosen fading. Unfortunately, this approach seems to be mathematically intractable. It is even not possible to employ numeric integration methods, since the parameter D which appears on the upper limit of summation in (2.8) is also a random variable that depends on the channel statistics and distribution, and is hard to compute.

A simple lower bound can be obtained by considering the fact that, any choice of power distribution different than the power distribution given by (2.6) yields a capacity value less than or equal to the maximum value [1]. Thus, if we uniformly distribute the total power over the subcarriers, then the resultant capacity will always be less than C_{max}. Then, lower bound for capacity is given by [1]:

$$C_l = \int_0^\infty W \log_2 \left(1 + \frac{P_R \gamma}{W N_0} \right) p(\gamma) d\gamma, \tag{2.9}$$

where $W = N \Delta f$. It should be noted here that this expression has the same form as given in (2.3), in which the average capacity of a constant power variable rate single carrier communication is evaluated.

2.2 Multipath Channels

The theory for dispersive channels, whether time-invariant or time-varying, has been reported systematically over the years [39-43]. Doubtless, the rapid advance in technology and the exploding demand for efficient high quality digital wireless communications over almost every possible media (cellular, personal, data networks, the ambitious wireless high rate ATM networks, point-to-point

9

microwave systems, underwater communications, satellite communications, etc.) plays a dramatic role in this trend. Information theoretic study of increasingly complicated fading channel models has accelerated to a degree where its impact on communications in a fading regime is notable. These studies have already led to interesting results, which matured to a large degree in the understanding of communications through fading media, under a variety of constraints and models.

A number of distributions exist that well describe the statistics of the mobile radio signals [39]. Extensive field trials have been used to validate these distributions and results showed agreement between measurements and theoretical formulas. The long-term signal variation is well characterized by the lognormal distribution whereas the short-term signal variation is described by several other distributions such as Rayleigh, Rice, Nakagami-m, and Weibull. It is generally accepted that the path strength at any delay is characterized by the short-term distributions over spatial dimensions of a few hundred wavelengths, and by the lognormal distribution over areas whose dimension is much larger. Composite distributions attempt to describe the transition from the local distribution to the global distribution of the path strength, thus combining both fast and slow fading. These distributions assume the local mean, which is the mean of fast fading distribution, to be lognormally distributed. The best-known composite distributions are Rayleigh-lognormal (also known as Suzuki), Rice-lognormal, and Nakagami-lognormal.

Among these, Nakagami-m distribution has been given a special attention for its ease of manipulation and wide range of applicability. Although, in general, it has been found that the fading statistics of the mobile radio channel may well be characterized by the Nakagami-m, situations are found for which Rice and even Weibull yield better results. Some studies even question the use of Nakagami-m distribution because its tail does not seem to yield a good fitting to experimental data, better fitting being found around the mean or median. More importantly, situations are encountered for which no distributions seem to adequately fit experimental data, though one or another may yield a moderate fitting.

2.2.1 Rayleigh Fading Channels

In macrocellular environments, fading appears as Rayleigh distributed, because the transmitted field is heavily scattered between the transmitter and the receiver. In fact, Rayleigh distribution constitutes a special case of the Rice, Nakagami-m, Weibull and the composite distributions and can be obtained in an exact manner by appropriately setting the parameters of these distributions.

Rayleigh distribution is used to model multipath fading with no direct line of sight (LOS) path. In this case, instantaneous SNR per symbol of the ith path, γ, is distributed according to an exponential distribution given by [39]:

$$p(\gamma) = \frac{1}{\bar{\gamma}} \exp\left(-\frac{\gamma}{\bar{\gamma}}\right); \quad \gamma \geq 0, \tag{2.10}$$

where $\bar{\gamma} = \frac{E_b}{N_0} E\{\alpha^2\}$ denotes the average SNR per symbol of the ith path. Here, α is the attenuation factor, and E_b is the bit energy.

MRC diversity technique is proved to be optimal in the sense that it achieves the maximum possible combiner output SNR at any instant of time. It is assumed that there are L diversity channels, carrying the same information-bearing signal, each channel is frequency nonselective and slowly fading. The fading processes among the L diversity channels are assumed to be mutually statistically independent. In the MRC, each demodulator output is multiplied by the corresponding complex-valued (conjugate) channel gain. The effect of this multiplication is to compensate for the phase shift in the channel and weight the signal by a factor that is proportional to the signal strength [39]. For a Rayleigh fading, the pdf of instantaneous SNR at the output of the MRC is [39]:

$$p(\gamma) = \frac{L^L \gamma^{L-1}}{(L-1)! \bar{\gamma}^L} \exp\left(-\frac{L\lambda}{\bar{\gamma}}\right); \quad \gamma \geq 0. \tag{2.11}$$

2.2.2 Nakagami-n (Rician) Fading Channels

Rician distribution is used to model propagation environments consisting of one strong direct LOS component and many random weaker components. In microcellular or picocellular environments, LOS paths are more likely to exist because cell size is smaller and the user is nearer to base stations. Thus, indoor fading is often expected to be Rician distributed.

In Rician fading, γ is distributed according to a non-central chi-square distribution given by [43-45]:

$$p(\gamma) = \frac{(1+K)}{\bar{\gamma}} \exp\left(-K - \frac{(1+K)\gamma}{\bar{\gamma}}\right) I_0\left(2\sqrt{\frac{K(1+K)\gamma}{\bar{\gamma}}}\right); \quad \gamma \geq 0, \qquad (2.12)$$

where K is the Rician factor, $\bar{\gamma}$ is the sum of the power in the LOS and local-mean scattered power, and $I_n(.)$ is the nth order modified Bessel function of the first kind. The K factor is the ratio of signal power in LOS component over the local-mean scattered power and ranges from $K = 0$ (Rayleigh fading) to $K \to \infty$ (no fading, constant amplitude). Typical value of K is in the range of 7-12 dB.

For a Rician fading channel, the pdf of instantaneous SNR at the output of MRC is given by [43-45]:

$$p(\gamma) = \frac{(L+K)}{\bar{\gamma}} \left(\frac{(L+K)\gamma}{K\bar{\gamma}}\right)^{\frac{L-1}{2}} \exp\left(-K - \frac{(L+K)\gamma}{\bar{\gamma}}\right) I_0\left(2\sqrt{\frac{K(L+K)\gamma}{\bar{\gamma}}}\right); \gamma \geq 0 \ (2.13)$$

where $K = \sum_{i=1}^{L} K_i$ and K_i is the Rician factor of ith diversity branch.

2.2.3 Nakagami-m Fading Channels

Nakagami-m distribution fits some urban empirical data well [39]; therefore it is often used in performance analysis for fading channels. Its general form takes

Rayleigh and one sided Gaussian distributions as special cases. It can also approximate Lognormal distribution when certain conditions are satisfied. Nakagami-m and Rician are found to approximate each other by some simple equations relating the physical parameters associated to each distribution. In particular, the approximation to Rician distribution is an attractive feature since the Nakagami-m distribution is mathematically more convenient to handle than the Rician. However, the approximation to Lognormal distribution is of less interest because of certain constraints.

In Nakagami-m, γ is distributed according to a gamma distribution. Then [39], [43]:

$$p(\gamma) = \frac{m^m \gamma^{m-1}}{\bar{\gamma}^m \Gamma(m)} \exp\left(-\frac{m\gamma}{\bar{\gamma}}\right); \quad \gamma \geq 0, \tag{2.14}$$

where $\Gamma(.)$ is the gamma function, and m is the Nakagami-m parameter that ranges from 0.5 to ∞. With $m = 0.5$, it becomes one-sided Gaussian distribution; $m = 1$ is Rayleigh fading, and in the limit $m \to \infty$ the Nakagami-m fading channel converges to a no-fading AWGN channel. Especially for high m, Nakagami-m can approximate Rician for $m = \dfrac{1}{1 - \left(K/(K+1)\right)^2}$.

Any single channel system with Nakagami-m fading, in which the parameter m is an integer, is equivalent to an L-channel diversity system for a Rayleigh fading channel. Consequently, it follows that a K-channel system transmitting in a Nakagami-m fading channel with independent fading is equivalent to an $L=K.m$ channel diversity in a Rayleigh fading channel. Under a Nakagami-m fading channel, pdf for L-branch MRC, where $m_i/\bar{\gamma}_i$ identical across the branches, is expressed as [39]:

$$p(\gamma) = \frac{m_T^{m_T} \gamma^{m_T-1}}{\bar{\gamma}_T^{m_T} \Gamma(m_T)} \exp\left(-\frac{m_T \gamma}{\bar{\gamma}_T}\right); \quad \gamma \geq 0, \tag{2.15}$$

where $m_T = \sum_{i=1}^{L} m_i$ is the total fading index, $\bar{\gamma}_T = \sum_{i=1}^{L} \bar{\gamma}_i$ is the total average SNR after combining. Here, m_i and $\bar{\gamma}_i$ are the fading index and the average SNR on the ith branch, respectively.

2.2.4 Nakagami-q (Hoyt) Fading Channels

The Hoyt fading channels are typically observed on satellite links subject to strong ionospheric scintillation. In this case, γ is distributed according to [8], [43], [46]:

$$p(\gamma) = \frac{(1+q^2)}{2q\bar{\gamma}} \exp\left(-\frac{(1+q^2)^2 \gamma}{4q^2\bar{\gamma}}\right) I_0\left(\frac{(1-q^4)\gamma}{4q^2\bar{\gamma}}\right); \quad \gamma \geq 0, \tag{2.16}$$

where q is the Hoyt fading parameter ranging from $q = 0$ for a one-sided Gaussian fading to $q = 1$ for a Rayleigh fading.

Under Hoyt fading channel with MRC, the pdf of the instantaneous SNR of the combiner output is given by [8], [52]:

$$p(\gamma) = \left(\frac{2q}{1+q^2}\right)^L \sum_{k=0}^{\infty} \frac{(L/2)k}{k!} \left(\frac{1-q^2}{1+q^2}\right)^{2k} f_{G\left(L+2k, \frac{4q^2\bar{\gamma}}{(1+q^2)^2}\right)}(\gamma); \quad \gamma \geq 0, \tag{2.17}$$

where $f_{G(\alpha,\beta)}(x) = \dfrac{x^{\alpha-1} e^{-\frac{x}{\beta}}}{\beta^{\alpha} \Gamma(\alpha)}$.

2.2.5 Weibull Fading Channels

The Weibull distribution was often used to model the time until failure of many different physicals systems. Following this, it is used for describing the indoor radio channel fading and has been identified as one of the major probability distributions for modeling amplitude fading in a multipath environment. It is a

flexible model providing a very good fit to experimental fading channel measurements for both indoor and outdoor environments.

The pdf of Weibull is [47-50]:

$$p(\gamma) = \frac{\beta}{2} \frac{\gamma^{\beta/2-1}}{(a\bar{\gamma})^{\beta/2}} \exp\left(-\left(\frac{\gamma}{a\bar{\gamma}}\right)^{\beta/2}\right); \quad a = \frac{1}{\Gamma(1+2/\beta)} \quad \text{and} \quad \gamma \geq 0, \quad (2.18)$$

where $\beta > 0$. For $\beta = 1$, the Weibull distribution is identical to the exponential distribution, while for $\beta = 2$ the Weibull distribution is equal to the Rayleigh distribution.

2.2.6 Lognormal Fading Channels

A problem with mobile radio propagation is the effect of shadowing of the signal due to large obstructions, such as large buildings, trees and hilly terrain between the transmitter and the receiver. Shadowing is usually modeled as a multiplicative and, generally, slowly time varying random process; as lognormally distributed.

The pdf of the instantaneous SNR γ is given by [39], [51]:

$$p(\gamma) = \frac{\xi}{\sqrt{2\pi}\sigma\gamma} \exp\left(-\frac{10\log_{10}\gamma - \mu}{2\sigma^2}\right); \quad \xi = \frac{10}{\ln 10} \quad \text{and} \quad \gamma \geq 0, \quad (2.19)$$

where μ and σ^2 are the mean and variance in decibels of $10\log_{10}\gamma$, the SNR. For typical cellular and microcellular environments, σ is in the range of 5-12 dB. The corresponding average SNR is given by:

$$\bar{\gamma} = \exp\left(\frac{\mu}{\xi} + \frac{\sigma^2}{2\xi^2}\right). \quad (2.20)$$

15

2.3   Capacity Bounds for Fading Channels

As already mentioned, the integral for the lower bound of channel capacity under Rayleigh fading can easily be evaluated. Lower bound for MRC output under Rayleigh fading is also given in 0 and stated below for $L=1, 2, 3$ and 4:

$$C_{l,rayleigh-MRC}(1) = \frac{W}{\ln 2}\left[e^{1/\gamma_a} Ei(1/\gamma_a)\right]$$

$$C_{l,rayleigh-MRC}(2) = \frac{W}{\ln 2}\left[e^{2/\gamma_a} Ei(2/\gamma_a)\left(1-\frac{2}{\gamma_a}\right)+1\right]$$

$$C_{l,rayleigh-MRC}(3) = \frac{W}{\ln 2}\left[e^{3/\gamma_a} Ei(3/\gamma_a)\left(1-\frac{3}{\gamma_a}+\frac{9}{2\gamma_a{}^2}\right)+\frac{3}{2}-\frac{3}{2\gamma_a}\right]$$

$$C_{l,rayleigh-MRC}(4) = \frac{W}{\ln 2}\left[e^{4/\gamma_a} Ei(4/\gamma_a)\left(1-\frac{4}{\gamma_a}+\frac{8}{\gamma_a{}^2}-\frac{32}{3\gamma_a{}^3}\right)+\frac{11}{6}-\frac{8}{3\gamma_a}+\frac{8}{3\gamma_a{}^2}\right]$$

$$(2.21)$$

The results given in (2.21) can be stated as lower bound under Nakagami-m fading, with $L=K.m$ if m is integer.

For Rician fading channels, evaluating the integral in (2.9) and obtaining closed form expression for the lower bound is not easy because of complex pdf. Therefore, in evaluating the integral we use a series expansion for the logarithm function. i.e,

$$\log_2(1+\gamma_b x) = \frac{\ln(1+\gamma_b x_0)}{\ln 2} + \frac{1}{\ln 2}\sum_{m=1}^{n}\frac{(-1)^{m-1}\gamma_b{}^m (x-x_0)^m}{m(1+\gamma_b x_0)^m}, \qquad (2.22)$$

where $\gamma_b = \frac{\gamma_a}{\bar{\gamma}} = \frac{P_R}{N_0 W}$ is the SNR, x_0 is the reference point for the series expansion, and n is the number of components that the series contain. Series convergence is guaranteed when $x < 1/\gamma_b + 2x_0$. For the lower bound of the channel capacity under Rician fading, we obtain the following expression:

$$C_{l,rician} = \frac{\ln(1+\gamma_b x_0)}{\ln 2} + \frac{1}{\ln 2}\sum_{m=1}^{n}\frac{\gamma_b^{m}(-1)^{m-1}}{m(1+\gamma_b x_0)^m(1+K)^m} \cdot$$
$$\sum_{i=0}^{m}(-x_0)^i(K+1)^i \bar{\gamma}^{m-i}\binom{m}{i}\sum_{j=0}^{m-i}K^{m-i-j}\binom{m-i}{j}\frac{(m-i)!}{(m-i-j)!} \tag{2.23}$$

Similarly, for Rician fading with MRC, the channel capacity lower bound is:

$$C_{l,rician-MRC} = \frac{\ln(1+\gamma_b x_0)}{\ln 2} + \frac{1}{\ln 2}\sum_{m=1}^{n}\frac{\gamma_b^{m}(-1)^{m-1}}{m(1+\gamma_b x_0)^m(L+K)^m} \cdot$$
$$\sum_{i=0}^{m}(-x_0)^i(K+L)^i \bar{\gamma}^{m-i}\binom{m}{i}\sum_{j=0}^{m-i}K^{m-i-j}\binom{m-i}{j}\frac{(L-1+m-i)!}{(L-1+m-i-j)!} . \tag{2.24}$$

When we substitute $K=0$ in the above expressions, we obtain Rayleigh fading expressions with and without diversity:

$$C_{l,rayleigh} = \frac{\ln(1+\gamma_b x_0)}{\ln 2} + \frac{1}{\ln 2}\sum_{m=1}^{n}\frac{\gamma_b^{m}(-1)^{m-1}}{(1+\gamma_b x_0)^m}\sum_{i=0}^{m}(-x_0)^i \bar{\gamma}^{m-i}\frac{(m-1)!}{i!} \tag{2.25}$$

$$C_{l,rayleigh-MRC} = \frac{\ln(1+\gamma_b x_0)}{\ln 2} +$$
$$\frac{1}{\ln 2}\sum_{m=1}^{n}\frac{\gamma_b^{m}(-1)^{m-1}}{m(1+\gamma_b x_0)^m}\sum_{i=0}^{m}(-x_0)^i L^{i-m}\bar{\gamma}^{m-i}\binom{m}{i}\frac{(L-1+m-i)!}{(L-1)!} \tag{2.26}$$

Further simplifications for the lower bound of channel capacity can be developed for specific conditions. For high SNR assumption, the bound in (2.9) becomes

$$C_l = \int_0^{\infty} W \log_2\left(\frac{P_R\gamma}{WN_0}\right)p(\gamma)d\gamma . \tag{2.27}$$

Following, the lower bounds for the fading channels are found easily:

$$C_{l,rician} = \frac{1}{\ln 2}\left[\text{Ei}(K) + \ln\left(\frac{K\gamma_a}{1+K}\right)\right], \tag{2.28}$$

$$C_{l,nakagami-m} = \frac{1}{\ln 2}\left[\frac{\Gamma'(m)}{\Gamma(m)} + \ln\left(\frac{\gamma_a}{m}\right)\right], \tag{2.29}$$

17

$$C_{l,weibull} = \frac{1}{\ln 2} \frac{2}{\beta} \left[-0.577216 + \ln \left((a\gamma_a)^{\frac{\beta}{2}} \right) \right], \tag{2.30}$$

$$C_{l,lognormal} = \frac{1}{\ln 2} \left[\frac{\mu}{\xi} + \ln \left(\frac{\gamma_a}{\bar{\gamma}} \right) \right]. \tag{2.31}$$

2.3.1 Simulation Results

We have employed Monte-Carlo simulation in determining the average capacity given in (2.8). For this purpose, we have generated 100,000 independent sets of channel coefficients for each fading, then (2.8) has been computed for each set. Finally, the average was found.

The results of the Monte-Carlo simulations for Rician, Nakagami-m, Hoyt, Weibull and Lognormal fading are shown in Figure 2.1 - Figure 2.5, respectively. In the figures, the average capacity per unit bandwidth, $R_{av} = C_{av}/W$, is plotted against the average received SNR, γ_a. The number of carriers N is chosen as 48 [1]. The capacity of the ideal bandlimited AWGN and Rayleigh fading channels are given for comparison. In the figures, the average channel capacity per unit bandwidth obtained by Monte-Carlo simulations are compared with the lower bound expressions by employing numeric integration of (2.9). It is clearly seen from the figures that the lower bounds are tight for all fading channels, except for Lognormal fading. For Rician, Nakagami-m and Weibull, as the fading factor increases, the capacity of channel approaches to the AWGN channel, as expected. Again, as the fading factor increases, the lower bounds of channel capacity get closer to the average channel capacity values. For the channel under Hoyt fading, as the fading factor increases, the capacity approaches to the capacity of Rayleigh fading channel, as expected. The lower bound of the channel capacity is tight for Hoyt fading, and as the fading factor increases, the bound becomes tighter. For the

---

[1] As shown in 0, there is no significant difference between N values greater than 8, for $R_{av} \geq 1$.

Lognormal fading channel, as the variance increases, the average capacity decreases, which is always lower than the Rayleigh fading channel, as expected. For this case, the lower bound of the average capacity is not tight especially for large variance. But, still the bound is acceptable for small variance values.
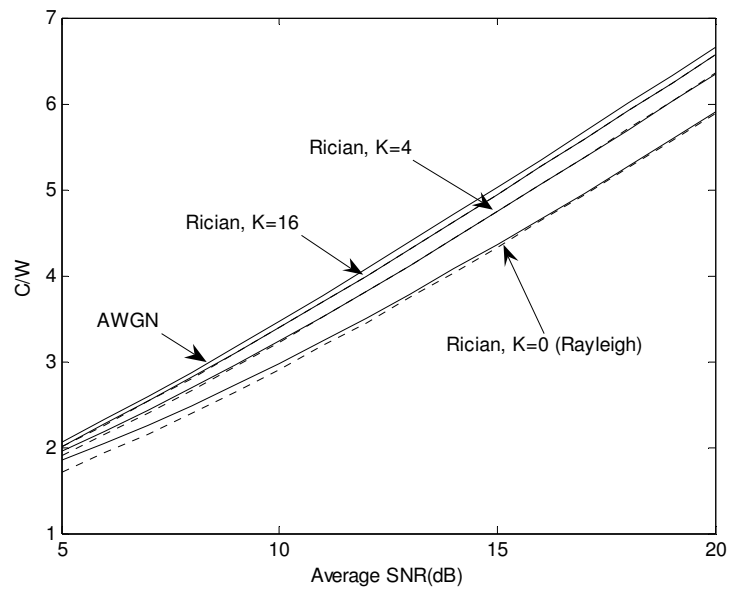
Figure 2.1 Average capacity per unit bandwidth (*C/W*) versus average SNR of OFDM: Rician channel (--: theoretical lower bound, -: simulation result).
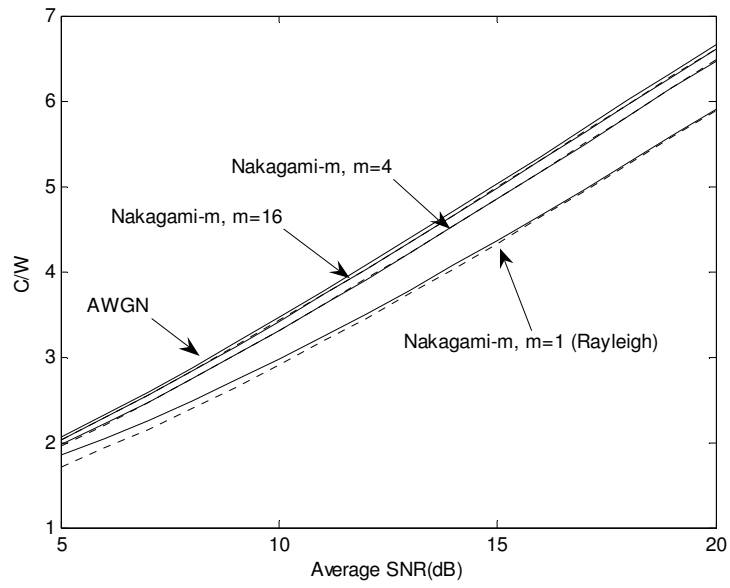
Figure 2.2 Average capacity per unit bandwidth (*C/W*) versus average SNR of OFDM: Nakagami-m channel (--: theoretical lower bound, -: simulation result).
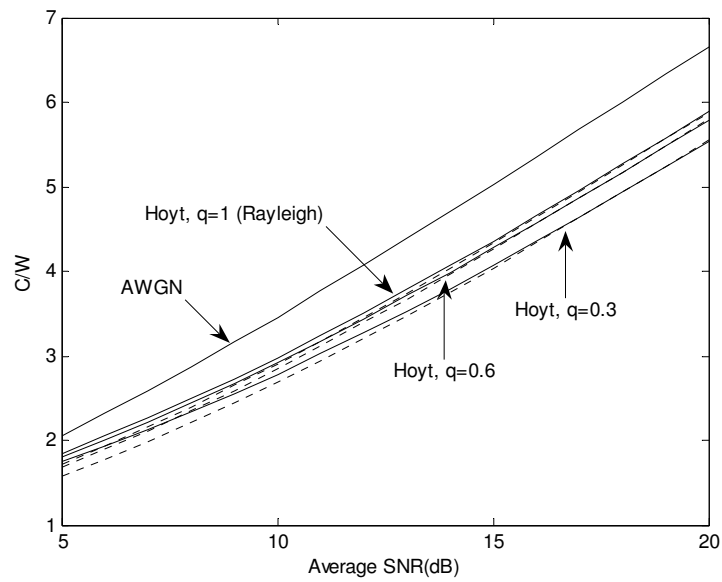
Figure 2.3 Average capacity per unit bandwidth (*C/W*) versus average SNR of OFDM: Hoyt channel (--: theoretical lower bound, -: simulation result).
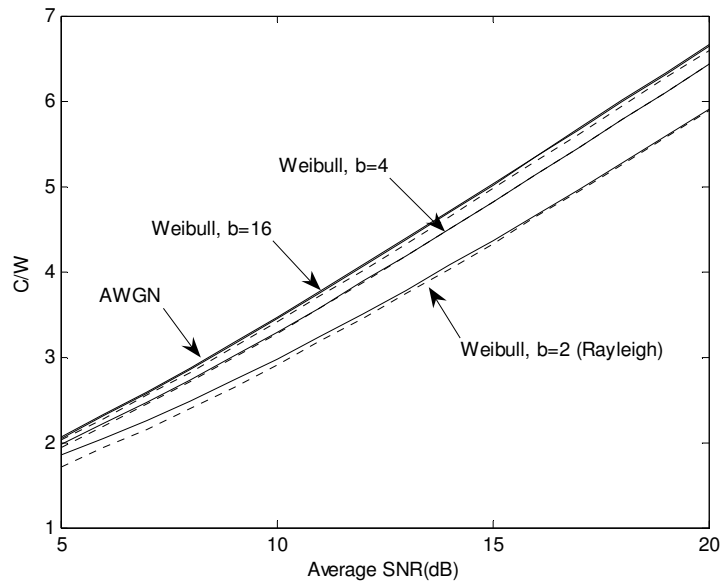
Figure 2.4 Average capacity per unit bandwidth (*C/W*) versus average SNR of OFDM: Weibull channel (--: theoretical lower bound, -: simulation result).
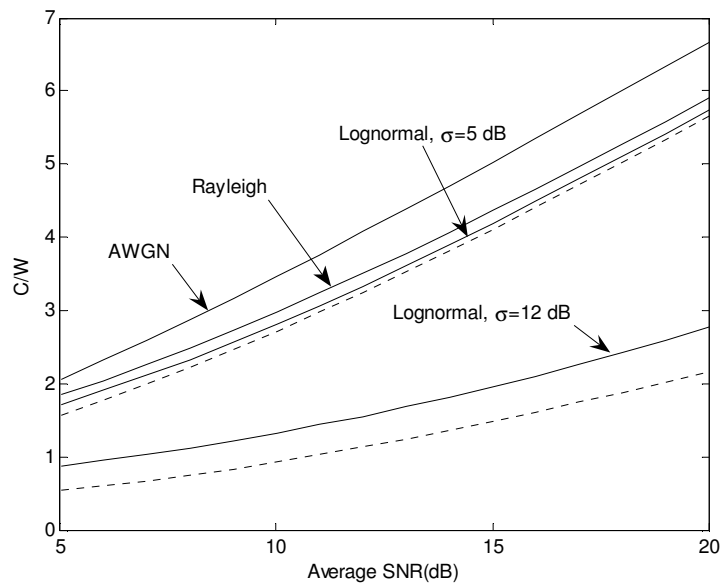
Figure 2.5 Average capacity per unit bandwidth (*C/W*) versus average SNR of OFDM: Lognormal channel (--: theoretical lower bound, -: simulation result).

In [43], it stated that for Rician channels, as K tends to infinity, the reception converges to the case of AWGN regardless of the order of diversity applied (This result is also seen in Figure 2.1.). Furthermore, the improvement in reception, using diversity, is most significant for the smaller values of K, especially for Rayleigh fading. This fact can be explained by the greater randomness of Rayleigh fading over other types of fading in which case the diversity techniques tend to be more efficient. For Rician channels, MRC diversity improvement in channel capacity is given in Figure 2.6. In the figure, average channel capacities per unit bandwidth obtained by Monte-Carlo simulations are compared with the lower bound expressions given by (2.9) by employing numeric integration, for Rician (K=4) fading, for no diversity case as well as for 2nd, 3rd and 4th diversity levels. It is observed that the lower bound expressions are tight for all values of L. As expected, when the order of diversity L is sufficiently large, the impact of channel fading on system performance is of little significance. The reception always reduces to the case of AWGN, regardless of the degree of fading, as L approaches infinity.

22
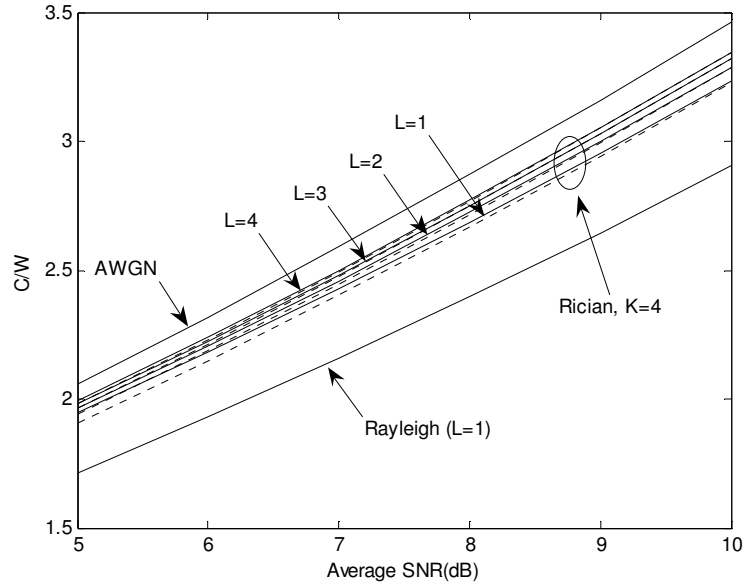
Figure 2.6 Average capacity per unit bandwidth (*C/W*) versus average SNR of OFDM: Rician channel (*K*=4), *L*=1[st,] 2nd, 3rd and 4th order MRC diversity reception, (--: theoretical lower bound, -: simulation result).

In Figure 2.7 and Figure 2.8, for Rician (*K*=4) fading, the channel capacity lower bounds per unit bandwidth obtained by numeric integrations are compared with lower bound expressions obtained by employing series expansion, given by (2.23) and (2.24), for *L*=1, 2, 3 and 4 diversity level. x_0 is chosen as 15 for *n*=100 to guarantee series convergence in Figure 2.7 and x_0=1 for *n*=2 in Figure 2.8. It is clearly seen that the expressions for lower bound of average capacity under Rician fading are highly accurate for all values of *L*. Selection of *n* and x_0 is quite important, because since Bessel function takes very small values, even small amount of divergence in series of logarithm causes great divergence in total integral value. As seen in Figure 2.8, *n*=2 gives results close enough to real values in the given range, which means we can express the formulas in a quite simple way.
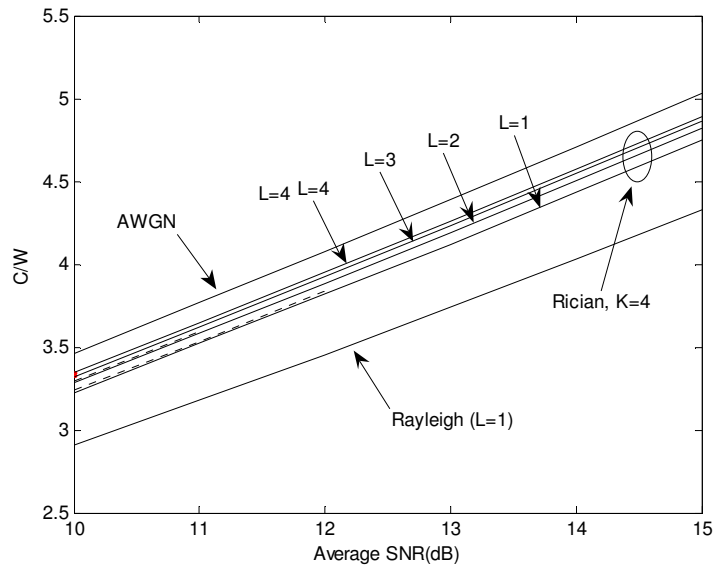
Figure 2.7 Average capacity per unit bandwidth (*C/W*) versus average SNR of OFDM: Rician channel (*K*=4), MRC diversity reception (--: series expansion (*n*=100, x_0=15) lower bound, -: lower bound).
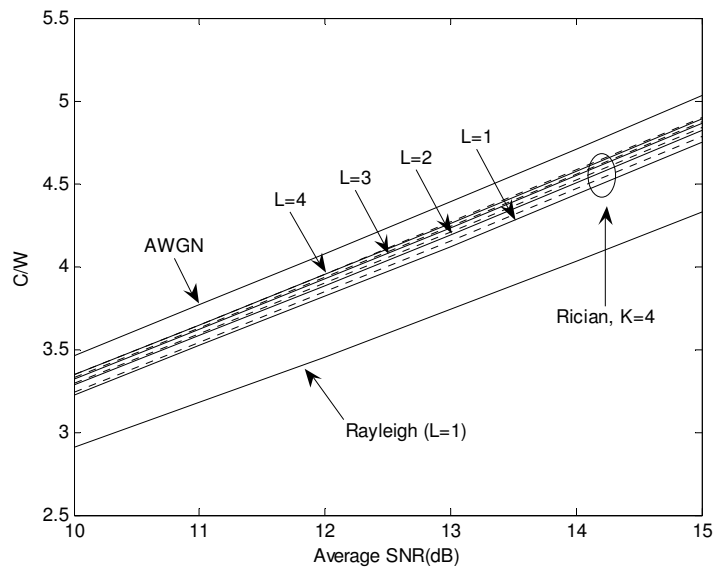
Figure 2.8 Average capacity per unit bandwidth (*C/W*) versus average SNR of OFDM: Rician channel (*K*=4), MRC diversity reception (--: series expansion (*n*=2, x_0=1) lower bound, -: lower bound).

Figure 2.9, Figure 2.10 and Figure 2.11 compare the channel capacity lower bound high SNR approximations provided by (2.28), (2.30) and (2.31), to the lower bound expressions, for Rician, Weibull and Lognormal fading, respectively. In the figures, channel capacities for AWGN and Rayleigh channels are also given for the sake of comparison. It is observed that the approximation given in (2.27) is highly accurate for average SNR values greater than 20 dB, for the given fading channels.
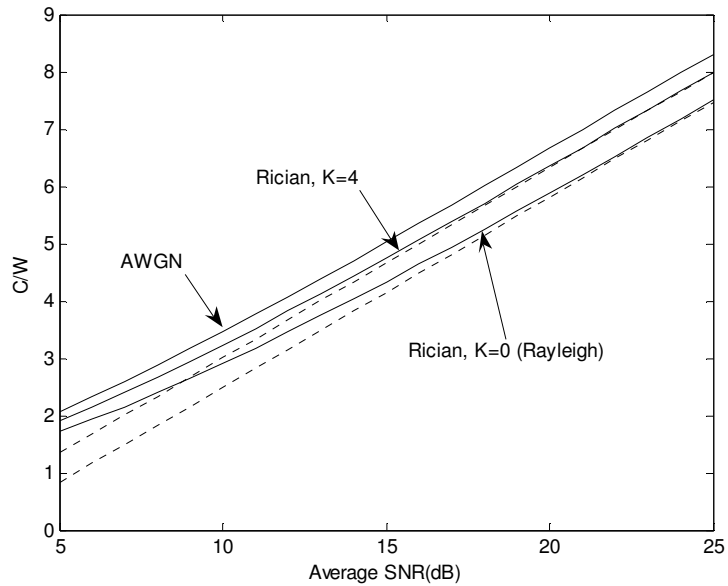
Figure 2.9 Average capacity per unit bandwidth (*C/W*) versus average SNR of OFDM: Rician channel (--: high SNR approximation, -: lower bound).
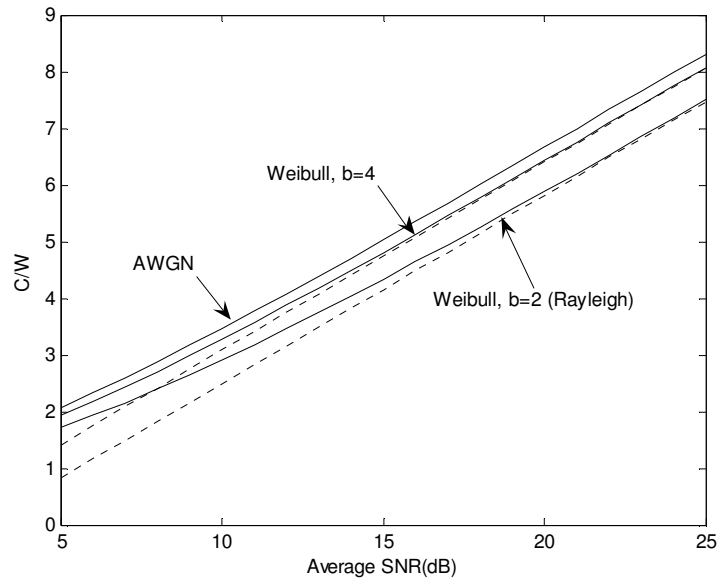
Figure 2.10 Average capacity per unit bandwidth (*C/W*) versus average SNR of OFDM: Weibull channel (--: high SNR approximation, -: lower bound).
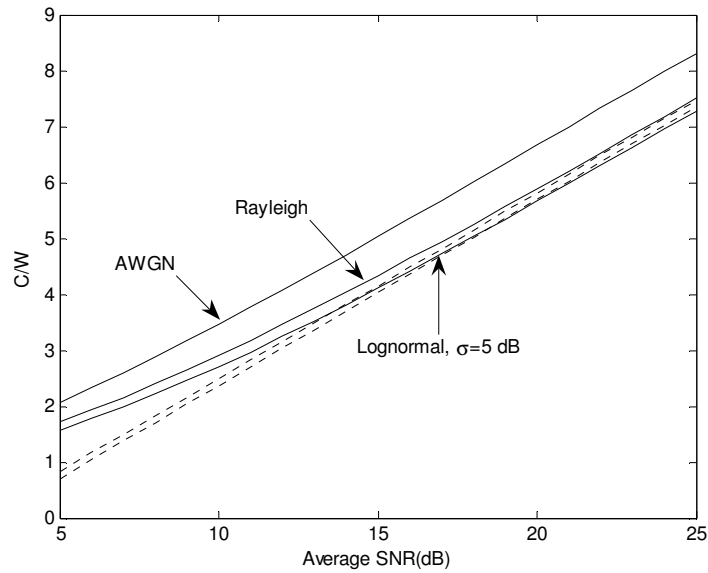
Figure 2.11 Average capacity per unit bandwidth (*C/W*) versus average SNR of OFDM: Lognormal channel (--: high SNR approximation, -: lower bound).

26

CHAPTER 3

CHANNEL ESTIMATION FOR OFDM SYSTEMS

In this chapter, we provide a brief theoretical background on multipath fading channels and OFDM transmission technique. Following, channel taps are estimated on the model developed for unmodulated OFDM assuming slowly time varying Rayleigh channel. We present the well known channel estimation methods, namely ML and MAP estimations, with their MSE and BER performances.

3.1 Multipath Channels [39, 41]

For a typical terrestrial wireless channel, the existence of multiple propagation paths between the transmitter and the receiver are assumed. With each path, a propagation delay and an attenuation factor are associated, which are usually time varying due to changes in propagation conditions resulting primarily from transceiver mobility. Then, we model the multipath fading channel by a time varying linear filter with impulse response $z(\tau,t)$ given by

$$z(\tau,t) = \sum_i a_i(t)\delta(\tau - \tau_i(t)),\qquad(3.1)$$

where $\delta(\cdot)$ stands for Dirac's delta function, $a_i(t)$ and $\tau_i(t)$ are the path attenuation and propagation delay on the ith path, respectively. By the central limit theorem, if a large number of paths between the transmitter and the receiver exists, the impulse response can be modeled by a complex valued Gaussian

random process, and further, the associated attenuation per path are independent and identically distributed. If the received signal has only a single diffuse multipath component $z(\tau, t)$ is characterized by a zero mean complex Gaussian random variable and the channel is called as *Rayleigh fading channel*. ($|z(\tau, t)|$ has a Rayleigh distribution). Alternately, if there are fixed scatterers or signal reflections in the medium, $z(\tau, t)$ has a nonzero mean value and therefore $|z(\tau, t)|$ has a Rician distribution. In this case, the channel is a *Rician fading channel*.

In many physical channels the fading statistics may be assumed approximately stationary for time intervals sufficiently long to make it meaningful to define a subclass of channels, called *wide-sense stationary* (WSS). When we assume the fading process $z(\tau, t)$ is WSS in *t*, then its autocorrelation function is:

$$\Phi_z(\tau_1, \tau_2; \Delta t) = \frac{1}{2} E\left\{ z(\tau_1, t) \cdot z(\tau_2, t + \Delta t)^* \right\}. \tag{3.2}$$

A further reasonable assumption for most mobile communication channels (e.g., troposcatter, chaff, moon reflection) is known as *uncorrelated scattering* (US). Thus, the attenuation and phase shift associated with path delay τ_1 are uncorrelated with the corresponding attenuation and phase shift associated with a different path delay τ_2. Then, (3.2) can be expressed as:

$$\Phi_z(\tau_1, \tau_2; \Delta t) = \Phi_z(\tau_1, \Delta t) \delta(\tau_1 - \tau_2), \tag{3.3}$$

where $\Phi_z(\tau, \Delta t)$ represents the average channel power as a function of the time delay τ and the difference Δt in observation time. The *multipath delay spread* of the channel, T_m, is the range of the values of the path delay τ for which $\Phi_z(\tau, 0)$, the *power delay profile* (the average power output of the channel) is essentially nonzero.

The *spaced frequency spaced time correlation function,* the Fourier transform of $\Phi_z(\tau, \Delta t)$ with respect of τ is given by

$$\Phi_z(\Delta f, \Delta t) = \Im_\tau \{\Phi_z(\tau, \Delta t)\}. \tag{3.4}$$

The *coherence bandwidth* of the channel, B_c, is the range of the values of frequency f for which *spaced frequency correlation function* $\Phi_z(\Delta f, 0)$ is essentially nonzero. Hence the multipath delay spread and the coherence bandwidth are related reciprocally, i.e., $B_c \approx 1/T_m$. Rougly speaking, the channel frequency response remains the same within the coherence bandwidth B_c. When the bandwidth of the transmitted signal is lager than the coherence bandwidth, the channel is called *frequency selective fading*; and when it is smaller, the channel is called *frequency nonselective (flat) fading*.

Now, for the time variations of the channel, in order to relate the Doppler effects to the time variations of the channel, we take the Fourier transform of $\Phi_z(\Delta f, \Delta t)$ with respect to Δt to obtain:

$$S_z(\Delta f, \lambda) = \Im_{\Delta t} \{\Phi_z(\Delta f, \Delta t)\}. \tag{3.5}$$

The *doppler spread* of the channel, B_d, is the range of the values of frequency λ for which *Doppler power spectrum* of the channel, $S_z(0, \lambda)$ is essentially nonzero. The channel *coherence time* is given by $T_c \approx 1/B_d$. Rougly speaking, the channel time response remains the same within the coherence time T_c. When the symbol interval of the transmitted signal is smaller than the coherence time (small Doppler), the channel is said to be *time-nonselective (slow) fading*; and when it is larger than the coherence time (large Doppler) the channel is said to be *time-selective (fast) fading*.

In the literature, there are various multipath channel models suitable for typical propagation environments. The most popular ones were developed by the European working group COST 207 (European Cooperation in the Field of Scientific and Technical Research) [41]. The typical propagation environments are classifiable into areas with rural character (rural area), areas typical for cities and suburban (typical urban), densely built urban areas with bad propagation

29

conditions (bad urban), and hilly terrains (hilly terrain). Basing on the WSSUS assumption, the working group COST 207 developed specifications for the power delay profile and Doppler power spectrum for these four classes of propagation environments.

The specification of typical power delay profile is based on the assumption that the corresponding function can be represented by one or more negative exponential functions. The power delay profile functions of the channel models according to COST 207 are shown in Table 3.1 and Figure 3.1.

Table 3.1 Specifications of typical power delay profiles of COST 207 channels.

Propagation area	Power delay profile	Delay Spread
Rural Area (RA)	$c_{RA}e^{-9.2\tau/\mu s}, \quad 0 \le \tau \le 0.7\mu s$ $0, \qquad\qquad else$	0.1 μs
Typical Urban (TU)	$c_{TU}e^{-\tau/\mu s}, \quad 0 \le \tau \le 7\mu s$ $0, \qquad\qquad else$	0.98 μs
Bad Urban (BU)	$c_{BU}e^{-\tau/\mu s}, \qquad 0 \le \tau \le 5\mu s$ $c_{BU}\dfrac{1}{2}e^{(5-\tau/\mu s)}, \quad 5 \le \tau \le 10\mu s$ $0, \qquad\qquad else$	2.53 μs
Hilly Terrain (HT)	$c_{HT}e^{-3.5\tau/\mu s}, \qquad 0 \le \tau \le 2\mu s$ $c_{HT}\dfrac{1}{2}e^{(15-\tau/\mu s)}, \quad 15 \le \tau \le 20\mu s$ $0, \qquad\qquad else$	6.88 μs
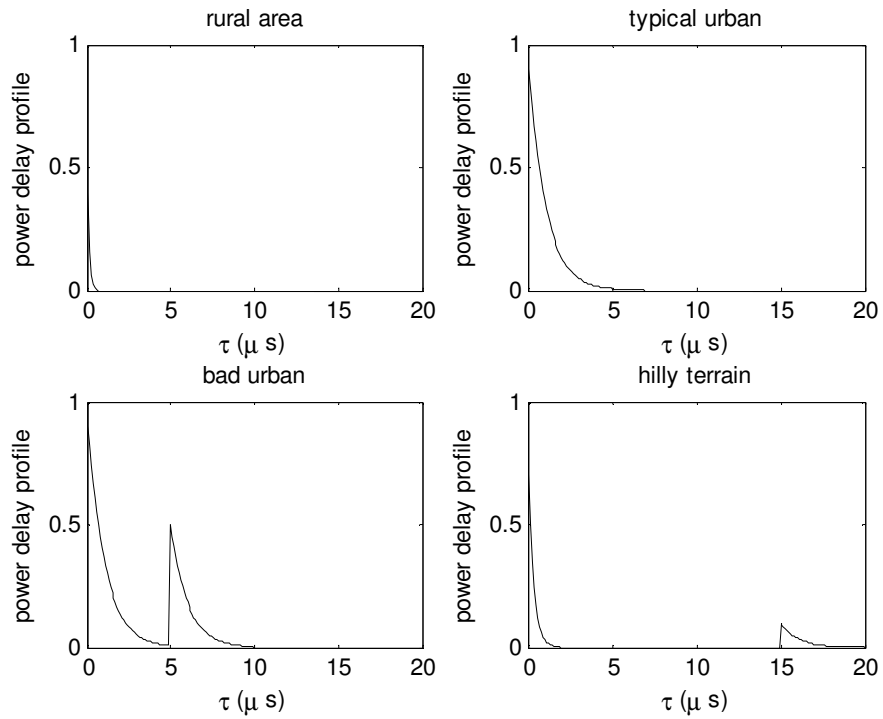
Figure 3.1 Power delay profile of the COST 207 channel models.

The real valued constant quantities introduced can in principle be chosen arbitrarily. Hence, they can be determined in such a way that the average delay power is equal to one, for example. In this case:

$$c_{RA} = \frac{9.2}{1 - e^{-6.44}}$$

$$c_{TU} = \frac{1}{1 - e^{7}}$$

$$c_{BU} = \frac{2}{3(1 - e^{-5})}$$

$$c_{HT} = \frac{1}{(1 - e^{-6.44})/3.5 + (1 - e^{-5})/10}$$

(3.6)

Table 3.2 shows the four types of Doppler power spectrum specified by COST 207, where $G(A_i, f_i, s_i) = A_i e^{-\frac{(f-f_i)^2}{2s_i^2}}$. They are also presented graphically in Figure 3.2 for better illustration. For the real valued constants A_1 and A_2, preferably the values are chosen as

$$
\begin{aligned}
A_1 &= 50 / \sqrt{2\pi} \, f_{max} \\
A_2 &= 10^{1.5} / \sqrt{2\pi} \left(\sqrt{10} + 15\right) f_{max}
\end{aligned}
\tag{3.8}
$$

since it is then ensured that average Doppler power is equal to one. The classical Jakes power spectral density only occurs in the case of very short propagation delays. Only in this case, the assumptions that the amplitudes of the scattering components are homogenous and the angles of arrival are uniformly distributed. For scattering components with medium and long propagation delays, however, it is assumed that the corresponding Doppler frequencies are normally distributed, resulting in a Doppler power spectral density with a Gaussian shape.

Table 3.2 Specifications of typical Doppler power spectral densities of COST 207 channels.

Type	Doppler Power Spectral Density	Propagation Delay	Doppler Spread
Jakes	$\dfrac{1}{\pi f_{max} \sqrt{1 - (f/f_{max})^2}}$	$0 \leq \tau \leq 0.5 \mu s$	$f_{max} / \sqrt{2}$
Gauss I	$G(A_1, -0.8 f_{max}, 0.05 f_{max})$ $+ G(A_1/10, 0.4 f_{max}, 0.1 f_{max})$	$0.5 \leq \tau \leq 2 \mu s$	$0.45 f_{max}$
Gauss II	$G(A_1, 0.7 f_{max}, 0.1 f_{max})$ $+ G(A_2/10^{1.5}, -0.4 f_{max}, 0.15 f_{max})$	$\tau \geq 2 \mu s$	$0.25 f_{max}$
Rice	$\dfrac{1}{\pi f_{max} \sqrt{1 - (f/f_{max})^2}} + 0.91^2 \delta(f - 0.7 f_{max})$	$\tau = 0 \mu s$	$0.39 f_{max}$

Figure 3.2 Doppler power spectral densities of the COST 207 channel models.

From Table 3.1 and Table 3.2, it can be seen that the power delay profile is independent of the Doppler frequencies, but the propagation delays have a decisive influence on the shape of the Doppler power spectrum. However, this is not valid for rural areas, where only the classical Jakes power spectral density is used. In this special case, the scattering function can be represented by the product of the power delay profile and the Doppler power spectrum functions. Channels with such a scattering function are called *independent time and frequency dispersive channels*. For this class of channels, the physical mechanism causing the propagation delays is independent from that which is responsible for the Doppler effect.

3.2 OFDM [39]

In recent years, OFDM systems have attracted an increasing interest due to their use in digital audio and video broadcasting services and to the possible adoption in Fourth Generation mobile communication standards. OFDM is a parallel transmission scheme, where a high rate serial data stream is split up into a set of low rate substreams, each of which is modulated on a separate subcarrier.

Figure 3.3 displays the conventional transceiver of an OFDM system. An OFDM signal can be represented as the sum of N independent QAM/PSK signals modulated onto subchannels of equal bandwidth. A serial-to-parallel buffer segments the information sequence into frames. The bits in each frame are parsed into N groups. Each group may be encoded separately. The complex valued signal points corresponding to the information symbols on the subchannels are denoted by X_k, $k=0,1\ldots,N-1$.

In order to modulate the subcarriers by the information symbol X_k, inverse Discrete Fourier Transform (IDFT) is employed. Then, the N-point IDFT yields the real-valued sequence

$$x_n = \frac{1}{\sqrt{N}}\sum_{k=0}^{N-1} X_k e^{j2\pi nk/N}, \quad n = 0,1\ldots,N-1 \quad .$$

(3.9)

The sequence $\{x_n, 0 \leq n \leq N-1\}$ corresponds to the samples of the sum $x(t)$ of N subcarrier signals, which is expressed by

$$x(t) = \frac{1}{\sqrt{N}}\sum_{k=0}^{N-1} X_k e^{j2\pi kt/T}, \quad 0 \leq t \leq T$$

(3.10)

where T is the symbol duration. The subcarrier frequencies are $f_k = k/T$. Furthermore, the discrete time sequence x_n represents the samples of $x(t)$ taken at times $t_n = nT/N$.
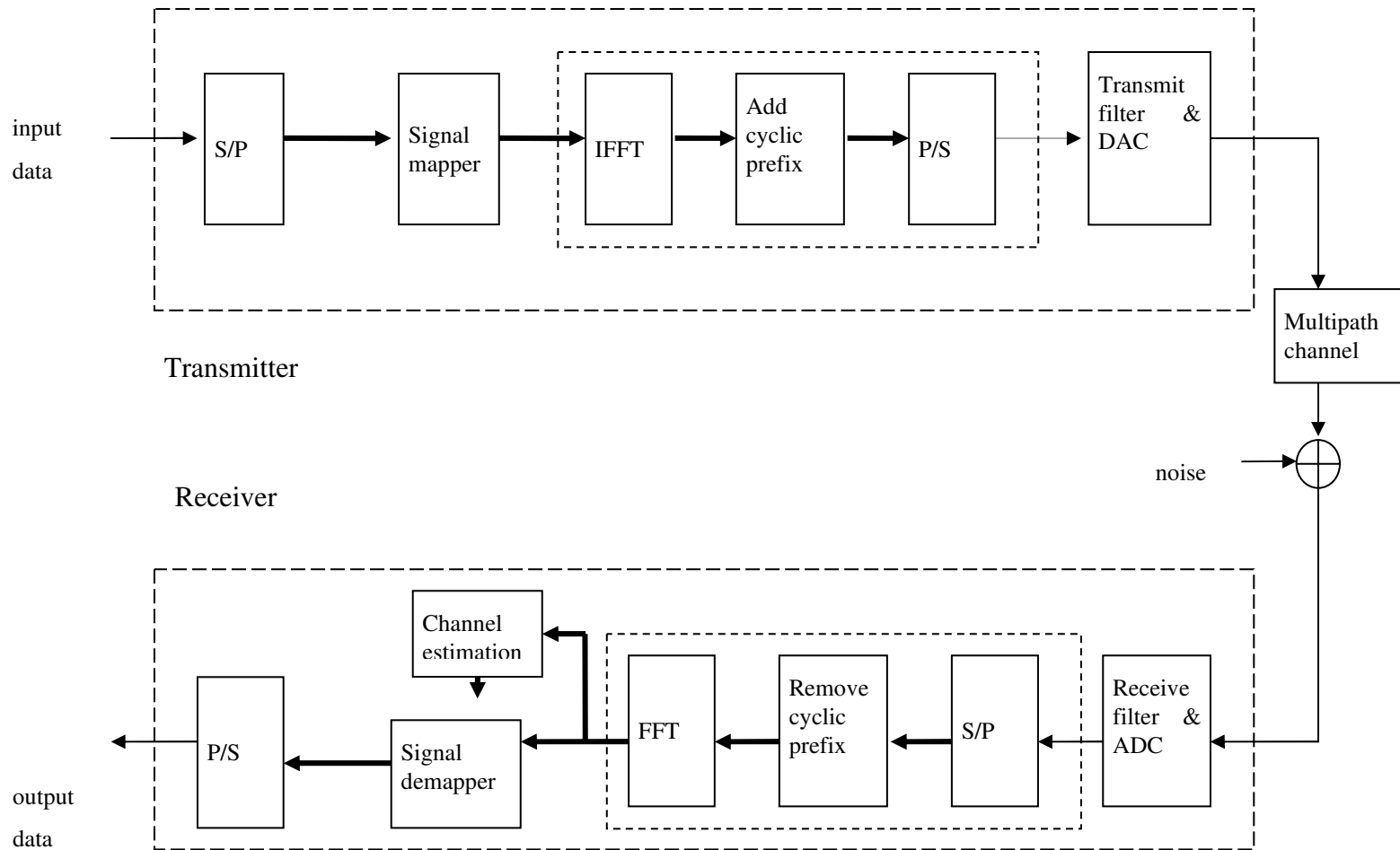
Figure 3.3 Schematic diagram of an OFDM system

The computation of the DFT is performed efficiently by the use of the Fast Fourier Transform (FFT) algorithm. Usually N is taken as an integer to the power of two, enabling the application of the highly efficient (inverse) FFT algorithms.

In practice, the signal samples x_n are passed through a digital-to-analog converter (DAC) whose output, ideally, would be the signal waveform $x(t)$. The output of the channel is the waveform

$$r(t) = x(t) * z(t) + w(t), \tag{3.11}$$

where $z(t)$ is the impulse response of the multipath channel, $w(t)$ is the additive noise and * denotes convolution. By selecting the bandwidth of each subchannel Δf to be very small, the symbol duration $T = 1/\Delta f$ is large compared to the channel time dispersion. Thereby, the bandwidth of the subchannels becomes small compared with the coherence bandwidth of the channel; that is, the individual subcarriers experience flat fading, which requires no traditional equalization. This implies that the symbol period of the substreams is made long compared to the delay spread of the time dispersive radio channel.

We assume that the use of a cyclic prefix both preserves the orthogonality of the tones and eliminates ISI between consecutive OFDM symbols. The information is demodulated by computing the DFT of the received signal after it has been passed through an analog-to-digital converter (ADC). As in the case of the modulator, the DFT is performed efficiently by the use of the FFT algorithm. Because of the cyclic prefix, successive blocks of the transmitted information sequence do not interfere and hence, the kth demodulated sequence may be expressed as

$$R_k = X_k Z_k + W_k, \tag{3.12}$$

where R_k is the output of the demodulator and W_k is the additive noise corrupting the signal. Z_k is the frequency response of the channel impulse at the subcarrier frequencies:

$$Z_k = Z\left(\frac{2\pi k}{N}\right) = \sum_{n=0}^{L_p} z_n e^{-j2\pi nk/N} \qquad (3.13)$$

Consequently, an OFDM receiver implements channel estimation and frequency domain equalization. Thus, channel factors are estimated and compensated prior to passing the data to the detector and decoder. The estimation and equalization methods used depend on the modeling of the channel and complexity invested in each task. The nature of the OFDM enables powerful estimation and equalization techniques. The equalization (signal demapping) required for detecting the data constellations is an elementwise multiplication of the FFT output by the inverse of the estimated channel. For phase modulation schemes, multiplication by the complex conjugate of the channel estimate can do the equalization.

3.3 Channel Estimation under Rayleigh Fading

In an OFDM link, modulated bits are disturbed during the transmission through the channel, since the channel introduces amplitude and phase shifts due to frequency selective and time varying nature of the radio channel. In order for the receiver to acquire the original bits, it needs to take into account these unknown changes. Channel equalization uses channel estimations and inverts the effect of non-selective fading on each subcarrier.

Classical methods estimate channel coefficients relying on known training sequences [4]. Training sequence dependent channel estimation methods for OFDM transmission systems have been developed under the assumption of a slowly varying channel, where the channel transfer function is assumed stationary within one OFDM data block. Thus, the channel transfer function for the previous OFDM data block is used as the transfer function for the present data block. The block diagram is given in Figure 3.4.
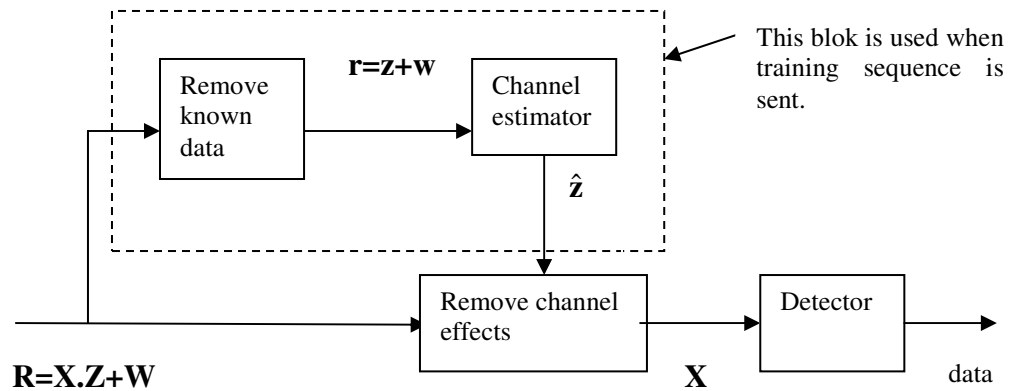
Figure 3.4 Block diagram of the channel estimation using training sequence.

When training sequences are used in order to cope with Doppler effect due to the mobility in wireless systems, the repetition period must not be too small in order not to lose much from the overhead. However, then one faces the problem of not tracking the channel variations properly. The classical method of decision directed channel estimation (DDCE) provides a suitable solution for this problem [4]. The simple philosophy of this method is that in the absence of transmission errors we can benefit from the availability of all information by using the detected subcarrier symbols as an a posteriori reference signal. The block diagram of DDCE scheme is shown in Figure 3.5.
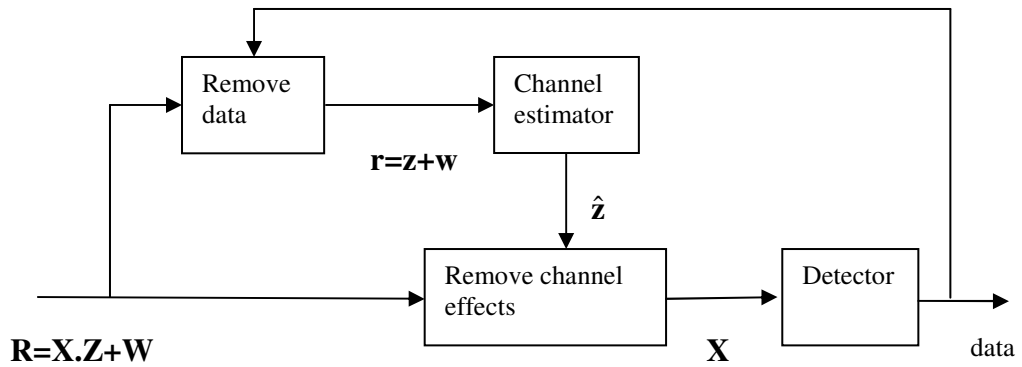
Figure 3.5 Block diagram of the decision directed channel estimation.

In certain cases, the channel transfer function of a wideband radio channel may have significant changes even within one OFDM data block [4]. For such channels, it can be preferable to estimate channel characteristic parameters in every OFDM symbol based on continuous pilot signals. In wideband mobile channels, the pilot based channel estimation scheme has been proven to be a feasible method for OFDM systems, if the channel is slowly fading. The block diagram of this scheme is given in Figure 3.6.

For pilot subcarrier arrangement, the total N subcarriers are divided into N_p groups, each with $L=N/N_p$ adjacent subcarriers. In each group, the first subcarrier is used to transmit pilot signal. The pilot signals are first extracted from the received signal, and the channel transfer function is estimated from the received known pilot signals. Then, the channel responses of subcarriers that carry data are interpolated by using the neighboring pilot channel responses. Theoretically, using high-order polynomial interpolation will fit the channel response better. However, the computational complexity grows as the order is increased.
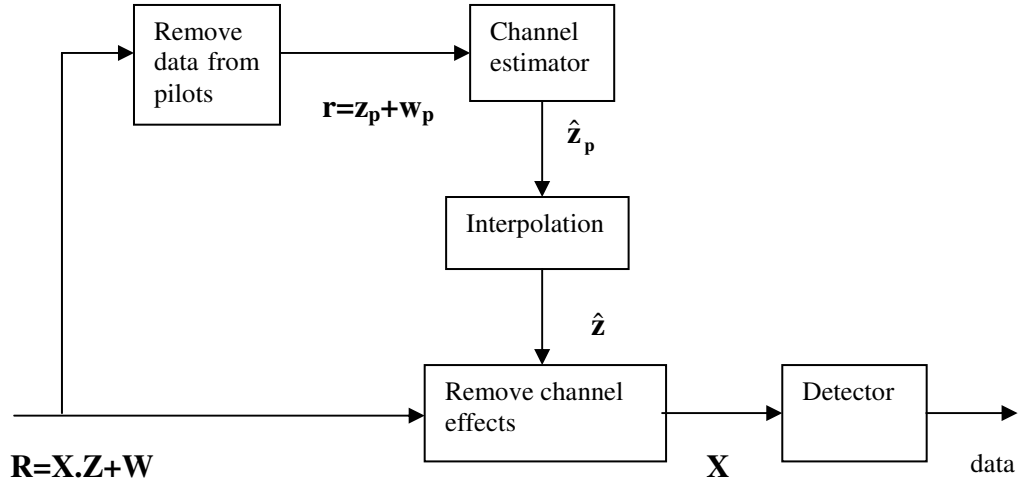
Figure 3.6 Block diagram of the pilot aided channel estimation.

We assume that the channel is frequency selective for the whole band, but is nearly flat for subbands. We take an OFDM system with N subcarriers (modulation effects are assumed to have been removed, e.g., as in a training section, pilots or by decision feedback), assume a channel which is stationary inside the observation interval and AWGN at the receiver. In vector notation, the received signal is

$$\mathbf{r} = \mathbf{z} + \mathbf{w}, \tag{3.14}$$

where the additive white Gaussian noise $\mathbf{w}$ are assumed to be samples from zero mean jointly Gaussian complex random processes with covariance matrix $\mathbf{C}_w$. (Please note that smaller cases of letters are used for frequency domain of signals after removing of modulation effects throughout the study.) The subchannel noise processes are mutually independent so that $\mathbf{C}_w$ can be taken as a diagonal matrix with equal entries. The channel coefficients, $\mathbf{z}$, are samples from a continuous and jointly Gaussian complex random process. We assume that $\mathbf{z}$ is zero mean; thus, it is completely characterized by its covariance matrix $\mathbf{C}_z$.

40

Channel estimation methods in the literature are generally based on ML or MAP estimation. The ML estimate of the coefficient vector is given by [53]:

$$\hat{\mathbf{z}}_{\mathbf{ML}} = \arg\max_{\mathbf{z}} \quad p(\mathbf{r/z}), \tag{3.15}$$

where the conditional probability density function is [54]

$$p(\mathbf{r}/\mathbf{z}) = \frac{1}{\pi^N |\mathbf{C}_{\mathbf{w}}|} \exp\left[-(\mathbf{r} - \mathbf{z})^{\mathbf{H}} \mathbf{C}_{\mathbf{w}}^{-1} (\mathbf{r} - \mathbf{z})\right]. \tag{3.16}$$

A necessary condition is obtained by differentiating the likelihood function with respect to $\mathbf{z}$ and setting the result equal to zero:

$$\left.\frac{\partial \ln p(\mathbf{r/z})}{\partial \mathbf{z}}\right|_{\mathbf{z} = \hat{\mathbf{z}}_{\mathbf{ML}}} = 0. \tag{3.17}$$

Then,

$$\ln p(\mathbf{r/z}) = -(\mathbf{r} - \mathbf{z})^{\mathbf{H}} \mathbf{C}_{\mathbf{w}}^{-1} (\mathbf{r} - \mathbf{z}) - \ln(\pi^N |\mathbf{C}_{\mathbf{w}}|) \tag{3.18}$$

$$\frac{\partial \ln p(\mathbf{r}/\mathbf{z})}{\partial \mathbf{z}} = \mathbf{C}_{\mathbf{w}}^{-1} (\mathbf{r} - \mathbf{z}) \tag{3.19}$$

and the ML estimate is

$$\hat{\mathbf{z}}_{\mathbf{ML}} = \mathbf{r}. \tag{3.20}$$

The MAP estimation of the coefficient vector [53] is found similarly:

$$\hat{\mathbf{z}}_{\mathbf{MAP}} = \arg\max_{\mathbf{z}} \quad p(\mathbf{z/r}), \tag{3.21}$$

where

$$p(\mathbf{z/r}) = \frac{p(\mathbf{r/z})\, p(\mathbf{z})}{p(\mathbf{r})}, \tag{3.22}$$

$$p(\mathbf{z}) = \frac{1}{\pi^N |\mathbf{C}_z|} \exp\left[-\mathbf{z}^H \mathbf{C}_z^{-1} \mathbf{z}\right]. \tag{3.23}$$

The necessary condition is,

$$\left.\frac{\partial \ln p(\mathbf{z}/\mathbf{r})}{\partial \mathbf{z}}\right|_{\mathbf{z}=\hat{\mathbf{z}}_{MAP}} = 0. \tag{3.24}$$

Following the steps given below

$$\ln p(\mathbf{z}/\mathbf{r}) = \ln p(\mathbf{r}/\mathbf{z}) + \ln p(\mathbf{z}) - \ln p(\mathbf{r}), \tag{3.25}$$

$$\frac{\partial \ln p(\mathbf{z}/\mathbf{r})}{\partial \mathbf{z}} = \mathbf{C}_w^{-1}(\mathbf{r} - \mathbf{z}) - \mathbf{C}_z^{-1}\mathbf{z}, \tag{3.26}$$

$$\mathbf{C}_w^{-1}\mathbf{r} - \mathbf{C}_w^{-1}\hat{\mathbf{z}}_{MAP} - \mathbf{C}_z^{-1}\hat{\mathbf{z}}_{MAP} = 0, \tag{3.27}$$

$$\left(\mathbf{C}_w^{-1} + \mathbf{C}_z^{-1}\right)\hat{\mathbf{z}}_{MAP} = \mathbf{C}_w^{-1}\mathbf{r}, \tag{3.28}$$

$$\hat{\mathbf{z}}_{MAP} = \left(\mathbf{C}_w^{-1} + \mathbf{C}_z^{-1}\right)^{-1}\mathbf{C}_w^{-1}\mathbf{r}, \tag{3.29}$$

and simplifying (3.29), MAP estimation expression is found to be

$$\hat{\mathbf{z}}_{MAP} = \mathbf{A} \cdot \mathbf{r} \quad \text{where} \quad \mathbf{A} = \mathbf{C}_z\left(\mathbf{C}_w + \mathbf{C}_z\right)^{-1}. \tag{3.30}$$

Notice that for the ML estimator (without a priori knowledge on the channel) $\mathbf{A}$ becomes the identity matrix.

The time invariant channel is modeled simply as attenuation and phase shift. i.e.,

$$\mathbf{z}(\boldsymbol{\alpha}, \varphi) = \boldsymbol{\alpha}\, e^{j\varphi} \tag{3.31}$$

Then, after estimation of the channel coefficients $\mathbf{z}$, we can compute the estimated channel phase, φ and attenuation, $\boldsymbol{\alpha}$ separately, from the amplitude and phase of the estimate $\mathbf{z}$.

3.4   Estimator Performance

MSE and BER performances of ML and MAP channel estimators are discussed briefly in the following sections. Estimators' performances are evaluated to see the degradation in the performance in case of channel estimation errors and to compare with other estimators.

3.4.1   MSE

The error variances (diagonal of MSE matrix), provide important quantitative information concerning the quality of the estimates that can be used in subsequent detection analysis. The MSE matrix of the estimates is defined by [54]:

$$\mathbf{MSE} = \mathbf{E}\left\{(\hat{\mathbf{z}} - \mathbf{z})(\hat{\mathbf{z}} - \mathbf{z})^{\mathbf{H}}\right\}, \tag{3.32}$$

where $\hat{\mathbf{z}}$ is the estimated channel vector. $(.)^{\mathbf{H}}$ is the notation for Hermitian of a matrix or a vector. Then, MSE of the ML estimates can be shown to be:

$$\begin{aligned}\mathbf{MSE_{ML}} &= \mathbf{E}\left\{(\mathbf{r} - \mathbf{z})(\mathbf{r} - \mathbf{z})^{\mathbf{H}}\right\} \\ &= \mathbf{C_w}\end{aligned}, \tag{3.33}$$

and for the MAP estimator, the MSE matrix is:

$$\begin{aligned}\mathbf{MSE_{MAP}} &= \mathbf{E}\left\{(\mathbf{Ar} - \mathbf{z})(\mathbf{Ar} - \mathbf{z})^{\mathbf{H}}\right\} \\ &= \mathbf{A C_w A^H} + [\mathbf{A} - \mathbf{I_N}]\mathbf{C_z}[\mathbf{A} - \mathbf{I_N}]^{\mathbf{H}}\end{aligned} \tag{3.34}$$

where $\mathbf{I_N}$ is the identity matrix with size NxN. It can easily be proven that,

$$\begin{aligned}\mathbf{MSE_{MAP}} &= (\mathbf{I_N} - \mathbf{A})\,\mathbf{C_z} \\ &= \mathbf{C_z} - \mathbf{C_z}(\mathbf{C_w} + \mathbf{C_z})^{-1}\mathbf{C_z}\end{aligned}. \tag{3.35}$$

Following this, using the Inversion Lemma [55], i.e.,

$$E = B^{-1} + CD^{-1}C^{H}$$
$$E^{-1} = B - BC(D + C^{H}BC)^{-1}C^{H}B$$
(3.36)

with $B = C_z$, $C = I_N$, $D = C_w$, we reach the final equation,

$$MSE_{MAP} = (C_w^{-1} + C_z^{-1})^{-1} = \sigma_w^2 A,$$
(3.37)

where σ_w^2 is the variance of the white noise component. As known, in linear signaling scheme with a Gaussian a priori density, as in our case, the MAP estimator is the efficient estimate, where the error variance is equal to the bound on MSE [53]. For independent fading, $C_z = \sigma_z^2 I_N$, where σ_z^2 is the variance of channel coefficients. Then, MSE is found to be

$$MSE_{MAP,ind} = \frac{\sigma_z^2 \sigma_w^2}{\sigma_z^2 + \sigma_w^2} I_N.$$
(3.38)

For a flat fading channel, $C_z = \sigma_z^2 1_N$, where 1_N is the notation we use for the NxN matrix with all entries equal to one. Then,

$$MSE_{MAP,flat} = \frac{\sigma_z^2 \sigma_w^2}{N\sigma_z^2 + \sigma_w^2} 1_N.$$
(3.39)

As seen from (3.38) and (3.39), for independent fading MSE does not depend on N, on the contrary for flat fading channel, as the number of subchannels increases, MSE decreases. A ratio on resulting from the correlation can be found by dividing the error variance of independent fading by the error variance of the flat fading. The result is:

$$c_{max} = \frac{N\sigma_z^2 + \sigma_w^2}{\sigma_z^2 + \sigma_w^2}.$$
(3.40)

In Figure 3.7, we show the ratio in (3.40) obtained for channel esimates versus number of subchannels for SNR=10 dB (σ_z^2=1 and σ_w^2=0.1). As seen, the ratio

for the rms error of independent fading with respect to flat fading is almost equal to square root of N (upper bound for the variance is about N as given in (3.40)).
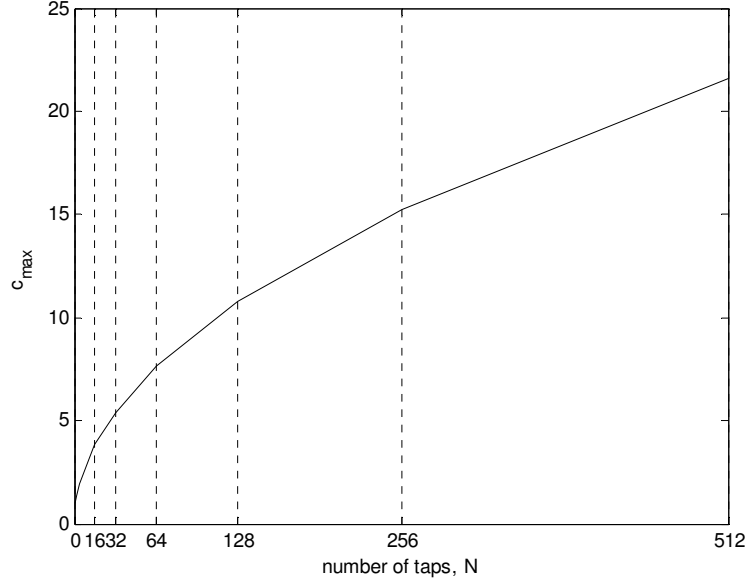
Figure 3.7 The ratio for the rms error of independent fading wrt flat fading.

The error variances of real part of the channel with real covariance matrix (real and imaginary parts of channel coefficients are independent) can be found similarly [54]:

$$
\begin{aligned}
\mathbf{MSE_r} &= \mathbf{E}\left\{ \left(\mathbf{Ar_r} - \mathbf{z_r}\right)\left(\mathbf{Ar_r} - \mathbf{z_r}\right)^{\mathbf{H}} \right\} \\
&= \mathbf{AC_{w_r} A^H} + [\mathbf{A} - \mathbf{I_N}]\mathbf{C_{z_r}}[\mathbf{A} - \mathbf{I_N}]^{\mathbf{H}}.
\end{aligned}
\tag{3.41}
$$

Determining the error variance of channel phase estimation (or attenuation estimation) is somewhat difficult and needs large number of integration. (Details

45

are given in Appendix A.) Then, we find the channel phase error variance for each path seperately. The variance of the phase error of kth path is given by [56]:

$$E\left\{\left(\hat{\phi}_k - \phi_k\right)^2\right\} = \int\limits_{-\pi}^{\pi}\int\limits_{-\pi}^{\pi}\left(\hat{\phi}_k - \phi_k\right)^2 p\left(\hat{\phi}_k, \phi_k\right) d\hat{\phi}_k \, d\phi_k \,. \tag{3.42}$$

We can find $p\left(\hat{\phi}_k, \phi_k\right)$ by transforming the Cartesian pdf $p(\hat{z}_k, z_k)$ to polar form, and then integrating. Thus,

$$p\left(\hat{\phi}_k, \phi_k\right) = \int\limits_{0}^{\infty}\int\limits_{0}^{\infty} p\left(\hat{\alpha}_k, \hat{\phi}_k, \alpha_k, \phi_k\right) d\hat{\alpha}_k \, d\alpha_k \,. \tag{3.43}$$

Note that, $(\hat{z}_k, z_k)$ are jointly Gaussian, then $p(\hat{z}_k, z_k)$ can be written as [56]:

$$p(\hat{z}_k, z_k) = \frac{1}{2\pi\sigma_z\sigma_{\hat{z}}\sqrt{1-r^2}}\exp\left\{-\frac{1}{2(1-r^2)}\left(\frac{\hat{z}_k^2}{\sigma_z^2} - 2r\frac{\hat{z}_k z_k}{\sigma_z\sigma_{\hat{z}}} + \frac{z_k^2}{\sigma_{\hat{z}}^2}\right)\right\}, \tag{3.44}$$

where correlation $r = \dfrac{C_{z\hat{z}}}{\sigma_{\hat{z}}\sigma_z}$ and $C_{z\hat{z}} = E\{z_k\hat{z}_k\}$. r can be found considering

$$\hat{z}_k = A_{k1}z_1 + A_{k2}z_2 + \cdots + A_{kN}z_N + A_{k1}w_1 + A_{k2}w_2 + \cdots + A_{kN}w_N\,, \tag{3.45}$$

which is also known to be a Gaussian variable. Then, we can evaluate the phase estimation error variance using (3.42). The error variance of the attenuation can be found similarly.

3.4.2 BER

Performance degradation due to channel estimation error can be best analyzed by finding the BER. The received signal for the kth subcarrier is given by

$$r_k = x_k z_k + w_k\,, \tag{3.46}$$

46

where x_k and r_k are the transmitted and received symbols, respectively; z_k accounts for the correlated, complex valued fading introduced by the frequency selective channel; and w_k denotes samples of an AWGN. Following [3], we start our analysis by defining the symbol transmitted as $x_{k,i}$, which is an element of the symbol set $\{x_{k,m}\}$, $m = \{1,2,\ldots,M\}$. (M is the order of the modulation scheme.) At the receiver's site, an optimum detector will detect the symbol $x_{k,n} \in \{x_{k,m}\}$, which minimizes the distance metric $M_d(x_{k,n}) = |r_k - \hat{z}_k x_{k,n}|^2$. $\hat{z}_k$ is the estimate channel coefficient. An error occurs when the metric calculated for a symbol $x_{k,n} \neq x_{k,i}$ is smaller than the metric for the transmitted symbol $x_{k,i}$. The probability of this event is

$$P_e = \Pr\{M_d(x_{k,n}) < M_d(x_{k,i})\} = \Pr\{D < 0\}, \tag{3.47}$$

where $D = M_d(x_{k,n}) - M_d(x_{k,i})$ is called *decision variable*. Then, D becomes

$$D = r_k \hat{z}_k^*(x_{k,i}^* - x_{k,n}^*) + r_k^* \hat{z}_k(x_{k,i} - x_{k,n}) + |\hat{z}_k|^2(|x_{k,n}|^2 - |x_{k,i}|^2). \tag{3.48}$$

r_k is known to be a complex Gaussian random variable. The same holds for $\hat{z}_k$. Thus, the decision variable D is a special case of the generic quadratic form and the error probability is found to be [3]

$$P_e = Q_1(a,b) - \frac{v_2/v_1}{1+v_2/v_1} I_0(ab) e^{-(a^2+b^2)/2}, \tag{3.49}$$

where $I_n(x)$ is the nth order modified Bessel function of the first kind and $Q_1(a,b)$ is Marcum's Q function. The parameters a, b, v_1 and v_2 are related to the moments [3]. For the Rayleigh channel, as in our case, it can easily be shown that $a = b = 0$. Then, the probability of error simplifies to

$$P_e = \frac{1}{1+v_2/v_1}, \tag{3.50}$$

where

$$v_{1,2} = \sqrt{w^2 + \frac{1}{4|C|^2\left(\mu_{xx}\mu_{rr} - |\mu_{xr}|^2\right)}} \mp w, \qquad (3.51)$$

$$w = \frac{A\mu_{xx} + B\mu_{rr} + C^*\mu_{xr} + C\mu_{xr}^*}{4|C|^2\left(\mu_{xx}\mu_{rr} - |\mu_{xr}|^2\right)}, \qquad \begin{aligned} \mu_{xx} &= \frac{1}{2}E\left\{|\hat{z}_k|^2\right\} \\ \mu_{rr} &= \frac{1}{2}E\left\{|r_k|^2\right\}. \\ \mu_{xr} &= \frac{1}{2}E\left\{|\hat{z}_k r_k^*|\right\} \end{aligned} \qquad (3.52)$$

The constants that are representing the properties of the modulation schemes are $A = |x_{k,n}|^2 - |x_{k,i}|^2$, $B = 0$ and $C = x_{k,n} - x_{k,i}$. Assigning different constellation values, the probability of error can be calculated.

For gray coded QPSK and perfect channel estimation, which means that the receiver has exact knowledge of the channel tap ($\hat{z}_k = z_k$), the BER can easily be shown to be

$$P_e = \frac{1}{2}\left(1 - \frac{1}{\sqrt{1 + 1/\gamma_b}}\right), \qquad (3.53)$$

where $\gamma_b = \dfrac{\sigma_z^2 E\left\{|x|^2\right\}}{K\sigma_w^2}$ is the bit SNR and K denotes the number of bits represented by one symbol ($K=2$ for QPSK).

For the MAP estimator,

$$\begin{aligned} \mu_{xx} &= \frac{1}{2}\mathbf{A}(k,:)[\mathbf{C_z} + \mathbf{C_w}]\mathbf{A}^H(:,k) \\ \mu_{rr} &= \frac{\sigma_z^2 + \sigma_w^2}{2} \\ \mu_{xr} &= \frac{1}{2}\mathbf{A}(k,:)\mathbf{C_z}(:,k) \end{aligned} \qquad (3.54)$$

Here $\sigma_z^2 = E\{z_k z_k^*\}$, $\mathbf{A}(k,:)$ and $\mathbf{A}(:,k)$ denote the kth row and the kth column of the matrix $\mathbf{A}$, respectively. Then P_e can be calculated using (3.50).

Another method for analytical calculation of BER is given in [32]. This paper presents a systematic approach for evaluating BER performance of OFDM receivers in Rayleigh fading when a linear pilot assisted channel estimate is used. These BER expressions are functions of the average bit SNR, and some correlation coefficients that depend on the true channel statistic and the estimation method used. The derivations are based on the facts that Rayleigh fading and a linear pilot assisted channel estimate is a linear function of the true channel responses at pilot symbol locations.

The equation for evaluating the BER of QPSK modulated OFDM receiver with linear channel estimate algorithms is given by

$$P_e = \frac{1}{2}\left[1 - \frac{1}{2\sqrt{2}}\frac{\rho_1 + \rho_2}{\sqrt{1 + \frac{1}{2\gamma_b} - \frac{(\rho_1 - \rho_2)^2}{2}}} - \frac{1}{2\sqrt{2}}\frac{\rho_1 - \rho_2}{\sqrt{1 + \frac{1}{2\gamma_b} - \frac{(\rho_1 + \rho_2)^2}{2}}}\right], \quad (3.55)$$

where

$$\begin{array}{ccc} \rho_1 = \dfrac{\mu_1}{\sigma_1 \sigma_2} & & \sigma_1^2 = \dfrac{1}{2}E\{|z_k|^2\} \\[2mm] & \text{and} & \sigma_2^2 = \dfrac{1}{2}E\{|\hat{z}_k|^2\} \\[2mm] \rho_2 = \dfrac{\mu_2}{\sigma_1 \sigma_2} & & \\[2mm] & & \mu_1 + j\mu_2 = \dfrac{1}{2}E\{\hat{z}_k z_k^*\} \end{array} \qquad . \qquad (3.56)$$

For gray coded QPSK and perfect channel estimation, since $\rho_1 = 1$, $\rho_2 = 0$, the BER expression given in (3.55) can be shown to be $P_e = \frac{1}{2}\left(1 - \frac{1}{\sqrt{1 + 1/\gamma_b}}\right)$, which is the same as (3.53).

For ML channel estimation, the probability of error is

$$P_e = \frac{1}{2}\left[1 - \frac{1}{\sqrt{2}}\frac{\rho_1}{\sqrt{1 + \frac{1}{2\gamma_b} - \frac{\rho_1^2}{2}}}\right],$$ (3.57)

where $\rho_1 = \dfrac{1}{\sqrt{1 + 1/2\gamma_b}}$.

For the MAP estimator,

$$\sigma_1^2 = \frac{\sigma_z^2}{2}$$

$$\sigma_2^2 = \frac{1}{2}\mathbf{A}(k,:)[\mathbf{C_z} + \mathbf{C_w}]\mathbf{A}^{\mathbf{H}}(:,k).$$ (3.58)

$$\mu_1 + j\mu_2 = \frac{1}{2}\mathbf{A}(k,:)\mathbf{C_z}(:,k)$$

After calculating these variables, P_e is found from (3.55).

CHAPTER 4

SIMPLIFIED MAP ESTIMATORS

Frequency selectivity of the channel caused by the multipath environment is characterized by the frequency domain correlation function (the spaced frequency correlation function) of the channel. Several frequency domain correlation estimation methods are found in the literature [57-63]. Frequency selectivity of the radio channel can be characterized using level crossing rate of the channel in frequency domain. The detected symbols in frequency domain can also be used to generate the frequency domain correlation function. These methods need computational effort since the entire correlation matrix must be estimated. Instead, we assign a structure to the frequency domain correlation, i.e., the correlation function is parameterized.

In this chapter, we have proposed two simplified MAP estimators which model the correlation of subchannels by a single parameter. These estimators differ from the parametric estimators presented in the literature, which estimate the channel tap number and delays. The first simplified estimator is based on the exponential frequency domain correlation assumption, while for the second one we assume that power delay profile is exponential.

4.1 Exponential Frequency Domain Correlation Assumption

4.1.1 Proposed Estimator (SMAP-efdc)

In this section, we assume that the frequency domain correlation function has an exponential form, i.e.,

$$\mathbf{C}_z(n,m) = \rho^{|n-m|} \quad , \tag{4.1}$$

where the correlation coefficient is $0 \leq \rho \leq 1$. The lower limit means independent fading, while upper limit is for flat fading channel. Note that this approximation is reasonable, because as the distance increases the correlation between subchannels decreases. Also note that covariance matrix has a fairly simple form. Then, we expect that the MAP estimator complexity reduces considerably.

For a channel with exponential covariance matrix, Figure 4.1 shows the frequency domain correlation of the center subchannel (n=512) with the other subchannels for N=1024 and ρ=0.9, 0.99 and 0.999. As seen, for ρ=0.9, the correlation drops below 0.1 when we go only 20 neigbour subchannel away. But for ρ=0.999 (almost flat channel), edge subchannels receive almost 60% of the full correlation.
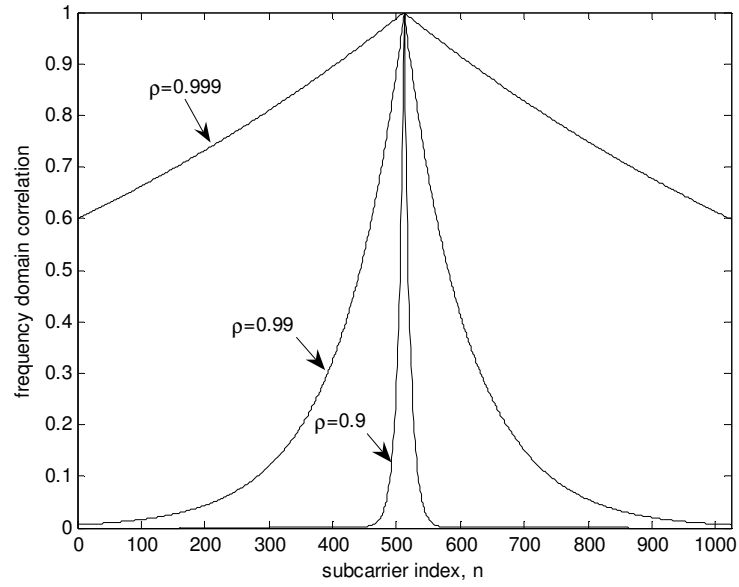
Figure 4.1 Frequency domain correlation of middle subchannel (n=512) with others, N=1024, channel with exponential frequency domain correlation.

Then, we propose the following simplified MAP (SMAP-efdc) estimator:

$$\hat{\mathbf{z}}_{\mathbf{SMAP}} = \mathbf{A}(\hat{\rho}) \cdot \mathbf{r} \quad \text{where} \quad \mathbf{A}(\hat{\rho}) = \mathbf{C}_{\mathbf{z}}(\hat{\rho})[\mathbf{C}_{\mathbf{w}} + \mathbf{C}_{\mathbf{z}}(\hat{\rho})]^{-1}. \tag{4.2}$$

$\hat{\rho}$ is the estimated ρ. The complete block diagram of the MAP estimator is shown in Figure 4.2.
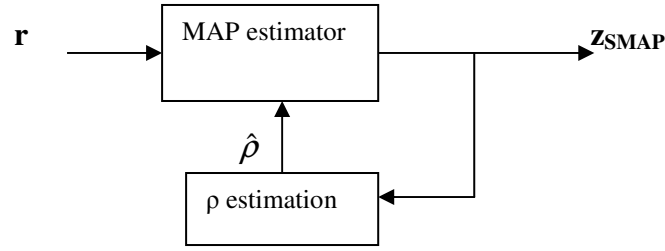
Figure 4.2 Block diagram of SMAP-efdc estimator

The instantaneous channel frequency response correlation values are calculated from the estimated fading by averaging neighbor subchannel correlations. Thus, the instantaneous correlation is found as

$$\hat{\rho}_{ins} = \frac{z_{SMAP,1} \cdot z_{SMAP,2}^* + z_{SMAP,2} \cdot z_{SMAP,3}^* + \cdots + z_{SMAP,N-1} \cdot z_{SMAP,N}^*}{\left| z_{SMAP,1} \right|^2 + \left| z_{SMAP,2} \right|^2 + \cdots + \left| z_{SMAP,N-1} \right|^2} \qquad (4.3)$$

The instantaneous correlation estimates are noisy, therefore an alpha tracker [57] can be used for averaging the instantaneous values:

$$\hat{\rho}^i = \alpha \, \hat{\rho}^{i-1} + \left(1 - \alpha\right) \hat{\rho}_{ins} \qquad (4.4)$$

where $0 < \alpha < 1$ is the tracking parameter and i is the symbol number. An alfa tracker with a high tracking parameter value will performs better, but obviously tracking time will be longer.

4.1.2 Performance

4.1.2.1 MSE Performance

For a channel with exponential frequency domain correlation, recognizing that matrix $\mathbf{A}$ is modeled as $\mathbf{A}(\rho)$, MSE expression of MAP estimator given in (3.34) becomes as below:

$$\begin{aligned} \mathbf{MSE} &= \mathbf{A}(\rho)\mathbf{C}_{\mathbf{w}}\mathbf{A}^{\mathbf{H}}(\rho) + [\mathbf{A}(\rho) - \mathbf{I}]\mathbf{C}_{\mathbf{z}}(\rho)[\mathbf{A}(\rho) - \mathbf{I}]^{\mathbf{H}} \\ &= \sigma_w^2 \mathbf{A}(\rho) \end{aligned}$$

(4.5)

Analytical results of rms error (square root of error variances) of channel estimation, channel amplitude and phase estimation versus correlation (ρ) for N=128, SNR=10 dB ($\mathrm{SNR} = 10\log_{10}\left(\sigma_z^2/\sigma_w^2\right)$) are shown in Figure 4.3, Figure 4.4, and Figure 4.5, respectively. In the plots, it is assumed that the channel has an exponential frequency domain correlation and ρ is known exactly. As seen from the figures, rms error gets smaller as the correlation between the subchannels increases. The improvement is more prominent for $0.9 < \rho < 1$. Note that the outer curves are for the edge subchannels (n=0 and n=N-1) estimation errors, the inner ones are for middle subchannels (n=N/2), and the others are for the remaining. The subchannels at the edges have largest error variances, while the variances of middle subchannels are the smallest, as expected. The error variances of subchannels in between decrease as the subchannels get closer to the center.

We have also investigated the effect of SNR on the rms error of center tap in Figure 4.6, for N=128. The channel has an exponential frequency domain correlation, with known ρ. The rms error decreases as SNR inreases, which is the expected result.
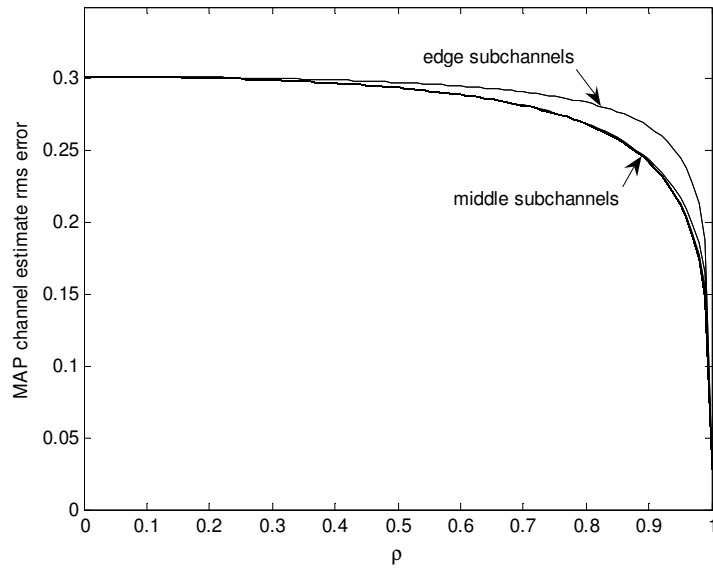
Figure 4.3 Channel MAP estimate rms error versus subchannel correlation (ρ), *N*=128, SNR=10 dB, channel with exponential frequency domain correlation.
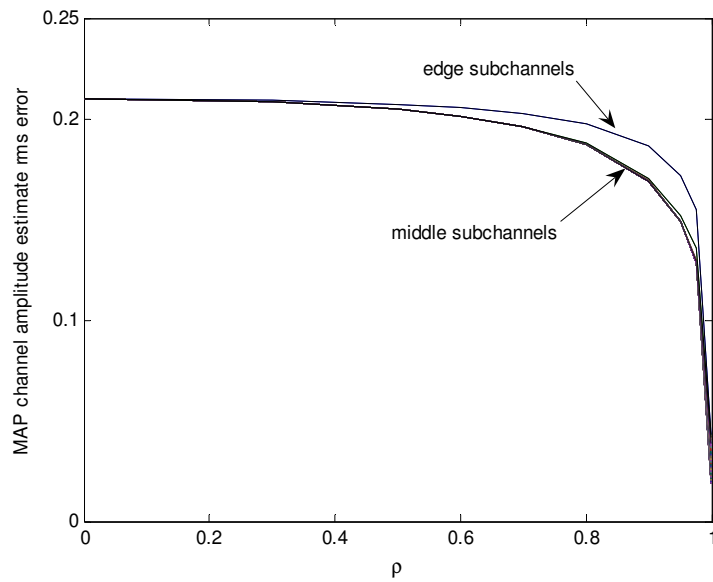
Figure 4.4 Channel amplitude MAP estimate rms error versus subchannel correlation (ρ), *N*=128, SNR=10 dB, channel with exponential frequency domain correlation.
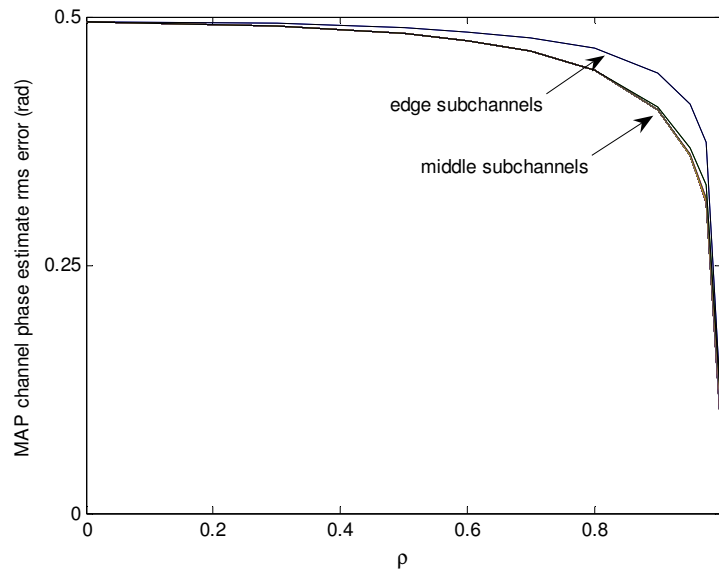
Figure 4.5 Channel phase MAP estimate rms error versus subchannel correlation (ρ), *N*=128, SNR=10 dB, channel with exponential frequency domain correlation.
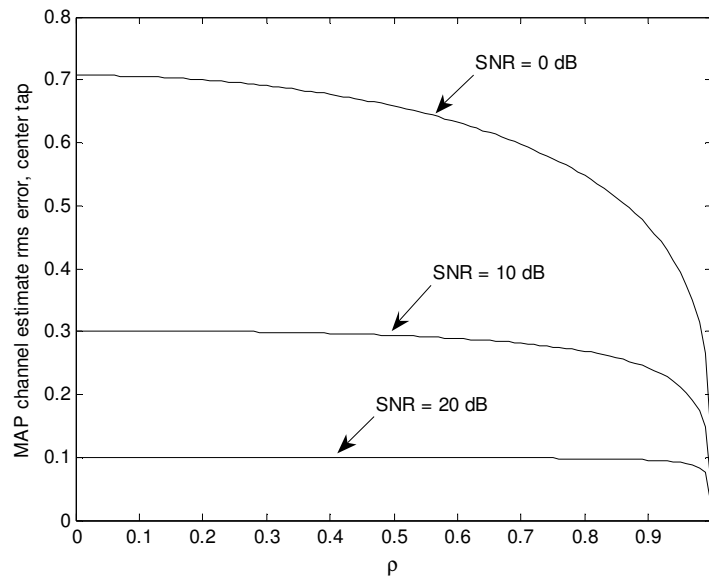
Figure 4.6 Channel MAP estimate rms error (center tap) versus subchannel correlation (ρ), *N*=128, SNR=0, 10 and 20 dB, channel with exponential frequency domain correlation.

We have done simulations for channels with known correlation ρ's to investigate the accuracy of estimation of ρ. We assume that the channel response is slowly time varying, that is, the channel correlation stays constant throughout the estimation process. The simulation parameters are selected as SNR=10 dB, α=0.9 and number of iterations is 1000. In Table 4.1, actual and estimated values of the correlation are given for various subchannel numbers. Slightly overestimation in the correlation parameter is observed and this deviation increases as N increases.

Table 4.1 Real and estimated correlation (ρ) values of channels with exponential frequency domain correlation, N=64, 128 and 256.

Correlation (ρ)	Estimated correlation ($\hat{\rho}$)		
	N=64	N=128	N=256
0	-0.0040	-0.0012	0.0005
0.20	0.2064	0.2133	0.2169
0.40	0.4159	0.4265	0.4319
0.60	0.6233	0.6366	0.6433
0.70	0.7252	0.7391	0.7460
0.80	0.8246	0.8381	0.8447
0.90	0.9189	0.9299	0.9350
1	1.00	1.00	1.00

4.1.2.2 Sensitivity Analysis

In what follows, we analyze the sensitivity of the SMAP-efdc estimator. For a channel with exponential frequency domain correlation, it is assumed that σ_w^2 is known and ρ is estimated. Then, the MSE in (3.34) becomes:

$$\mathbf{MSE} = \mathbf{A}(\hat{\rho})\mathbf{C_w}\mathbf{A^H}(\hat{\rho}) + [\mathbf{A}(\hat{\rho}) - \mathbf{I}]\mathbf{C_z}[\mathbf{A}(\hat{\rho}) - \mathbf{I}]^\mathbf{H}. \qquad (4.6)$$

Figure 4.7, Figure 4.8 and Figure 4.9 give the graphs of center tap rms error of SMAP-efdc estimator versus $\hat{\rho}$, for N=128, SNR=10 and 20 dB, $\rho = 0.5, 0.97$ and 0.999, respectively. The proposed estimator is not sensitive to correlation estimation errors for low correlation, but it is very sensitive for $\rho \geq 0.9$.
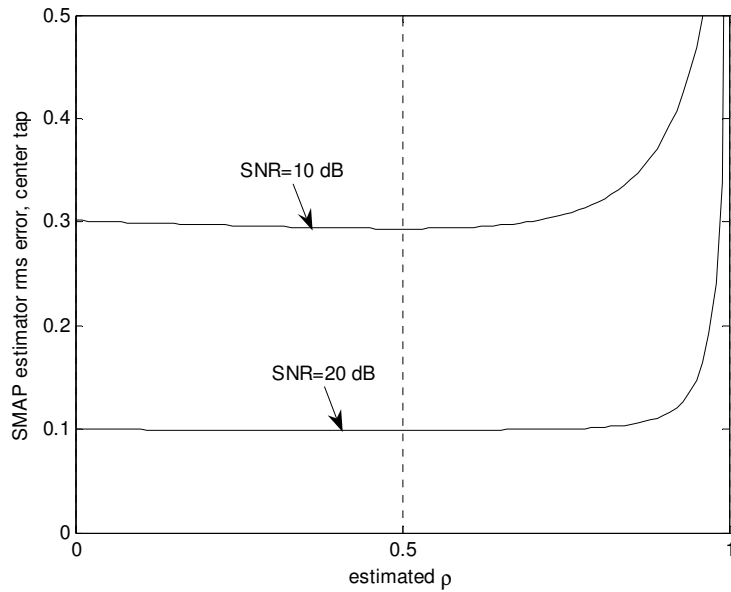
Figure 4.7 SMAP-efdc estimator rms error (center tap) versus estimated correlation ($\hat{\rho}$), $\rho = 0.5$, N=128, SNR=10 and 20 dB.
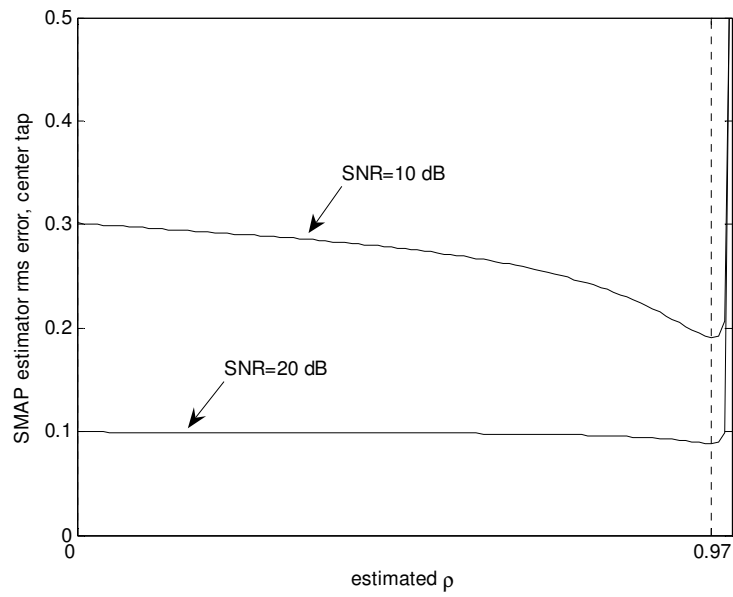
Figure 4.8 SMAP-efdc estimator rms error (center tap) versus estimated correlation ($\hat{\rho}$), $\rho = 0.97$, *N*=128, SNR=10 and 20 dB.
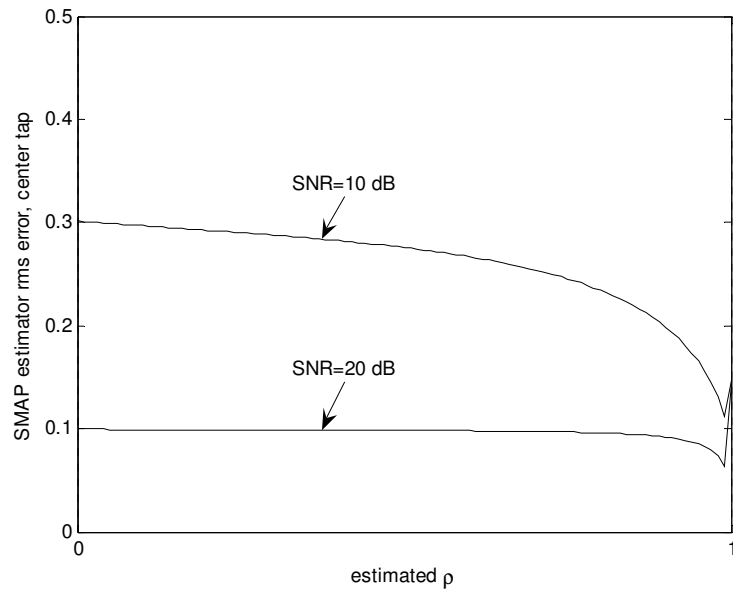
Figure 4.9 SMAP-efdc estimator rms error (center tap) versus estimated correlation ($\hat{\rho}$), $\rho = 0.999$, *N*=128, SNR=10 and 20 dB.

Similarly, for a channel with known ρ and estimated σ_w^2, the MSE of SMAP-efdc estimator is:

$$\mathbf{MSE} = \mathbf{A}(\hat{\sigma}_w^2)\mathbf{C_w}\mathbf{A^H}(\hat{\sigma}_w^2) + [\mathbf{A}(\hat{\sigma}_w^2) - \mathbf{I}]\mathbf{C_z}[\mathbf{A}(\hat{\sigma}_w^2) - \mathbf{I}]^{\mathbf{H}}. \tag{4.7}$$

Figure 4.10, Figure 4.11 and Figure 4.12 give the graphs of center tap rms error of SMAP-efdc estimator versus $\hat{\sigma}_w^2$, for N=128, SNR=0,10 and 20 dB, and ρ=0.5, 0.9 and 0.999, respectively. As seen from the figures, the proposed estimator is rather insensitive to the errors in $\hat{\sigma}_w^2$, especially when SNR is high and/or channel is highly correlated especially if error occurs as underestimation. For low SNRs, and for low correlated channels the proposed estimator is sensitive to errors. Rms error increases dramatically if noise variance is fairly overestimated for highly correlated channels.
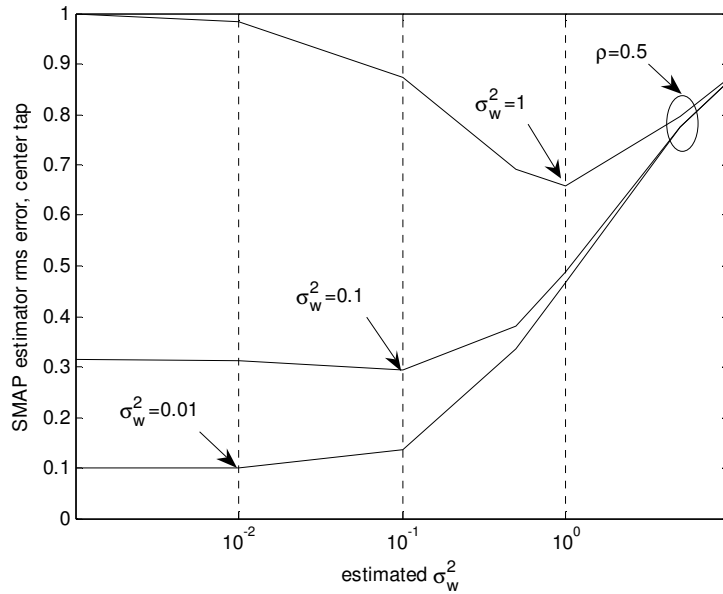
Figure 4.10 SMAP-efdc estimator rms error (center tap) versus estimated noise variance ($\hat{\sigma}_w^2$), $\rho = 0.5$, N=128, SNR=0, 10 and 20 dB.
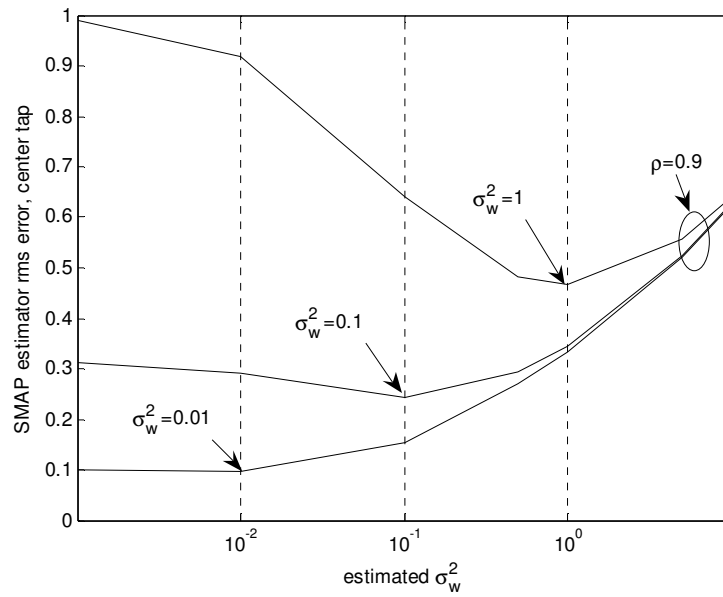
Figure 4.11 SMAP-efdc estimator rms error (center tap) versus estimated noise
variance ($\hat{\sigma}_w^2$), $\rho = 0.9$, *N*=128, SNR=0, 10 and 20 dB.
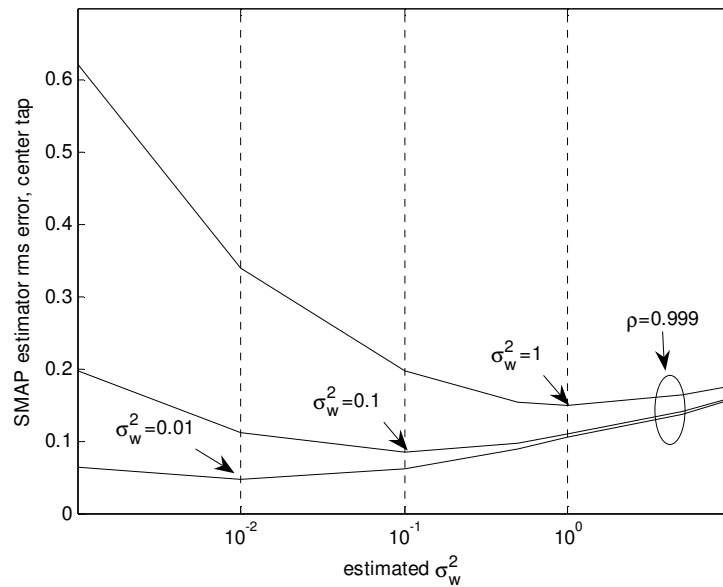
Figure 4.12 SMAP-efdc estimator rms error (center tap) versus estimated noise
variance ($\hat{\sigma}_w^2$), $\rho = 0.999$, *N*=128, SNR=0, 10 and 20 dB.

4.1.3 Approximate SMAP-efdc

The proposed SMAP-efdc estimator has a lower complexity compared to the MAP estimator, but it is still complicated because of matrix inversion in its expression. However, notice that when we assume that the covariance matrix is exponential as given in (4.1), the inverse of the covariance matrix is a tridiagonal matrix, i.e.,

$$
\mathbf{C_z}^{-1} = \frac{1}{1-\rho^2}
\begin{bmatrix}
1 & -\rho & 0 & \cdots & 0 \\
-\rho & 1+\rho^2 & \ddots & & \vdots \\
0 & \ddots & \ddots & & 0 \\
\vdots & & & 1+\rho^2 & -\rho \\
0 & \cdots & 0 & -\rho & 1
\end{bmatrix}
\tag{4.8}
$$

Then, the matrix **A** (matrix of the SMAP-efdc estimator) is the inverse of a tridiagonal matrix. Thus,

$$
\mathbf{A} = \left(1-\rho^2\right) \cdot
$$

$$
\begin{bmatrix}
\sigma_w^2 + 1 - \rho^2 & -\rho\sigma_w^2 & 0 & \cdots & 0 \\
-\rho\sigma_w^2 & \left(1+\rho^2\right)\sigma_w^2 + 1 - \rho^2 & \ddots & & \vdots \\
0 & \ddots & \ddots & & 0 \\
\vdots & & & \left(1+\rho^2\right)\sigma_w^2 + 1 - \rho^2 & -\rho\sigma_w^2 \\
0 & \cdots & 0 & -\rho\sigma_w^2 & \sigma_w^2 + 1 - \rho^2
\end{bmatrix}^{-1}
$$

$$
\tag{4.9}
$$

The need to find the inverse of tridiagonal matrices arises in many scientific and engineering applications and has been investigated for a few decades with an attempt to find a simple and explicit analytic expression for the inverse [62], [63]. For an NxN tridiagonal matrix **T** given by

63

$$T = \begin{bmatrix} a_1 & b_1 & 0 & \cdots & & 0 \\ c_1 & a_2 & b_2 & & & \vdots \\ 0 & c_2 & \ddots & \ddots & & 0 \\ \vdots & & \ddots & \ddots & & b_{N-1} \\ 0 & \cdots & 0 & & c_{N-1} & a_N \end{bmatrix},$$

(4.10)

the inverse of the matrix T is given by [64], [65]

$$\left(T^{-1}\right)_{ij} = \begin{cases} (-1)^{i+j} b_i \cdots b_{j-1} \theta_{i-1} \phi_{j+1} / \theta_N, & i \le j \\ (-1)^{i+j} c_j \cdots c_{i-1} \theta_{j-1} \phi_{i+1} / \theta_N, & i > j \end{cases},$$

(4.11)

where θ_i's and ϕ_i's verify the recurrence relation,

$$\theta_i = \begin{cases} 1, & i = 0 \\ a_1, & i = 1 \\ a_i \theta_{i-1} - b_i c_i \theta_{i-2}, & i = 2, \cdots, N \end{cases},$$

(4.12)

$$\phi_i = \begin{cases} 1, & i = N+1 \\ a_N, & i = N \\ a_i \phi_{i+1} - b_i c_i \phi_{i+2}, & i = 1, \cdots, N-1 \end{cases}.$$

(4.13)

Observe that $\theta_N = |T|$, the determinant of the matrix. The inverse of tridiagonal matrix can be computed in $N^2 + 7N - 7$ arithmetic operations [64], [65].

Using these results for our case, and noting that the matrix given in (4.9) is also symmetric, it follows that $b_1 = \cdots = b_{N-1} = c_1 = \cdots = c_{N-1} = b$, and the inverse formula will simplify to

$$\left(A^{-1}\right)_{ij} = \begin{cases} (-1)^{i+j} b^{j-i} \theta_{i-1} \phi_{j+1} / \theta_N, & i \le j \\ (-1)^{i+j} b^{i-j} \theta_{j-1} \phi_{i+1} / \theta_N, & i > j \end{cases}$$

(4.14)

where

$$\theta_i = \begin{cases} 1, & i = 0 \\ a_1, & i = 1 \\ a_i \theta_{i-1} - b^2 \theta_{i-2}, & i = 2, \cdots, N \end{cases}$$

$$\phi_i = \begin{cases} 1, & i = N+1 \\ a_N, & i = N \\ a_i \phi_{i+1} - b^2 \phi_{i+2}, & i = 1, \cdots, N-1 \end{cases} \qquad (4.15)$$

We conclude that, we may eliminate matrix inversion and thus **A** can be computed analytically, but this requires recursive calculations. This can be computationally expensive, especially for large N values. As a further simplification, we used series expansion of the matrix entries with respect to ρ, and took the first terms for an approximation. We realized that, only three diagonals are effective, especially when correlation is small and SNR is high. Because the others contain order of 4 or higher ρ and σ_w^2. Then, the final simplified matrix can be written as

$$\mathbf{A} = \begin{bmatrix} x_{0,1} & x_{1,1} & 0 & \cdots & & & 0 \\ x_{1,1} & x_{0,2} & x_{1,2} & & & & \vdots \\ 0 & x_{1,2} & \ddots & \ddots & & & \\ \vdots & & \ddots & \ddots & x_{1,2} & & 0 \\ & & & x_{1,2} & x_{0,2} & x_{1,1} \\ 0 & \cdots & & 0 & x_{1,1} & x_{0,1} \end{bmatrix} \qquad (4.16)$$

$$x_{0,1} = \frac{1}{\left(1+\sigma_w^2\right)} + \frac{\left(-\sigma_w^2\right)}{\left(1+\sigma_w^2\right)^3}\rho^2 + \frac{\left(-\sigma_w^2\right)}{\left(1+\sigma_w^2\right)^5}\rho^4$$

$$x_{0,2} = \frac{1}{\left(1+\sigma_w^2\right)} + \frac{3\left(-\sigma_w^2\right)}{\left(1+\sigma_w^2\right)^3}\rho^2 + \frac{3\left(-\sigma_w^2\right)}{\left(1+\sigma_w^2\right)^5}\rho^4$$

$$x_{1,1} = \frac{\sigma_w^2}{\left(1+\sigma_w^2\right)^2}\rho + \frac{\sigma_w^2\left(1-\sigma_w^2\right)}{\left(1+\sigma_w^2\right)^4}\rho^3 + \frac{\sigma_w^2\left(1-\sigma_w^2\right)^2}{\left(1+\sigma_w^2\right)^6}\rho^5$$

$$x_{1,2} = \frac{\sigma_w^2}{\left(1+\sigma_w^2\right)^2}\rho + \frac{\sigma_w^2\left(1-\sigma_w^2\right)}{\left(1+\sigma_w^2\right)^4}\rho^3 + \frac{2\sigma_w^2\left(1-\sigma_w^2\right)^2}{\left(1+\sigma_w^2\right)^6}\rho^5$$

$$(4.17)$$

Figure 4.13 shows the rms error (center tap) of the approximate SMAP-efdc estimator given in (4.16) and (4.17) for α=0.9, N=128 and SNR=10 dB, for an

exponential frequency domain correlation channel assuming that ρ and σ_w^2 are known exactly. The rms error of exact MAP estimator is drawn with solid lines for comparison. As seen from the figure, Approximate SMAP-efdc estimator gives highly accurate results for $0 \leq \rho \leq 0.95$. But, for higher correlation there is a notable degradation.
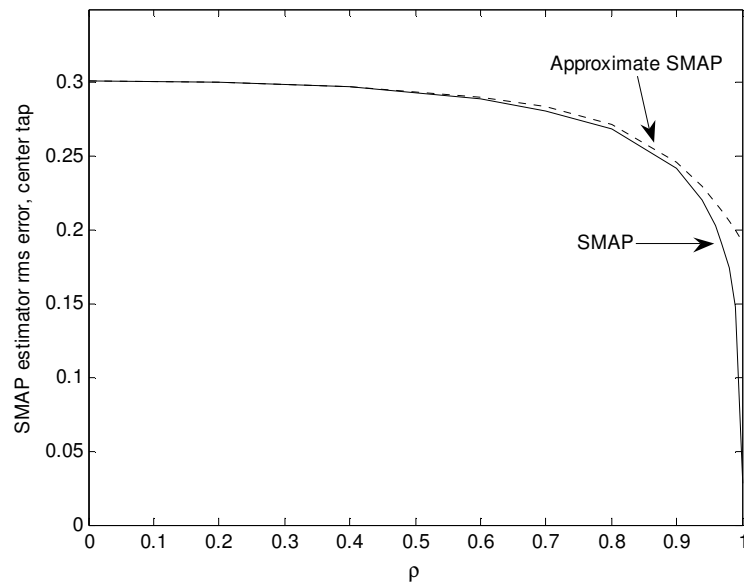
Figure 4.13 Approximate SMAP-efdc estimator rms error (center tap) versus subchannel correlation (ρ), N=128, SNR=10 dB, channel with exponential frequency domain correlation.

4.2 Exponential Power Delay Profile Assumption

4.2.1 Proposed Estimator (SMAP-epdp)

It is convenient to find the frequency response correlation from the power delay profile, which is the inverse Fourier transform of spaced frequency correlation function. Generally, in the literature a model is assigned to the power delay profile. Smulders' and exponential power delay profile models are the most common and realistic ones. For the Smulders' model, which is widely used for Rician channels, the power delay profile is [60], [61]

$$\Phi_z(\tau) = \begin{cases} 0, & \tau < 0 \\ \kappa^2 \delta(\tau), & \tau = 0 \\ \Pi, & 0 < \tau < \tau_1 \\ \Pi e^{-\gamma(\tau - \tau_1)}, & \tau \geq \tau_1 \end{cases} \tag{4.18}$$

where κ is the normalized power of the direct path (which is 0 for the Rayleigh channel), Π is the normalized power density of the constant level part, τ_1 is the duration of the constant level part and γ is the decay component of the decaying part. The Smulders' model power delay profile figure is given in Figure 4.14.

The spaced frequency correlation function is given by [60], [61]:

$$\Phi_z(\Delta f) = \kappa^2 + \Pi \left[\tau_1 \operatorname{sinc}(\tau_1 \Delta f) e^{j\pi\tau_1\Delta f} + \frac{e^{j2\pi\tau_1\Delta f}}{\gamma + j2\pi\Delta f} \right] \tag{4.19}$$

Generally $\tau_1 \approx 0$ is used in (4.18), which yields the exponential decaying power delay profile. As stated in the literature, exponentially decaying power delay profile is a good approximation for most practical channels.
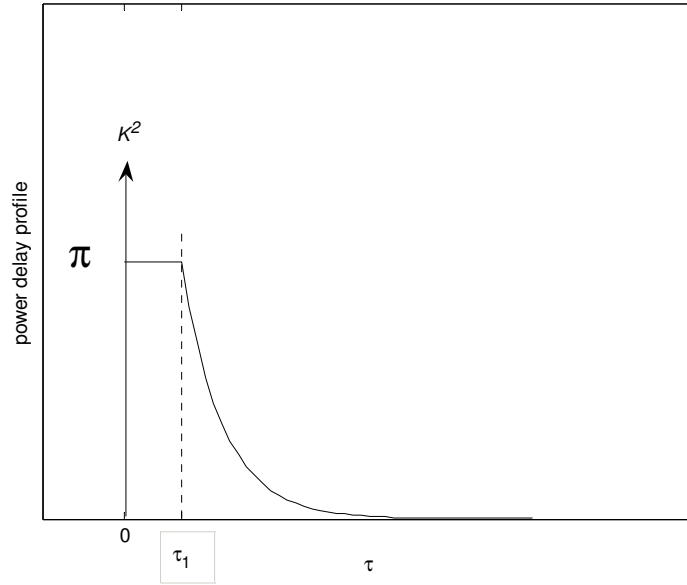
Figure 4.14 The Smulders' power delay profile model.

Then, for Rayleigh channel,

$$\Phi_z(\tau) = \frac{1}{\tau_{rms}} \exp\{-\tau/\tau_{rms}\} u(\tau) \tag{4.20}$$

where τ_{rms} is the absolute rms delay spread of the channel, and the spaced frequency correlation function for an OFDM system with N subcarrier is given by [62], [63]

$$\mathbf{C}_z(n,m) = \frac{1}{1 + j\,2\pi\tau_c(n-m)/N} . \tag{4.21}$$

where n, m are subchannel indices and $\tau_c = \tau_{rms}/T$ is the rms delay spread normalized to the duration T of the OFDM symbol. $\tau_c = \infty$ corresponds to perfect independent fading while $\tau_c = 0$ means flat fading. For the channel

68

$$z(\tau, t) = \sum_{i=1}^{L_p} a_i \delta(\tau - \tau_i), \tag{4.22}$$

where L_p is the total number of paths, a_i and τ_i are the complex amplitude and the delay of the ith path, respectively. Absolute rms delay spread can be calculated as [62]

$$\tau_{rms} = \sqrt{\frac{\sum_{i=1}^{L_p} (\tau_i - \bar{\tau})^2 |a_i|^2}{\sum_{i=1}^{L_p} |a_i|^2}} \quad \text{and} \quad \bar{\tau} = \frac{\sum_{i=1}^{L_p} \tau_i |a_i|^2}{\sum_{i=1}^{L_p} |a_i|^2} \tag{4.23}$$

For a channel with exponential power delay profile, Figure 4.15 shows the plot of frequency domain correlation of the center tap (n=512) with the other taps for N=1024 and τ_c=1, 5, and 50. As τ_c increases, subchannel correlation decreases.
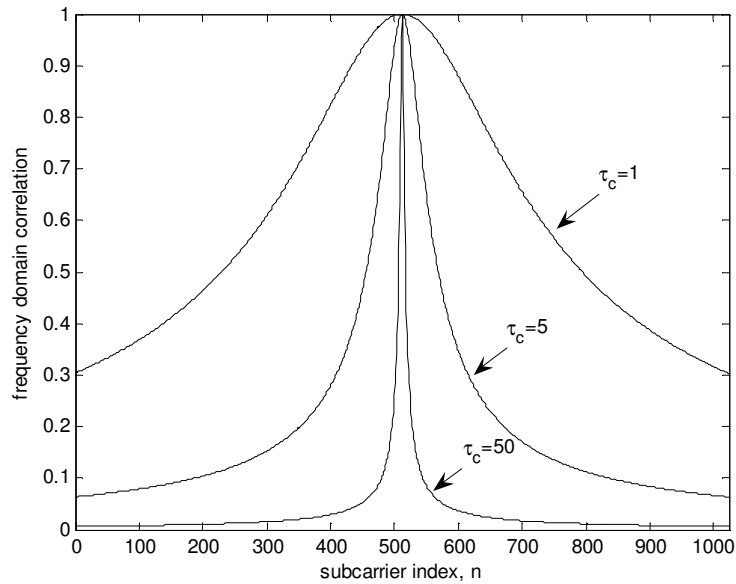
Figure 4.15 Frequency domain correlation of middle subchannel (n=512) with others, N=1024, channel with exponential power delay profile.

An approximation of (4.21) can be made when subchannels are almost independent. Thus, if $2\pi\tau_c(n-m)/N \gg 1$, then subchannel correlation is

$$C_z(n,m) \approx \frac{1}{j\,2\pi\tau_c(n-m)/N} . \tag{4.24}$$

Similarly, for highly correlated (nearly flat fading) channels τ_c is small. Thus, $\frac{2\pi\tau_c}{N} \ll 1$. Then $\left(\frac{2\pi\tau_c}{N}\right)^{(n-m)}$ is negligibly small for $(n\text{-}m)=2,3,\ldots,N\text{-}1$. The correlation function simplifies to

$$\mathbf{C}_z(n,m) \approx \frac{1}{\left(1 + j\,2\pi\tau_c/N\right)^{(n-m)}} . \tag{4.25}$$

Indeed, this is equivalent to the assumption that the channel frequency domain correlation is exponential, but the correlation coefficient is complex. i.e.,

$$\rho = \frac{1}{1 + j\,2\pi\tau_c/N} .$$

We propose the following simplified MAP (SMAP-epdp) estimator:

$$\hat{\mathbf{z}}_{\mathbf{SMAP}} = \mathbf{A}(\hat{\tau}_c)\cdot\mathbf{r} \quad \text{where} \quad \mathbf{A}(\hat{\tau}_c) = \mathbf{C}_z(\hat{\tau}_c)\left[\mathbf{C}_w + \mathbf{C}_z(\hat{\tau}_c)\right]^{-1} \tag{4.26}$$

where $\hat{\tau}_c$ is the estimated τ_c. Thus, once τ_c is estimated, it is fed to the MAP channel estimator. Accordingly, the block diagram of the estimator becomes the one shown in Figure 4.16.
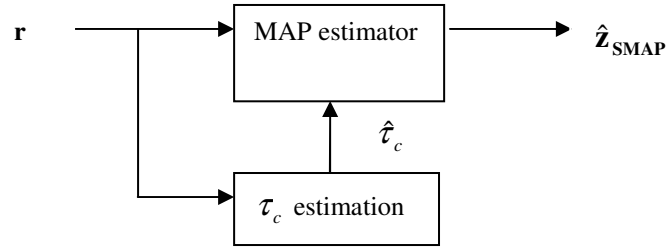
Figure 4.16 Block diagram of SMAP-epdp estimator

τ_c is estimated from the instantaneous channel frequency response correlation values. Details will be given in section 4.2.1.1. Since the detected values fluctuate from packet to packet (or OFDM symbols), they may not yield a good statistic, which may be a problem especially when the number of carriers is low. In addition, the use of detected values for correlating the received samples provides poor results when operating at low SNR values. Therefore, an alpha tracker [57] is used for averaging:

$$\hat{\tau}_c^i = \alpha \, \hat{\tau}_c^{i-1} + (1-\alpha) \, \hat{\tau}_{c,ins} \tag{4.27}$$

where $0 < \alpha < 1$ is the tracking parameter and i is the symbol number. The sensitivity of the alpha tracker can be increased, if the value of α is increased, by paying the price of increased tracking time which can be a problem in relatively fast fading channels.

4.2.1.1 Estimation of the Correlation Parameter

The sample covariance matrix (classical optimal ML estimation procedure) for independent samples is well known [66] to be

$$\hat{\mathbf{C}}_{\mathbf{z}} = \frac{1}{M} \sum_{i=1}^{M} \mathbf{r_i r_i^H} \ , \tag{4.28}$$

where $\mathbf{r_i} = \mathbf{z_i} + \mathbf{w_i}$ and M is the number of observations. Then, when we assume an unstructured covariance matrix, $\hat{\tau}_{c,ins}$ is obtained from the instantaneous channel frequency response correlation values, which are, in turn, found from the received instantaneous subchannel tap values. i.e.,

$$C_z(1,2) = \frac{r_1 \cdot r_2^* + r_2 \cdot r_3^* + \cdots + r_{N-1} \cdot r_N^*}{|r_2|^2 + |r_3|^2 + \cdots + |r_{N-1}|^2} \tag{4.29}$$

Then, $\hat{\tau}_{c,ins}$ can easily be found using (4.29) and (4.21).

The covariance matrix of a stationary signal is Hermitian and Toeplitz. However, the sample covariance matrix obtained from a finite number of observations seldom has this structure and to improve the precision it is necessary to make M as large as possible. However, in practice M cannot exceed a certain value because the observation time is limited. Further, the description of the samples as a set of independent random vector variables is an idealization and the question is whether it is possible to neglect this dependence, because when samples are dependent, the estimate (4.28) is no longer optimal. As it is shown in [66], the standard deviation of the estimate in this situation monotonically increases when the correlation coefficient between the samples becomes larger.

Estimating structured covariance matrices is of particular interest in a variety of applications [67-72]. Since the exact ML estimation of a Hermitian Toeplitz covariance matrix has no closed-form solution [71], the ML methods proposed in the literature are iterative and computationally involved, yet they are not guaranteed to yield the global optimal solution. This limits the interest in using the exact ML structured covariance matrix estimate in practical applications.

The exact ML estimate of τ_c is obtained by maximizing the likelihood function [73]:

$$\hat{\tau}_c = \arg \max_{\tau_c} L(\tau_c) \qquad (4.30)$$

where

$$\begin{aligned} L(\tau_c) &= \ln p(\mathbf{r}/\tau_c) \\ &= -\ln \pi^N - \ln \left| \mathbf{C}_{\mathbf{r}/\tau_c} \right| - \mathbf{r}\, \mathbf{C}_{\mathbf{r}/\tau_c}^{-1} \mathbf{r} \end{aligned} \qquad (4.31)$$

and $\mathbf{C}_{\mathbf{r}/\tau_c} = \mathbf{C}_\mathbf{z}(\tau_c) + \mathbf{C}_\mathbf{w}$. Then, we can find the ML estimate $\hat{\tau}_{c,ins}$ numerically, using (4.31).

If we impose no structure on the covariance matrix except for the Hermitian symmetry then it is known that the ML estimate is given by sample covariance matrix $\hat{\mathbf{C}}_\mathbf{z}$, whereas if we observe the structure of $\mathbf{C}_\mathbf{z}$ is implied by the parameterization of $\mathbf{C}_\mathbf{z}(\tau_c)$, the ML estimate of $\mathbf{C}_\mathbf{z}$ is given by $\mathbf{C}_\mathbf{z}(\hat{\tau}_c)$. Asymptotically, $\mathbf{C}_\mathbf{z}(\hat{\tau}_c)$ will have better accuracy than $\hat{\mathbf{C}}_\mathbf{z}$. However, solving for the ML solution for structured covariance matrix turns out to be very complicated because of the nonlinearity of the cost function.

Figure 4.17 gives simulation results of τ_c estimation, for comparison of structured and unstructured covariance matrix assumption, for $\tau_c = 10, 50$ and 100. An alpha-tracker is used with both methods. The initial value of $\hat{\tau}_c$ is set to the actual value for the iterations. Obviously, this is for clarity in the presentation. Actually, arbitrary initial values will be more realistic. As seen in the figure, structured matrix estimation method (solid line) finds τ_c nearly exactly, while unstructured matrix estimation (dotted line) overestimate τ_c, with an error about %12.
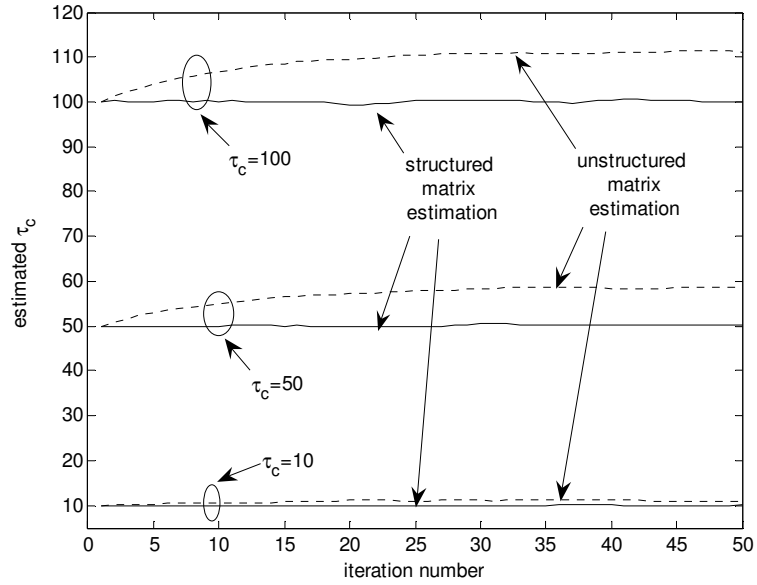
Figure 4.17 ML estimation of τ_c versus iteration number, with structured and unstructured matrix, $\tau_c = 10, 50$ and 100, SNR=10 dB, N=1024.

4.2.1.2 Estimation of Noise Variance

Noise variance is needed by the MAP estimator for optimal performance. Noise variance estimation for OFDM systems is a well investigated topic in the literature [74-77]. MMSE (minimum mean square error) and ML based noise variance estimators use channel estimates whereas moment based algorithms are blind, as well as many ad-hoc algorithms.

In section 4.2.2.2, it will be shown that the proposed SMAP estimator is quite insensitive to noise variance estimation errors. Therefore, in the rest of this report it is assumed that noise variance is estimated correctly. For the sake of completeness, below we give the MMSE estimation of noise variance and no further details are given related to this topic.

The MMSE estimation of noise variance σ_w^2, using the estimated channel coefficients, is given by [77],

$$\hat{\mathbf{C}}_{w,\mathbf{MMSE}} = (\mathbf{r} - \hat{\mathbf{z}})(\mathbf{r} - \hat{\mathbf{z}})^{\mathbf{H}}$$
$$\hat{\sigma}_{w,MMSE}^2 = \frac{1}{N}(\mathbf{r} - \hat{\mathbf{z}})^{\mathbf{H}}(\mathbf{r} - \hat{\mathbf{z}})$$

(4.32)

The graph of MMSE noise variance estimation for $N=1024$, $\tau_c = 10, 50$ and 100 and $\sigma_w^2 = 0.01, 0.1$ and 1 is given in Figure 4.18. The channel has an exponential power delay profile and τ_c is known. The initial value of $\hat{\sigma}_w^2$ is set to the actual value σ_w^2 for the iterations for the clarity in the presentation. As seen from the figure, (4.32) always underestimates the values. Estimation error increases as the noise variance decreases or as the channel correlation decreases, i.e. τ_c increases.
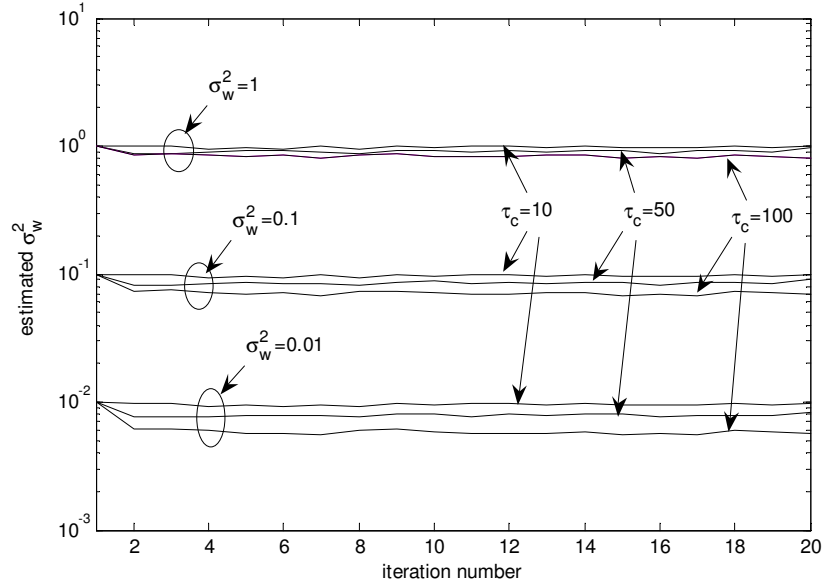
Figure 4.18 MMSE estimation of σ_w^2 ($\hat{\sigma}_w^2$) versus iteration number,
$\sigma_w^2 = 1, 0.1$ and 0.01, $\tau_c = 10, 50$ and 100, SNR=10 dB, $N=1024$.

4.2.2 Performance

4.2.2.1 MSE Performance

For a channel with exponential power delay profile, it is assumed that σ_w^2 and τ_c are known. Then, the MSE in (3.34) becomes:

$$\begin{aligned} \mathbf{MSE} &= \mathbf{A}(\tau_c)\mathbf{C_w}\mathbf{A^H}(\tau_c)+[\mathbf{A}(\tau_c)-\mathbf{I}]\mathbf{C_z}(\tau_c)[\mathbf{A}(\tau_c)-\mathbf{I}]^{\mathbf{H}} \\ &= \sigma_w^2\mathbf{A}(\tau_c) \end{aligned}. \qquad (4.33)$$

Figure 4.19 shows the graph of the MAP estimator rms error (square root of error variances) versus τ_c, for N=1024 and SNR=10 dB ($\text{SNR} = 10 \log_{10}\left(\sigma_z^2 / \sigma_w^2\right)$), assuming the channel is exponential and τ_c is exactly known. As seen from the figure, the rms error gets larger as the correlation of the channel decreases (τ_c increases). It should be noted that, the outer curves are for the edge subchannels (n=0 and n=N-1) estimation errors, the inner ones are for middle subchannels (n=N/2), and the others are for the remaining. The subchannels at the edges have largest error variances, while the variances of center subchannels are the smallest, as expected. The error variances of subchannels in between decrease as the subchannels get closer to the center.

Next, we have investigated the effect of SNR on the rms error. The graph of the rms error of the center tap versus τ_c for SNR=0, 10 and 20 dB (N=1024), for exponential power delay profile channels with known τ_c is given in Figure 4.20.
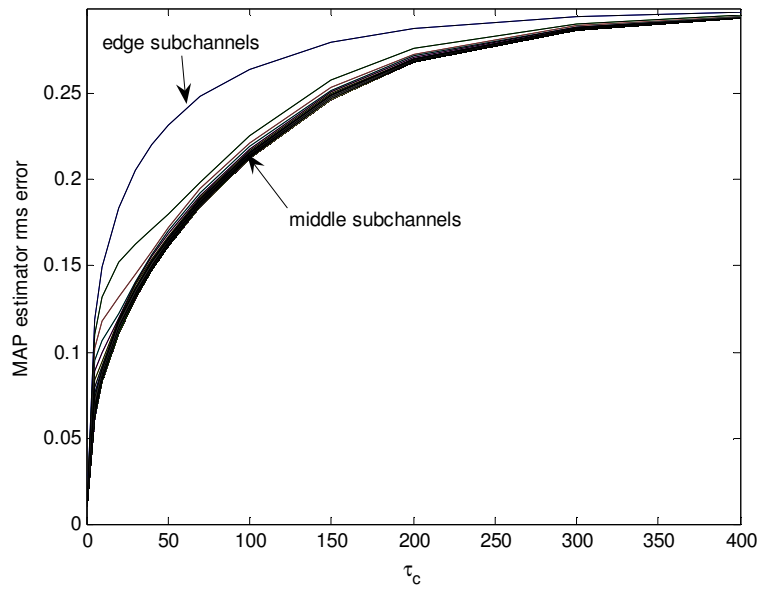
Figure 4.19 Channel MAP estimate rms error versus τ_c, SNR=10 dB, N=1024, channel with exponential power delay profile.
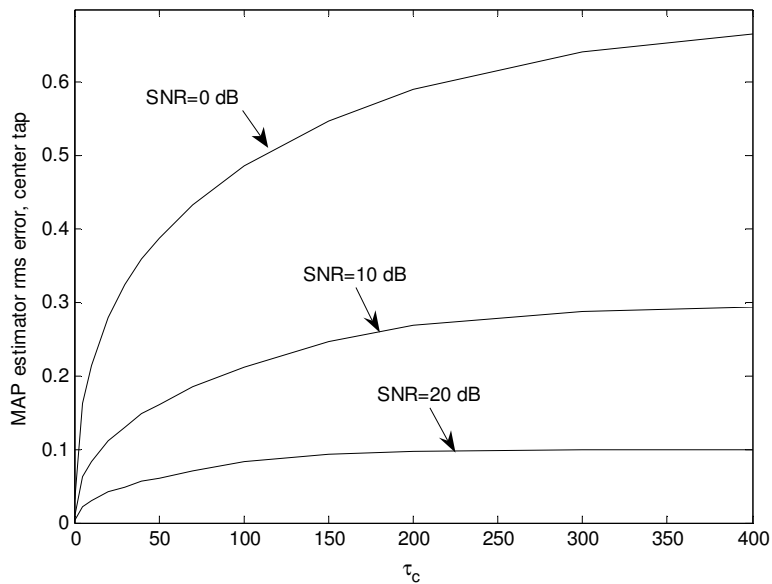
Figure 4.20 Channel MAP estimate rms error (center tap) versus τ_c, SNR=0, 10 and 20 dB, N=1024, channel with exponential power delay profile.

In Figure 4.21, for exponential power delay profile channels with known τ_c we provide the graph of rms error of the center tap as a function of N, the number of subchannels (SNR=10 dB). The results are consistent with the expressions given in (3.38) and (3.39). Thus, the rms error for independent fading does not depend on N, while for highly or fully correlated case, the error decreases as N increases, yielding very significant advantages for practical OFDM systems.
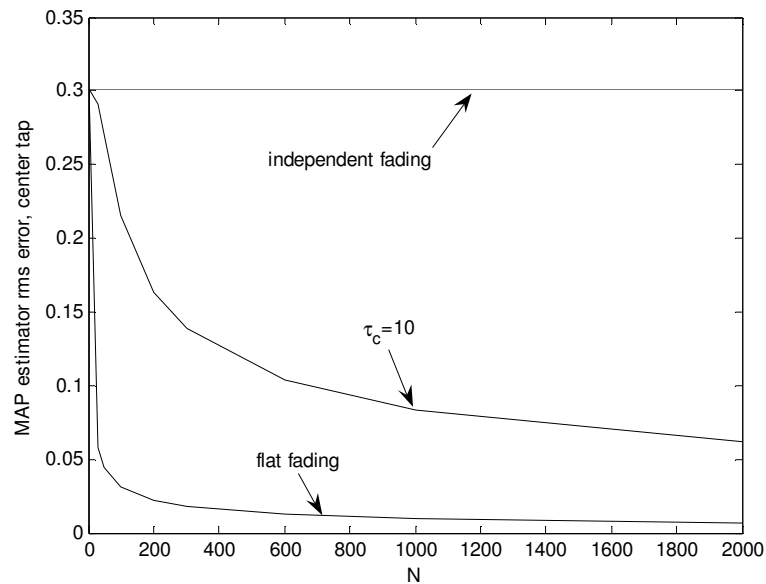
Figure 4.21 Channel MAP estimate rms error (center tap) versus number of subcarriers (*N*), SNR=10 dB, channel with exponential power delay profile.

4.2.2.2 Sensitivity Analysis

The MSE of SMAP-epdp estimator (for exponential power delay profile channels with τ_c is estimated and σ_w^2 is known) is given by:

$$\mathbf{MSE} = \mathbf{A}(\hat{\tau}_c)\mathbf{C_w}\mathbf{A^H}(\hat{\tau}_c) + [\mathbf{A}(\hat{\tau}_c) - \mathbf{I}]\mathbf{C_z}[\mathbf{A}(\hat{\tau}_c) - \mathbf{I}]^{\mathbf{H}}. \tag{4.34}$$

Figure 4.22 - Figure 4.24 give the graphs of rms error of SMAP-epdp estimator versus $\hat{\tau}_c$, for N=1024, SNR=10, 20 dB, and $\tau_c = 10, 50$ and 100, respectively. As seen, the proposed estimator is not much sensitive to the estimation errors in $\hat{\tau}_c$, especially if the error occurs as an over-estimation. Therefore, we conclude that there is no need to estimate τ_c exactly, e.g., by structured matrix estimation by paying the price of high complexity.
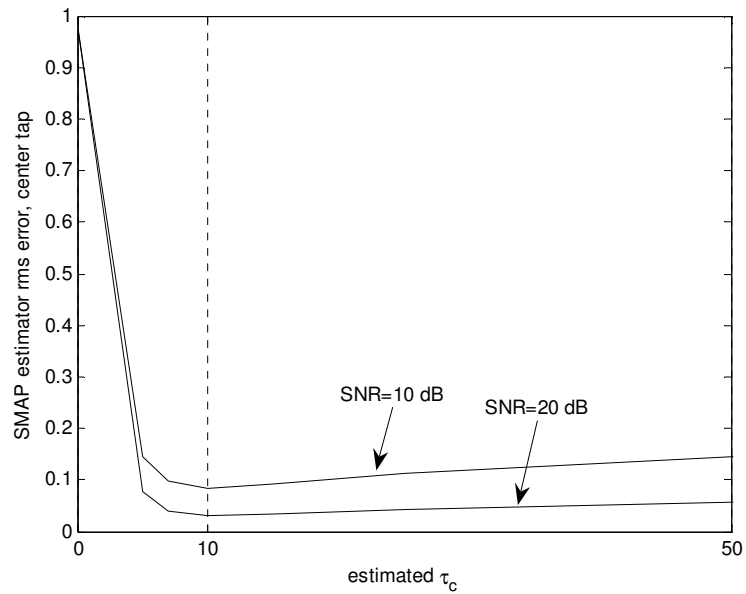
Figure 4.22 SMAP-epdp estimator rms error (center tap) versus estimated τ_c ($\hat{\tau}_c$), $\tau_c = 10$, N=1024, SNR=10 and 20 dB.
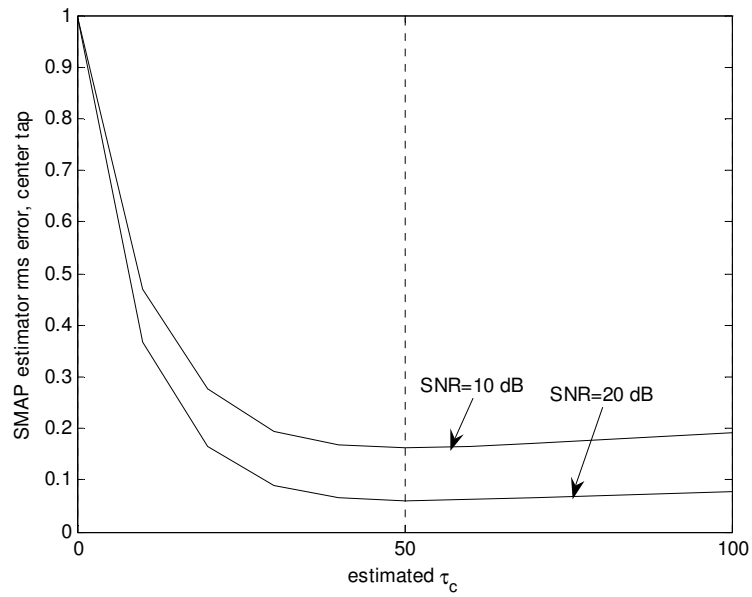
Figure 4.23 SMAP-epdp estimator rms error (center tap) versus estimated τ_c ($\hat{\tau}_c$), $\tau_c = 50$, N=1024, SNR=10 and 20 dB.
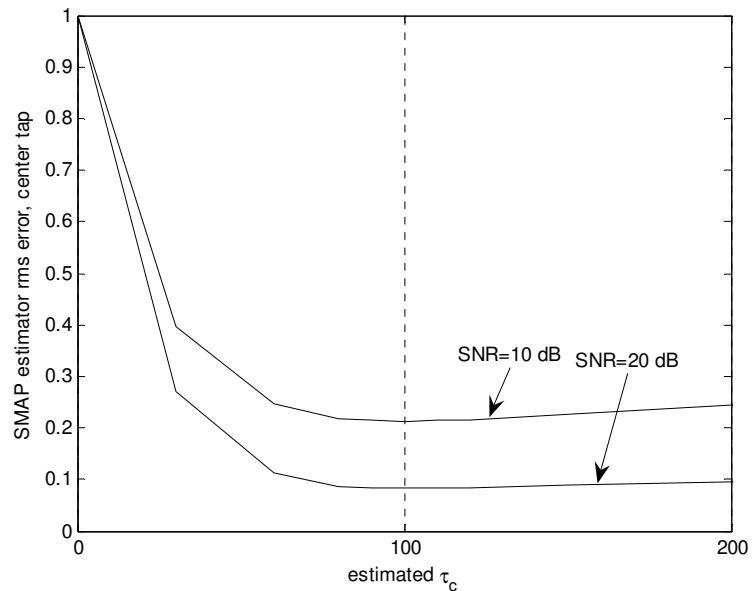
Figure 4.24 SMAP-epdp estimator rms error (center tap) versus estimated τ_c ($\hat{\tau}_c$), $\tau_c = 100$, N=1024, SNR=10 and 20 dB.

For exponential power delay profile channels with known τ_c, but σ_w^2 is estimated, the MSE of SMAP-epdp estimator is:

$$\mathbf{MSE} = \mathbf{A}(\hat{\sigma}_w^2)\mathbf{C_w}\mathbf{A^H}(\hat{\sigma}_w^2) + [\mathbf{A}(\hat{\sigma}_w^2) - \mathbf{I}]\mathbf{C_z}[\mathbf{A}(\hat{\sigma}_w^2) - \mathbf{I}]^{\mathbf{H}}. \tag{4.35}$$

Figure 4.25, Figure 4.26 and Figure 4.27 give the graphs of rms error of SMAP-epdp estimator versus $\hat{\sigma}_w^2$, for N=1024, SNR=0,10 and 20 dB, and $\tau_c = 10, 50$ and 100, respectively. As seen from the figures, the proposed SMAP-epdp estimator is rather insensitive to the errors in $\hat{\sigma}_w^2$, especially when SNR is high and/or channel is highly correlated. Rms error increases dramatically if noise variance is fairly overestimated.
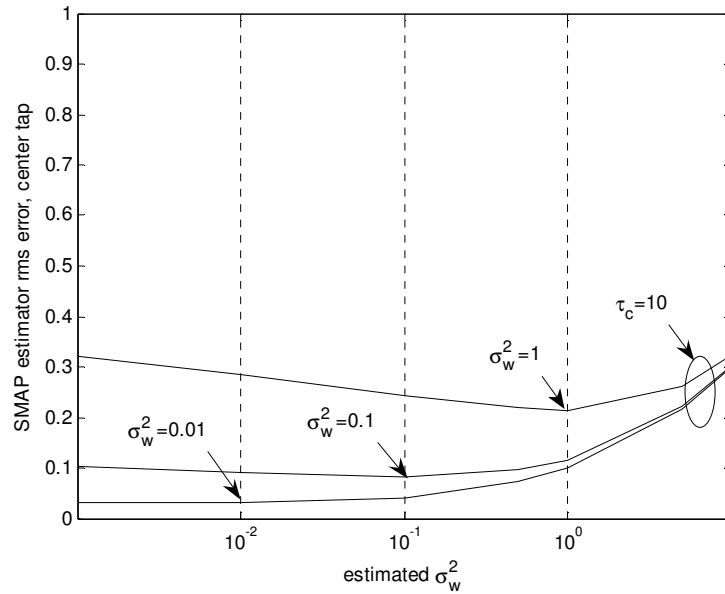
Figure 4.25 SMAP-epdp estimator rms error (center tap) versus estimated noise variance ($\hat{\sigma}_w^2$), $\tau_c = 10$, N=1024, SNR=0, 10 and 20 dB.
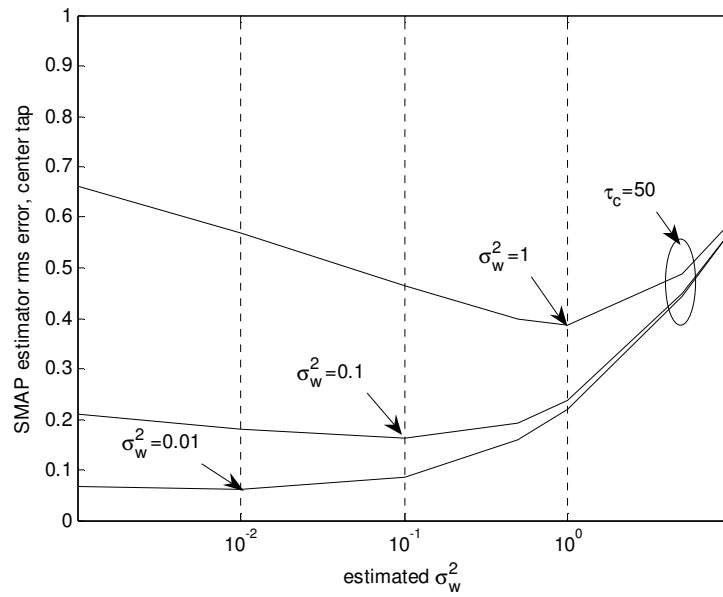
Figure 4.26 SMAP-epdp estimator rms error (center tap) versus estimated noise variance ($\hat{\sigma}_w^2$), $\tau_c = 50$, N=1024, SNR=0, 10 and 20 dB.
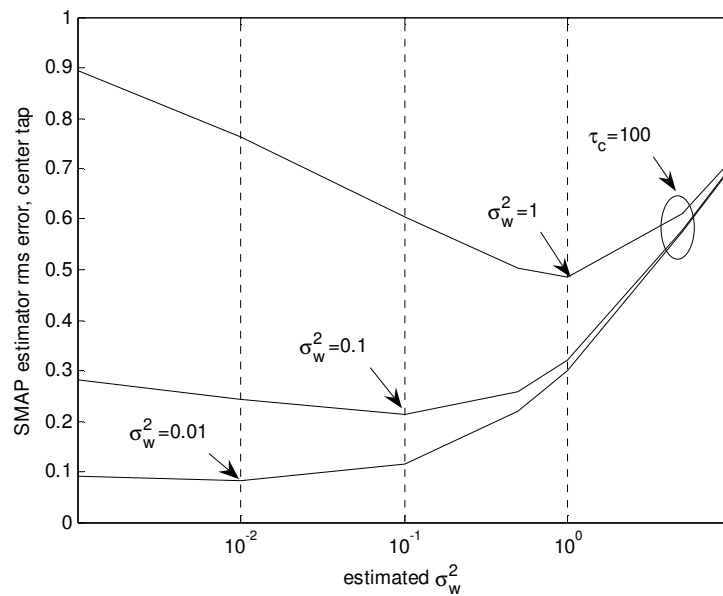
Figure 4.27 SMAP-epdp estimator rms error (center tap) versus estimated noise variance ($\hat{\sigma}_w^2$), $\tau_c = 100$, N=1024, SNR=0, 10 and 20 dB.

In order to investigate the sensitivity of SMAP-epdp to rms delay spread and noise variance estimation errors together, we analyze MSE of SMAP-epdp estimator when both τ_c and σ_w^2 are estimated. Thus,

$$\mathbf{MSE} = \mathbf{A}(\hat{\tau}_c, \hat{\sigma}_w^2)\mathbf{C_w}\mathbf{A^H}(\hat{\tau}_c, \hat{\sigma}_w^2) + \left[\mathbf{A}(\hat{\tau}_c, \hat{\sigma}_w^2) - \mathbf{I}\right]\mathbf{C_z}\left[\mathbf{A}(\hat{\tau}_c, \hat{\sigma}_w^2) - \mathbf{I}\right]^{\mathbf{H}}. \quad (4.36)$$

Figure 4.28, Figure 4.29 and Figure 4.30 give the graphs of rms error of SMAP-epdp estimator versus $\hat{\sigma}_w^2$ and $\hat{\tau}_c$, for SNR=10dB, and $\tau_c = 10, 50$ and 100, respectively.
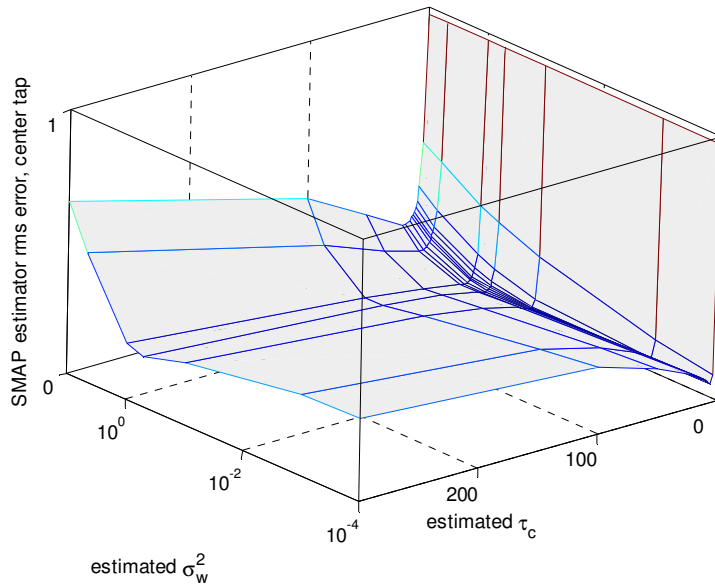
Figure 4.28 SMAP-epdp estimator rms error (center tap) versus estimated noise variance ($\hat{\sigma}_w^2$) and estimated τ_c ($\hat{\tau}_c$), $\tau_c = 10$, $\sigma_w^2 = 0.1$, N=1024.
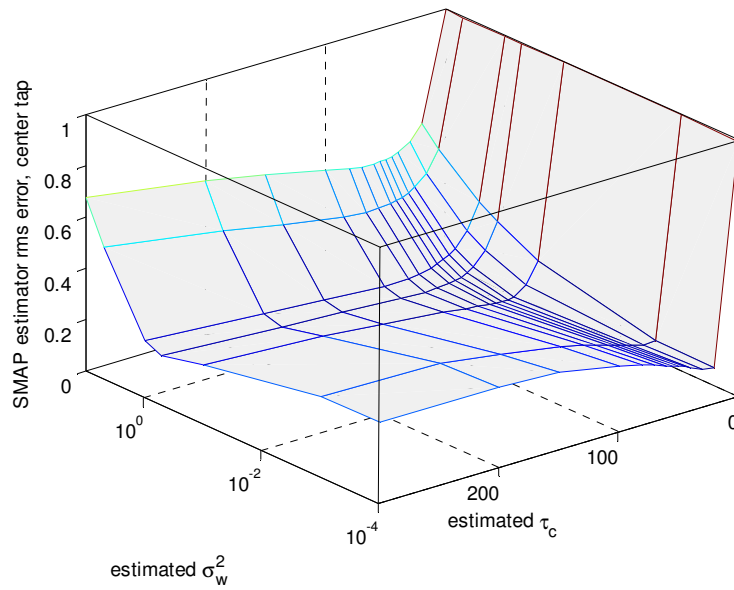
Figure 4.29 SMAP-epdp estimator rms error (center tap) versus estimated noise variance ($\hat{\sigma}_w^2$) and estimated τ_c ($\hat{\tau}_c$), $\tau_c = 50$, $\sigma_w^2 = 0.1$, N=1024.
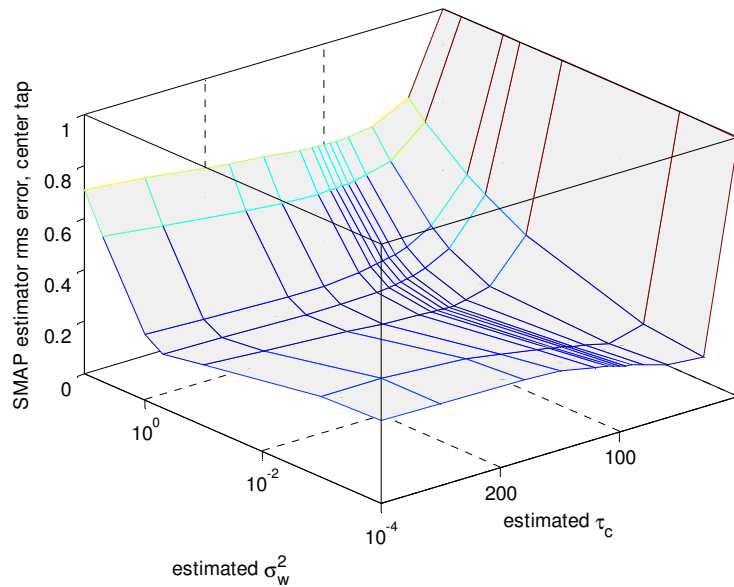
Figure 4.30 SMAP-epdp estimator rms error (center tap) versus estimated noise variance ($\hat{\sigma}_w^2$) and estimated τ_c ($\hat{\tau}_c$), $\tau_c = 100$, $\sigma_w^2 = 0.1$, N=1024.

4.2.2.3 Time Varying Channel Tracking

In this section, the performance of SMAP-epdp estimator under time varying channel conditions, i.e., τ_c is changing [2], is investigated. When we say τ_c is changing, this may be possible for a mobile receiver in rapidly changing environment. For example, for a car traveling from a crowded city to outside, to the rural area (e.g. from bad urban to rural area) τ_c will change. In such a situation τ_c is expected to change slightly.

The simulation result for the channel where initially $\tau_c = 10$, then $\tau_c = 50$ and finally $\tau_c = 100$, for N=1024, SNR=10 dB and α=0.9 is given in Figure 4.31. Indeed τ_c will change slightly in a real case, but in the simulations the difference between τ_c's are selected quite large to test the estimator performance. As seen from the figure, SMAP-epdp estimator can follow the variation in τ_c if there is enough time for iterations. The time needed for reaching the new value depends on the difference in τ_c value and selected α value.

---

[2] Note that, this is somehow different than the known time varying channel, i.e., τ_c is almost constant but the channel impulse response is varying by time. Channel impulse response changes when the receiver is stationary but environment (traffic, weather etc.) is varying. Another possible scenario is that the receiver is mobile, but its motion is in a range that the channel structure does not change so much, thus τ_c is stable (i.e., a car travelling in a rural area).
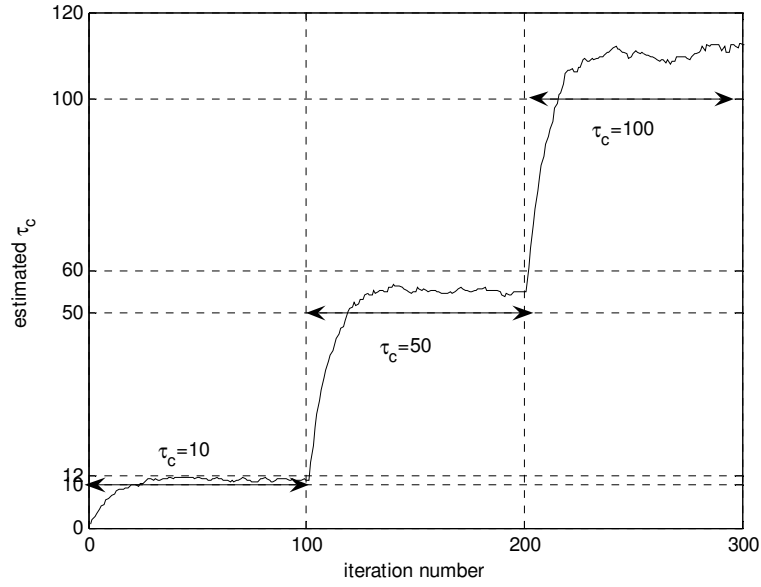
Figure 4.31 Estimated τ_c ($\hat{\tau}_c$) versus iteration number, SMAP-epdp estimator, N=1024, SNR=10 dB, τ_c varying channel ($\tau_c = 10$, 50 and 100).

4.2.3 Approximate SMAP-epdp

The proposed SMAP-epdp estimator has a reduced complexity compared to the conventional MAP estimator. However, since it involves a matrix inversion, the implementation is still complicated. Therefore, we have developed further approximations to avoid inversion.

Using Taylor series expansion of matrix $\mathbf{A}(\hat{\tau}_c)$,

$$\mathbf{A}(\hat{\tau}_c) = \sum_{k=0}^{\infty} \frac{\mathbf{A}^{(k)}(\tau_0)}{k!}(\hat{\tau}_c - \tau_0)^k \tag{4.37}$$

where τ_0 is the center point of the Taylor series, $k!$ is the factorial of k and $\mathbf{A}^{(k)}(\tau_0)$ denotes the kth derivative of $\mathbf{A}$ at the point τ_0, we obtain the Approximate SMAP-epdp estimator equation below:

$$\hat{\mathbf{z}}_{\mathbf{SMAP}} = \left[\mathbf{A}(\tau_0) + \mathbf{A}^{(1)}(\tau_0)(\hat{\tau}_c - \tau_0) + \mathbf{A}^{(2)}(\tau_0)\frac{(\hat{\tau}_c - \tau_0)^2}{2} + \cdots \right] \cdot \mathbf{r} \qquad (4.38)$$

Thus, we have expressions that can be implemented with only a limited number of computations, without the need for matrix inversion.

As another approach, recalling that SMAP-epdp estimator is not much sensitive to estimation errors in τ_c, we suggest to keep an array of matrices for a set of τ_c values and update the matrix $\mathbf{A}$ as τ_c changes significantly only. Then, we obtain the approximate estimator formula below:

$$\hat{\mathbf{z}}_{\mathbf{SMAP}} = \mathbf{A}(\tau_0) \cdot \mathbf{r}, \qquad (4.39)$$

where τ_0 is the selected value which is the closest to the estimated τ_c. The set of τ_0 is selected noticing that SMAP-epdp estimator is tolerable to approximately 20% underestimation and 50% overestimation in τ_c estimation. Accordingly, the set we use is:

$$\tau_0 = \begin{bmatrix} 1 & 3 & 5 & 7 & 10 & 15 & 20 & 30 & 45 & 70 & 100 \end{bmatrix}. \qquad (4.40)$$

Note that the upper limit can be changed according to the channel that the Approximate SMAP-epdp estimator will operate, or the set elements can be selected more frequently for finer performance, which will increase the memory used.

In Figure 4.32 and Figure 4.33, for exponential power delay profile channels with $\tau_c = 12$ and $\tau_c = 50$, the histograms of τ_0 selection with 1000 samples are given for several SNR values, respectively (N=1024). As seen from the figure, for low

SNRs, overestimation is more probable, therefore higher values of τ_0 are selected. As SNR increases, the estimation gets closer to the real value of τ_c, but still slightly overestimation is observed. Thus, selecting $\tau_0 = 15$ is more probable compared to selecting $\tau_0 = 10$ for $\tau_c = 12$. For a channel with $\tau_c = 50$ channel, although overestimation occurs, since it is closer, $\tau_0 = 45$ is selected.
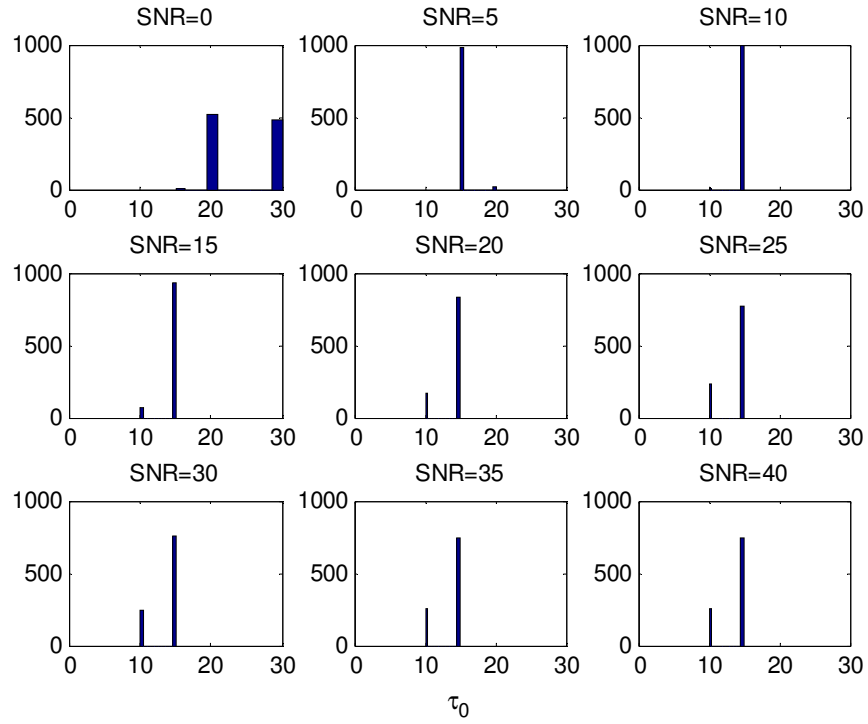
Figure 4.32 Histogram of τ_0 selection, Approximate SMAP-epdp estimator, channel with exponential power delay profile, $\tau_c = 12$, N=1024.
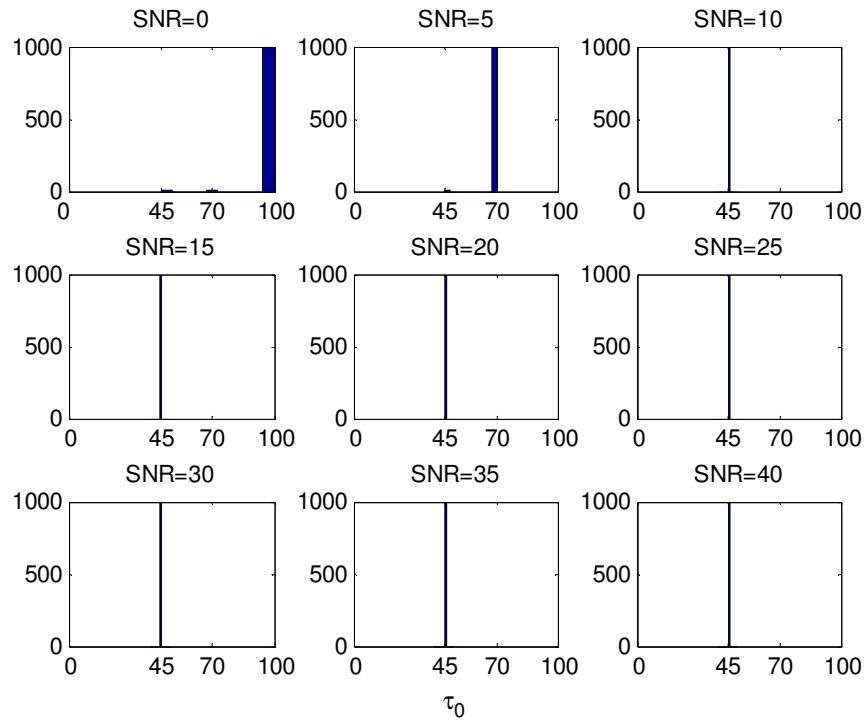
Figure 4.33 Histogram of τ_0 selection, Approximate SMAP-epdp estimator, channel with exponential power delay profile, τ_c=50, N=1024.

4.2.4 Computational Complexity

It is useful to compare the complexity of the proposed algorithm with existing estimators. As the ML estimator performance is not comparable to MAP based estimators, it is more relevant to make a comparison with respect to the exact MAP estimator.

The computational complexity of the channel estimators can be anticipated by the total number of multiplications required in a symbol time.

- The MAP estimator requires approximately $O(N^3+N^2+N^2)$ multiplications. (First terms are for the MAP estimator, the third one is for covariance matrix estimation.)

- The proposed SMAP-epdp estimator needs $O(N^3+N^2+N)$ multiplication. Since we still take the inverse of the matrix, the first term is the same.

- For both of the Approximate SMAP-epdp, $O(N^2+N)$ operation is needed.

CHAPTER 5

SIMULATION RESULTS

In this chapter, we evaluate the performance of the estimators using computer simulations. In order that the simulations are as realistic as possible, we use the DVB-T standards [78] as our guideline and use the COST 207 [41] and DVB-T channel models, which are widely accepted as good models in the community.

5.1 DVB-T Standards [78]

According to the DVB-T standard, the transmitted signal is organized in frames, which consist of 68 OFDM symbols. Each symbol is constituted by a set of carriers and transmitted with a duration composed of two parts, a data part and a guard interval. All symbols contain data and reference information. Since the OFDM signal comprises many separately modulated carriers, each symbol can in turn be considered to be divided into cells, each corresponding to the modulation carried on one carrier during one symbol.

The numerical values for the OFDM parameters for the 2k mode are given in Table 5.1 for 8 MHz channels. The values for the various time related parameters are given in multiples of the elementary period and in microseconds.

Table 5.1 Numerical values of the OFDM parameters for DVB-T 2k mode.

Number of active carriers	K	1705
Value of carrier number	$[K_{min}, K_{max}]$	[0,1705]
Number of data carriers	K_d	1512
Elementary period	T	7/64 µs
Symbol period	$T_s=N.T$	224 µs
Carrier spacing	$1/T_s$	4464 Hz
Spacing between carriers K_{min} and K_{max}	$(K-1)/T_s$	7,61 MHz

5.2 Channel Models

5.2.1 DVB-T Channels

We have chosen two different multipath channels taken from the literature for the simulations. The first channel model is a 30-path multipath Rayleigh model, which is noted to be suitable for wireless systems operating at the outdoor dispersive environment [17]. The second channel has 20 path, and is taken from ETSI EN 300 744 final draft document [78].

Model parameters delay τ_i (µs), amplitude ρ_i and phase θ_i (rad) are listed in Table 5.2.

Table 5.2 Parameters of DVB-T channels, 20 and 30-path models.

Path no	Channel 1			Channel 2		
	Delay (μs)	**Amp-litude**	**Phase** (rad)	**Delay** (μs)	**Amp-litude**	**Phase** (rad)
1	0.0120	0.4213	5.9010	1,003019	0,057662	4,855121
2	0.2892	0.1543	0.2147	5,422091	0,176809	3,419109
3	0.5593	0.4401	3.9968	0,518650	0,407163	5,864470
4	0.6919	0.4380	4.6862	2,751772	0,303585	2,215894
5	1.0266	0.1864	4.4331	0,602895	0,258782	3,758058
6	1.2347	0.0669	1.1484	1,016585	0,061831	5,430202
7	1.3056	0.0809	4.0282	0,143556	0,150340	3,952093
8	1.9643	0.1647	3.3214	0,153832	0,051534	1,093586
9	2.0906	0.1503	4.0649	3,324866	0,185074	5,775198
10	2.3076	0.1714	3.8432	1,935570	0,400967	0,154459
11	2.3907	0.1289	2.8815	0,429948	0,295723	5,928383
12	2.8962	0.2123	2.8152	3,228872	0,350825	3,053023
13	3.7334	0.3531	5.0859	0,848831	0,262909	0,628578
14	3.7415	0.0982	6.2326	0,073883	0,225894	2,128544
15	3.7630	0.0808	0.7662	0,203952	0,170996	1,099463
16	4.0452	0.1157	5.6671	0,194207	0,149723	3,462951
17	5.4348	0.2199	2.3719	0,924450	0,240140	3,664773
18	5.5246	0.2016	6.0266	1,381320	0,116587	2,833799
19	5.9653	0.1228	5.1854	0,640512	0,221155	3,334290
20	6.6460	0.2004	1.1537	1,368671	0,259730	0,393889
21	6.8295	0.2102	1.3142			
22	7.5086	0.2630	4.4436			
23	7.9602	0.1199	6.0964			
24	8.2400	0.3210	5.0876			
25	8.8824	0.1907	1.4835			
26	9.7827	0.2379	4.7438			
27	10.1142	0.1800	0.1396			
28	11.1587	0.2539	1.8221			
29	17.6513	0.2767	1.7052			
30	18.3765	0.1208	5.3582			

The following time invariant multipath model was employed for the channel impulse response:

$$z(\tau) = \sum_{i=1}^{L_p} a_i \delta(\tau - \tau_i) \quad \text{and} \quad a_i = \rho_i e^{j\theta_i}, \tag{5.1}$$

where ρ_i and θ_i are the amplitude and phase of the path associated with the delay τ_i and L_p is the number of paths. The random variables a_i's are zero mean complex valued Gaussian and are mutually independent. The actual amplitudes and phases are determined from the samples taken from the amplitude and the phase spectra of the dispersive channel,

$$\begin{array}{l} \alpha_k = |Z(k/NT)| \\ \phi_k = \arg(Z(k/NT)) \end{array} \quad \text{where} \quad Z(f) = \sum_{i=1}^{L_p} a_i e^{-j2\pi f \tau_i} \quad . \tag{5.2}$$

Figure 5.1 depicts amplitude and phase response of DVB-T channels, for $N=2048$, $T_s=224$ µs.
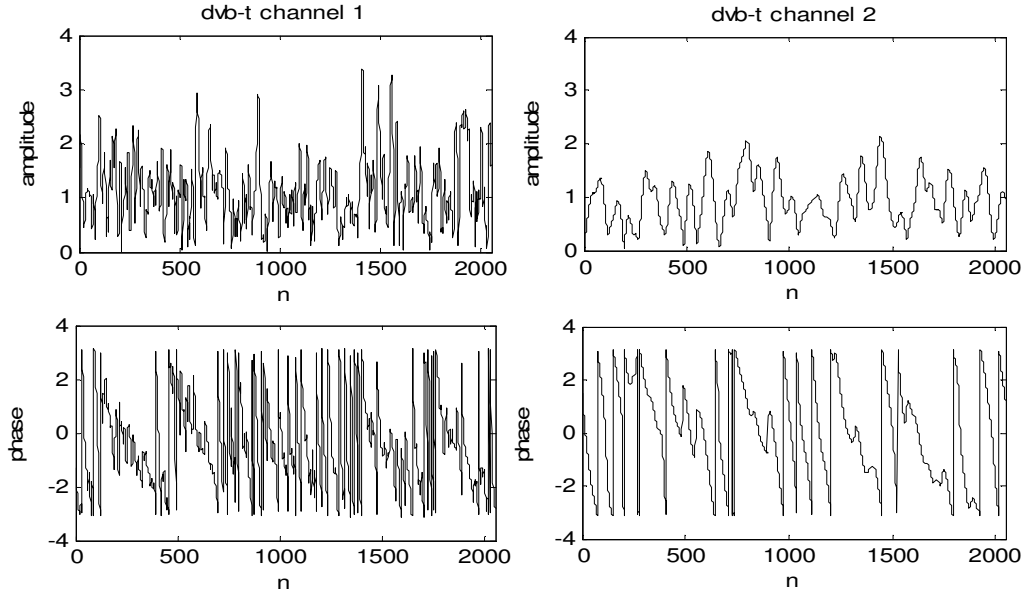
Figure 5.1 Amplitude and phase response of DVB-T channels versus subcarrier index (n), $N=2048$.

94

5.2.2 COST 207 Channels

Specifications of the sample multipath channel models according to COST 207 for the four propagation areas, namely rural area, typical urban, bad urban and hilly terrain are given in Table 5.3 - Table 5.6, respectively [41].

Note that in the tables, alternative 6-path channel models as well as more complex, but therefore more exact, 12-path channel models have been presented.

Table 5.3 Parameters of COST 207 Rural Area channels, 4 and 6-path models.

Path no	Channel 1		Channel 2	
	Delay (μs)	Power	Delay (μs)	Power
1	0	1	0	1
2	0.2	0.63	0.1	0.4
3	0.4	0.1	0.2	0.16
4	0.6	0.01	0.3	0.06
5			0.4	0.03
6			0.5	0.01

Table 5.4 Parameters of COST 207 Typical Urban channels, 6 and 12-path models.

Path no	Channel 1		Channel 2		Channel 3		Channel 4	
	Delay (μs)	Power	Delay (μs)	Power	Delay (μs)	Power	Delay (μs)	Power
1	0	0.5	0	0.5	0	0.4	0	0.4
2	0.2	1	0.2	1	0.2	0.5	0.1	0.5

3	0.6	0.63	0.5	0.63	0.4	1	0.3	1
4	1.6	0.25	1.6	0.25	0.6	0.63	0.5	0.55
5	2.4	0.16	2.3	0.16	0.8	0.5	0.8	0.5
6	5	0.1	5	0.1	1.2	0.32	1.1	0.32
7					1.4	0.2	1.3	0.2
8					1.8	0.32	1.7	0.32
9					2.4	0.25	2.3	0.22
10					3	0.13	3.1	0.14
11					3.2	0.08	3.2	0.08
12					5	0.1	5	0.1

Table 5.5 Parameters of COST 207 Bad Urban channels, 6 and 12-path models.

Path no	**Channel 1**		**Channel 2**		**Channel 3**		**Channel 4**	
	Delay (µs)	**Power**	**Delay (µs)**	**Power**	**Delay (µs)**	**Power**	**Delay (µs)**	**Power**
1	0	0.5	0	0.56	0	0.2	0	0.17
2	0.4	1	0.3	1	0.2	0.5	0.1	0.46
3	1	0.5	1	0.5	0.4	0.79	0.3	0.74
4	1.6	0.32	1.6	0.32	0.8	1	0.7	1
5	5	0.63	5	0.63	1.6	0.63	1.6	0.59
6	6.6	0.4	6.6	0.4	2.2	0.25	2.2	0.28
7					3.2	0.5	3.1	0.18
8					5	0.79	5	0.72
9					6	0.63	6	0.69
10					7.2	0.2	7.2	0.21
11					8.2	0.1	8.1	0.1
12					10	0.03	10	0.03

Table 5.6 Parameters of COST 207 Hilly Terrain channels, 6 and 12-path models.

Path no	Channel 1		Channel 2		Channel 3		Channel 4	
	Delay (μs)	Power	Delay (μs)	Power	Delay (μs)	Power	Delay (μs)	Power
1	0	1	0	1	0	0.1	0	0.1
2	0.2	0.63	0.1	0.71	0.2	0.16	0.1	0.16
3	0.4	0.4	0.3	0.35	0.4	0.25	0.3	0.25
4	0.6	0.2	0.5	0.18	0.6	0.4	0.5	0.4
5	15	0.25	15	0.16	0.8	1	0.7	1
6	17.2	0.06	17.2	0.02	2	1	1	1
7					2.4	0.4	1.3	0.4
8					15	0.16	15	0.16
9					15.2	0.13	15.2	0.13
10					15.8	0.1	15.7	0.1
11					17.2	0.06	17.2	0.06
12					20	0.04	20	0.04

Multipath characteristic (channel amplitude and phase response as explained in (5.2)) of COST 207 channels are shown in Figure 5.2 - Figure 5.8, for N=2048 and T_s=224 μs. An arbitrary instance of the stochastic model is generated using a computer program to make the plots. Phase is uniformly distributed in the interval $[0,2\pi)$. As seen, frequency selectivity increases as we go from rural area to hilly terrain. A typical rural area channel is very close to a flat fading channel, while a hilly terrain channel is closer to a channel with a noisy correlation. i.e., a correlated channel is multiplied with an independent fading channel. This is because of the separately placed two exponential in the power delay profile.
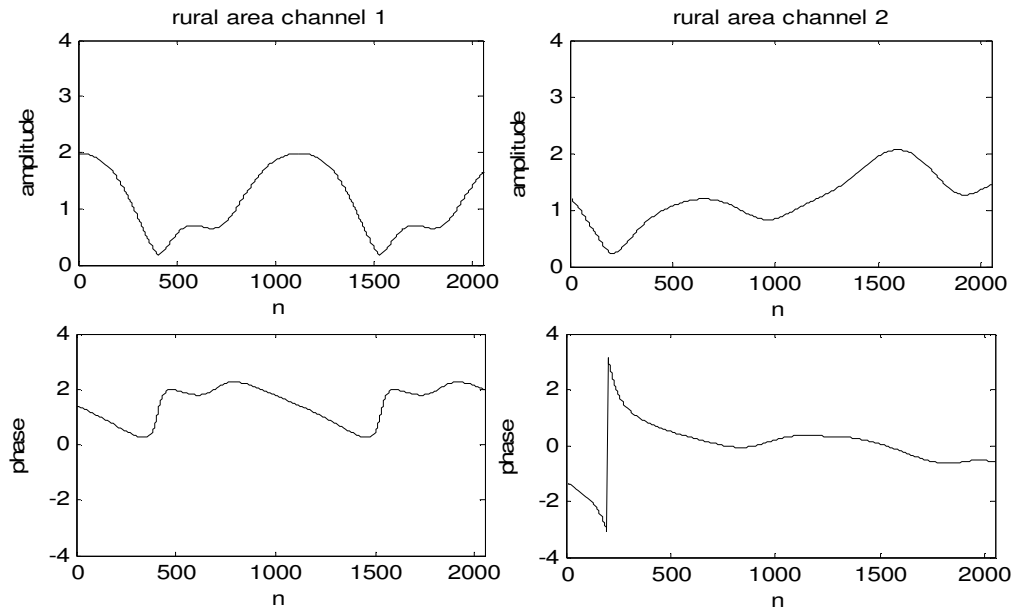
Figure 5.2 Amplitude and phase response of COST 207 rural area channels versus subcarrier index (n), *N*=2048.
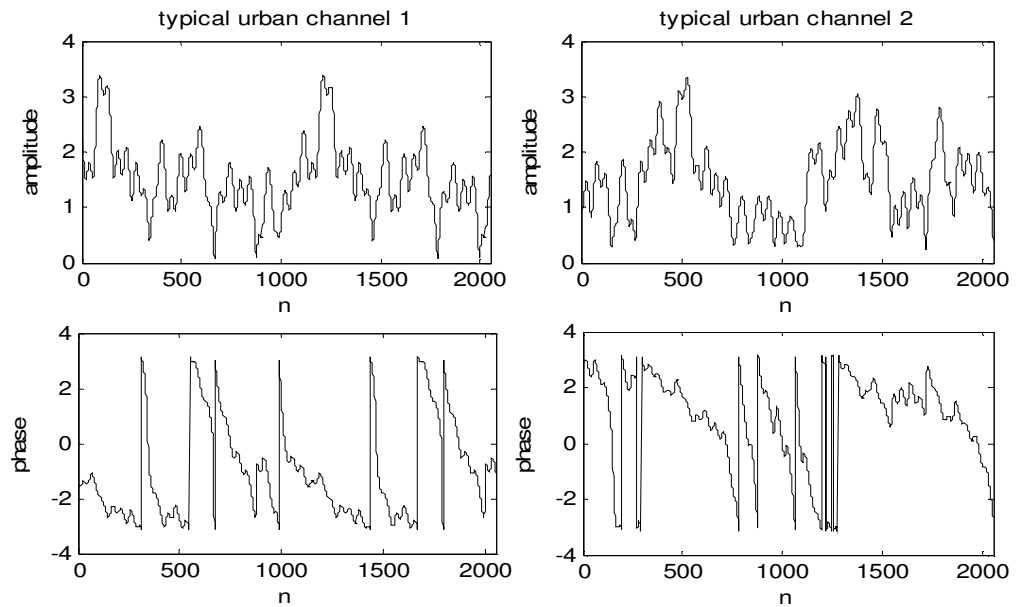
Figure 5.3 Amplitude and phase response of COST 207 typical urban channels (1 and 2) versus subcarrier index (*n*), *N*=2048.
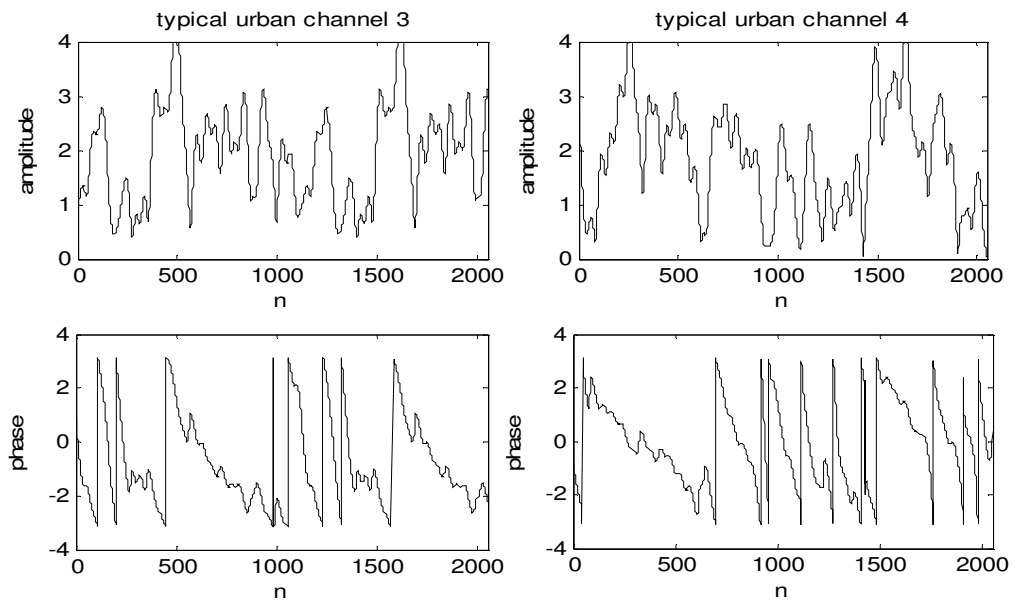
Figure 5.4 Amplitude and phase response of COST 207 typical urban channels (3 and 4) versus subcarrier index (*n*), *N*=2048.
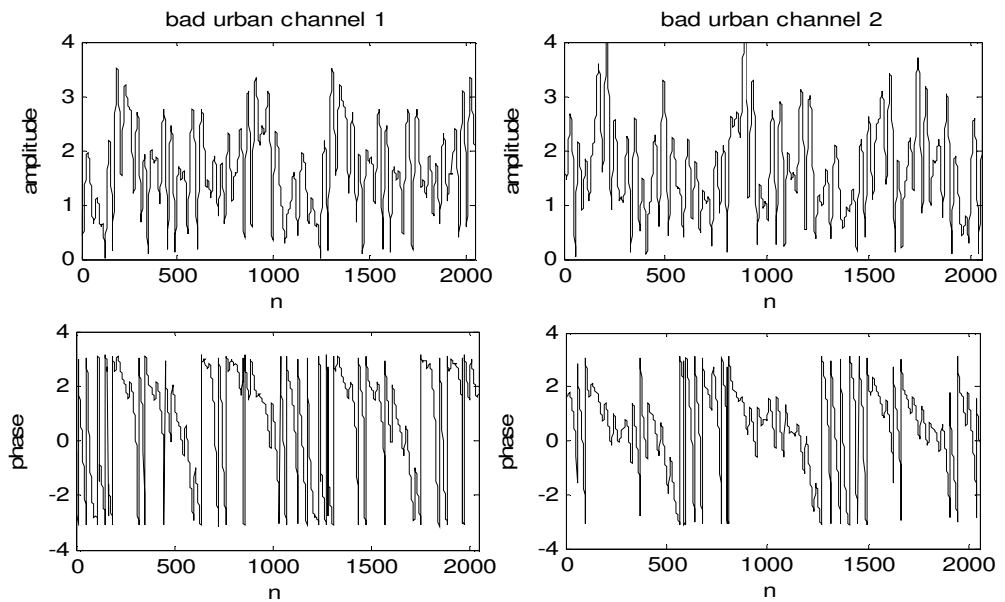
Figure 5.5 Amplitude and phase response of COST 207 bad urban channels (1 and 2) versus subcarrier index (*n*), *N*=2048.
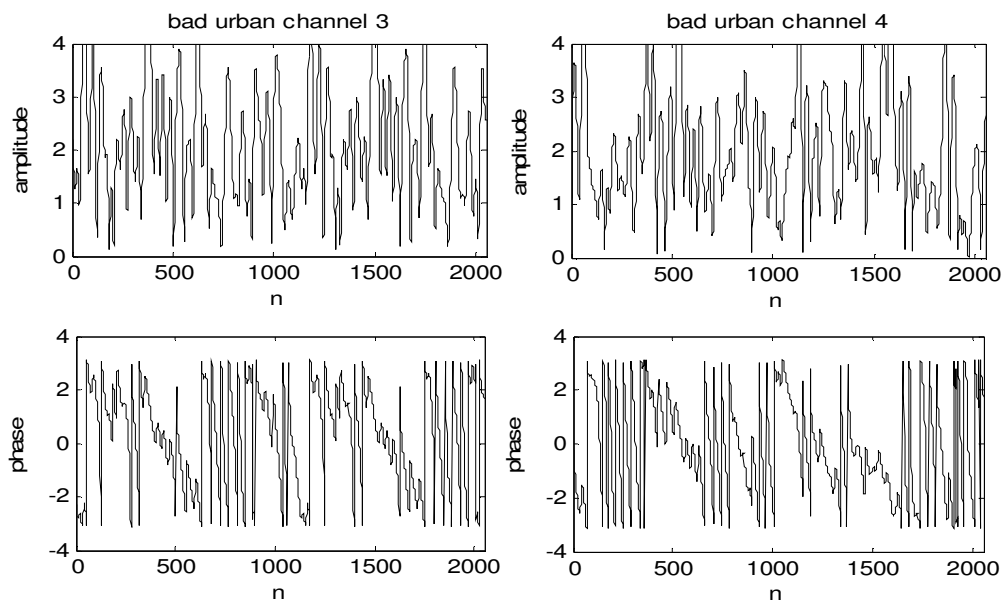
Figure 5.6 Amplitude and phase response of COST 207 bad urban channels (3 and 4) versus subcarrier index (*n*), *N*=2048.
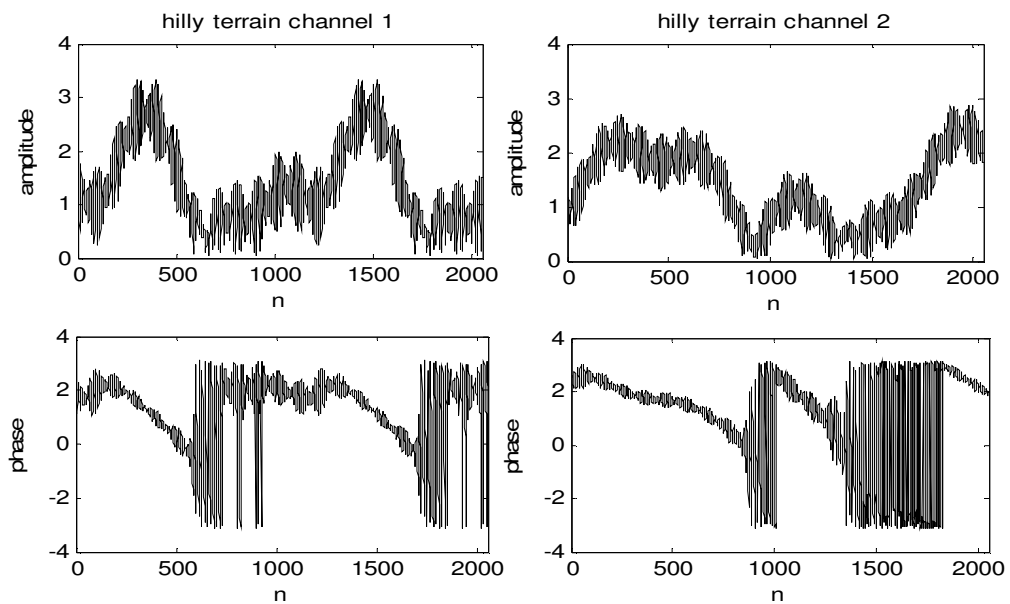
Figure 5.7 Amplitude and phase response of COST 207 hilly terrain channels (1 and 2) versus subcarrier index (*n*), *N*=2048.
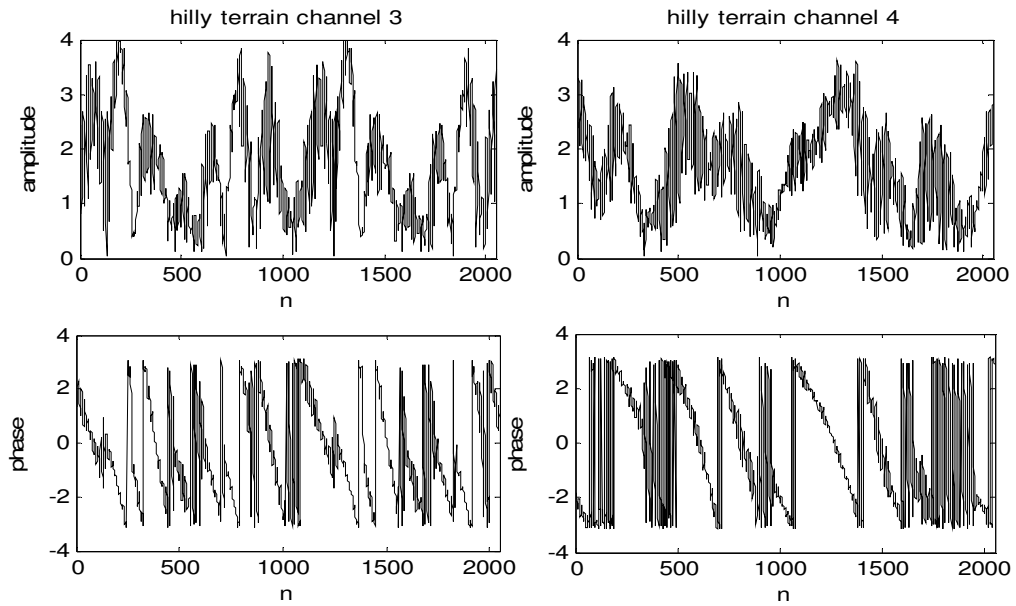
Figure 5.8 Amplitude and phase response of COST 207 hilly terrain channels (3 and 4) versus subcarrier index (*n*), *N*=2048.

5.2.3 Frequency Domain Correlation

We have used autocorrelation method [54] to estimate correlation matrix, which results with a biased, positive definite Toeplitz matrix. According to autocorrelation method, with N_s data points $x[0], x[1], \ldots x[N_s - 1]$, to estimate a *P*x*P* correlation matrix (for $P \leq N_s$) we form the matrix

101

$$\mathbf{X} = \begin{bmatrix} x[0] & 0 & \cdots & 0 \\ x[1] & x[0] & \cdots & 0 \\ \vdots & \vdots & \ddots & \vdots \\ x[P-1] & x[P-2] & \cdots & x[0] \\ x[P] & x[P-1] & \cdots & x[1] \\ \vdots & \vdots & & \vdots \\ x[N_s-1] & x[N_s-2] & \cdots & x[N_s-P] \\ 0 & x[N_s-1] & \cdots & \\ \vdots & \vdots & & \vdots \\ 0 & 0 & \cdots & x[N_s-1] \end{bmatrix} \tag{5.3}$$

This data matrix $\mathbf{X}$ is of size $(N_s+P\text{-}1)\mathrm{x}P$. The columns of $\mathbf{X}$ contain the entire data sequence $x[0], x[1], \ldots x[N_s-1]$ successively displaced and zero-padded. The rows contain the data samples that would appear under a sliding window just P samples long that moves along the data sequence. (These samples are in reverse order.) The correlation matrix estimate is then given by

$$\hat{\mathbf{C}}_{\mathbf{x}} = \frac{1}{N_s} \mathbf{X}^{\mathbf{H}}\mathbf{X} \tag{5.4}$$

Figure 5.9 gives the correlation of the middle subchannel with the other subchannels computed by autocorrelation method for DVB-T channels. Note that in the figure $N_s=P=N$. Similarly, Figure 5.10 - Figure 5.13 give subchannel correlation for COST 207 rural area, typical urban, bad urban and hilly terrain channels, respectively. As seen, although all channels are somewhat correlated, the rural area correlation is the highest. Note that, if we classify according to frequency domain correlation, DVB-T channel 1 can be called as a bad urban channel while channel 2 is a typical urban channel according to COST 207 channel classifications.
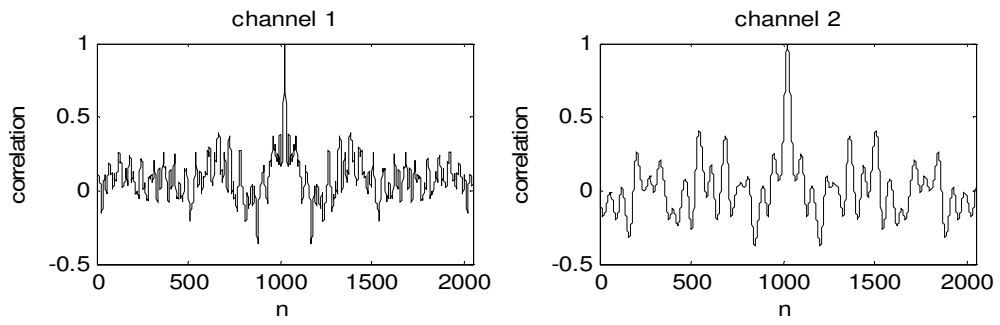
Figure 5.9 Frequency domain correlation of middle subchannel (*n*=1024) with others versus subcarrier index (*n*), *N*=2048, DVB-T channels.
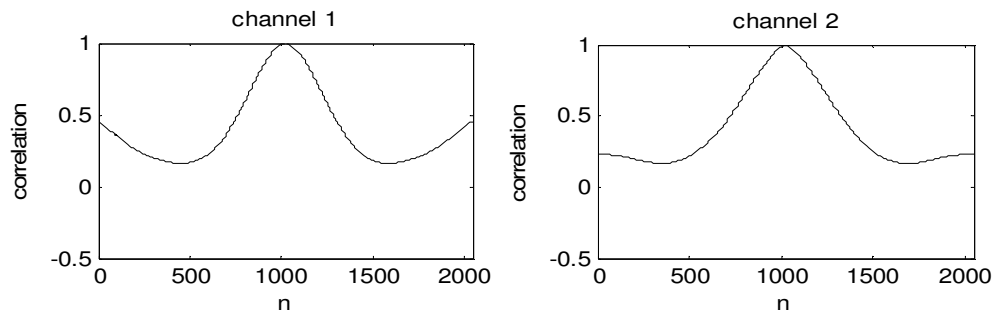
Figure 5.10 Frequency domain correlation of middle subchannel (*n*=1024) with others versus subcarrier index (*n*), *N*=2048, COST 207 rural area channels.
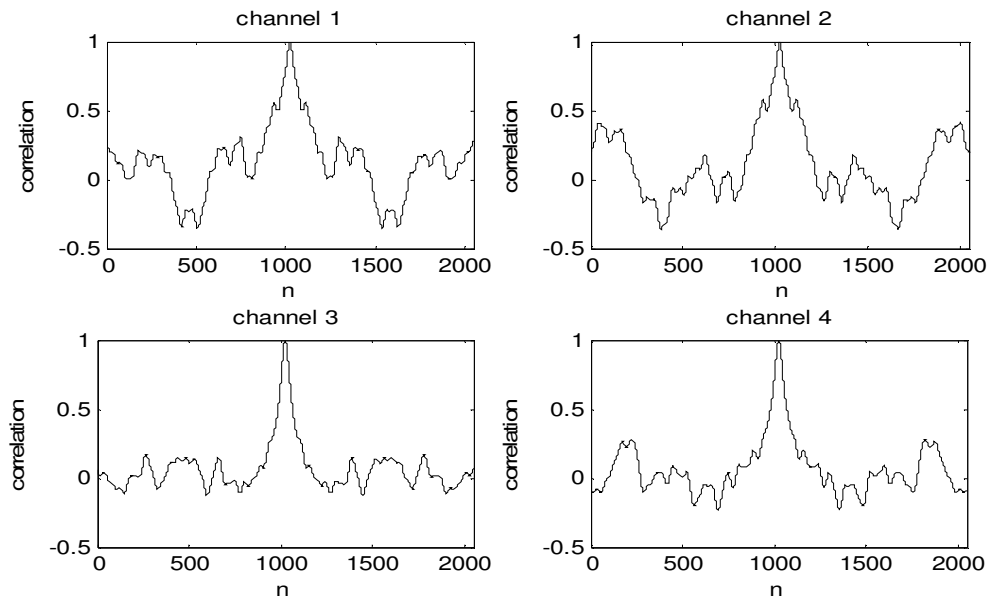
Figure 5.11 Frequency domain correlation of middle subchannel (*n*=1024) with others versus subcarrier index (*n*), *N*=2048, COST 207 typical urban channels.
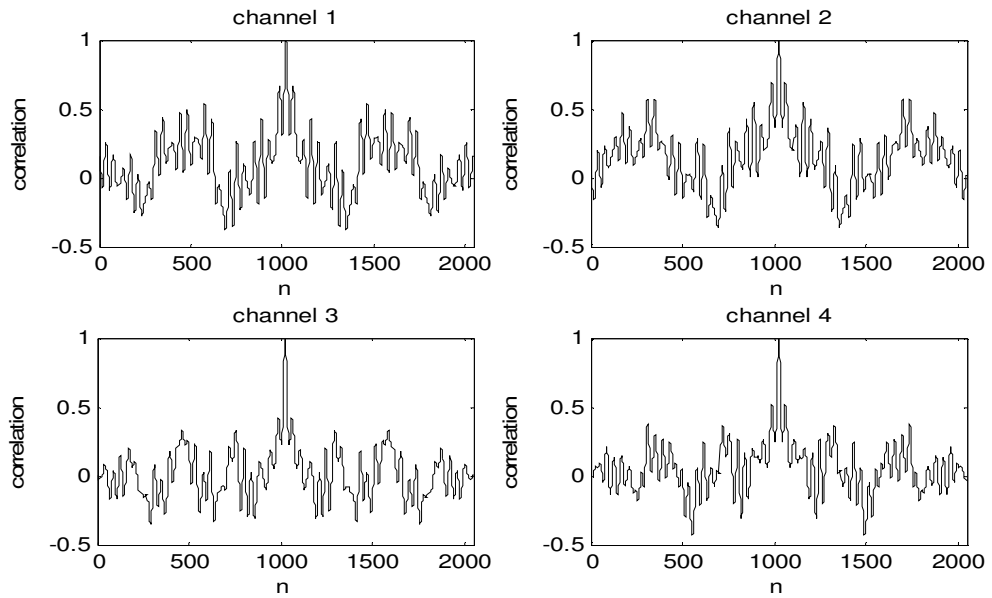
Figure 5.12 Frequency domain correlation of middle subchannel (*n*=1024) with others versus subcarrier index (*n*), *N*=2048, COST 207 bad urban channels.
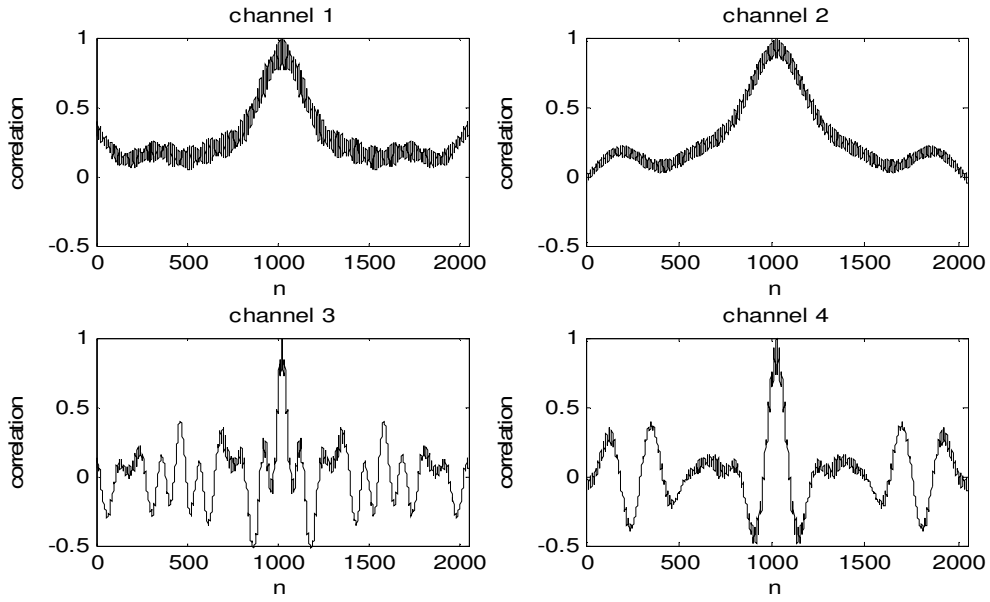
Figure 5.13 Frequency domain correlation of middle subchannel (n=1024) with others versus subcarrier index (n), N=2048, COST 207 hilly terrain channels.

5.3 SMAP-efdc Results

Following, the performance of SMAP-efdc channel estimator with the DVB-T and COST 207 channels is investigated. SMAP-efdc estimator assumes that the channel has an exponential frequency domain correlation, and estimate the correlation between subchannels. Then, it computes the covariance matrix and use it for MAP estimation (details are given in section 4.1).

5.3.1 Real Channel Simulations

Estimated ρ values for DVB-T and COST 207 channels are given in Table 5.7, for SNR=10 dB, N=2048, K=1705, α=0.9. For the simulations, it is assumed that the channels are stationary during channel estimation. Initial values of $\hat{\rho}$ are set to

the 0.99 for simplicity. Estimated values are computed as the mean of 1000 runs. As seen, all channels are highly correlated, $\rho > 0.97$ and rural area channels are found to be almost flat i.e., $\rho \approx 1$.

Table 5.7 Estimated correlation ($\hat{\rho}$) values of DVB-T and COST 207 channels, found using SMAP-efdc channel estimator.

Channel no	$\hat{\rho}$				
	DVB-T channels	COST 207			
		Rural area channels	Typical urban channels	Bad urban channels	Hilly terrain channels
1	0.977	1	0.999	0.994	1
2	0.998	1	0.999	0.995	1
3			0.998	0.993	0.999
4			0.999	0.992	1

Simulation results for the rms error versus subchannel index for the real channels are given in Figure 5.14 - Figure 5.18, with the given parameter values above. The dashed line (--) is the MAP estimator rms error, with covariance matrix computed by autocorrelation method [54] that uses channel coefficients, and the dotted line (…) is for SMAP-efdc estimator performance. It is concluded that, the proposed estimator can be used safely for typical urban and bad urban channels. The rms error of SMAP-efdc is lower than the ML estimator's, but the performance is poor compared to MAP estimator with computed covariance matrix. This is because for highly correlated case, SMAP-efdc estimator is very sensitive to ρ estimation error, as shown in section 4.1.2.2. Thus, a small variation in estimation causes a large deviation in the error variance. Unfortunately, rural area and hilly terrain

area simulations give intolerable results. Rural area channels are estimated to be flat fading (indeed they are not), which causes very high rms errors.
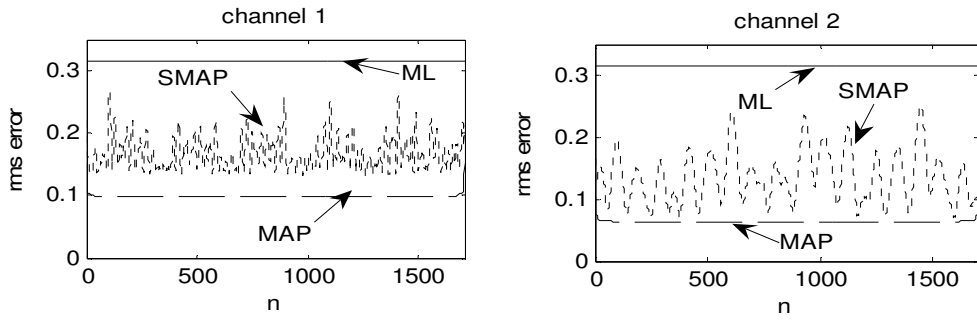
Figure 5.14 SMAP-efdc channel estimator rms error versus subcarrier index (n), SNR=10 dB, DVB-T channels.

Figure 5.15 SMAP-efdc channel estimator rms error versus subcarrier index (n), SNR=10 dB, COST 207 rural area channels.

Figure 5.16 SMAP-efdc channel estimator rms error versus subcarrier index (n),
SNR=10 dB, COST 207 typical urban channels.

Figure 5.17 SMAP-efdc channel estimator rms error versus subcarrier index (n),
SNR=10 dB, COST 207 bad urban channels.

Figure 5.18 SMAP-efdc channel estimator rms error versus subcarrier index (n), SNR=10 dB, COST 207 hilly terrain channels.

5.4 SMAP-epdp Results

In this section we have investigated the performance of SMAP-epdp channel estimator with the DVB-T and COST 207 channels. This estimator assumes that power delay profile of the channel is exponential, and estimate τ_c, rms delay spreads relative to the sampling interval T_s of the OFDM system. Then, it computes the covariance matrix and use it for MAP estimation (details are in section 4.2).

5.4.1 Real Channel Simulations

For DVB-T and COST 207 channels, τ_c's are calculated using (4.21) and presented in Table 5.8. Note that, when we compute τ_c, we assume that the

channel is exponential. For the same channels the estimated values of τ_c ($\hat{\tau}_c$), are also presented in the same table for comparison. Simulation parameters are selected to be SNR=10 dB, N=2048, K=1705, α=0.9. For the simulations, it is assumed that the channels are stationary during channel estimation. Initial values of $\hat{\tau}_c$ are set to the computed values for simplicity. Estimated values given are the mean of 1000 runs. (Note that tracking parameter α is selected high, therefore the deviation of estimation is low.) Generally estimated values are slightly different from the computed ones, but since SMAP-epdp is not much sensitive to estimation errors, dramatic degradation in the rms error performance is not expected. Since hilly terrain channels do not have exponential power delay profile (combinations of two exponential) computed and estimated τ_c differs dramatically.

Simulation results of rms error versus subchannel index for DVB-T and COST 207 channels are given in Figure 5.19 - Figure 5.23, for the same parameter values given above. The dashed line is the rms error of the MAP estimator with computed covariance matrix using autocorrelation method [54]. MSE of the proposed estimator is very low compared to ML estimator and nearly the same with the performance of MAP estimator with computed covariance, except for hilly terrain channels. Since the channel data is randomly generated, the computed covariance matrix is not equal to the actual one obtained by using expectation. Therefore, the performance of estimator with a computed covariance matrix will not give the exact MSE. Thus, the proposed estimator performance may come out to be better than that of MAP procedure, as in the case of rural area and typical urban channels. For hilly terrain channels, as stated before, since they do not fit to exponential power delay profile well, higher errors occur. But still SMAP-epdp estimator can be used as a crude approximation.

Table 5.8 Calculated and estimated rms delay spread (τ_c) values of DVB-T and COST 207 channels, found using SMAP-epdp channel estimator.

| Channels		Ch. no	Computed τ_c	Estimated τ_c
DVB-T channels		1	43.58	48.15
		2	11.34	16.48
COST 207	Rural area channels	1	1.15	1.05
		2	0.90	0.90
	Typical urban channels	1	9.71	6.45
		2	9.71	7.18
		3	9.15	8.35
		4	9.38	9.83
	Bad urban channels	1	21.87	22.18
		2	22.02	20.58
		3	22.15	26.90
		4	23.26	25.98
	Hilly terrain channels	1	45.73	17.80
		2	36.35	14.41
		3	45.59	31.48
		4	46.63	24.92
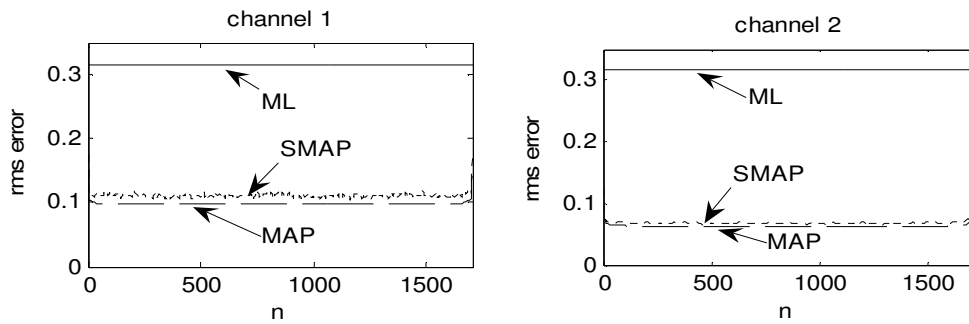
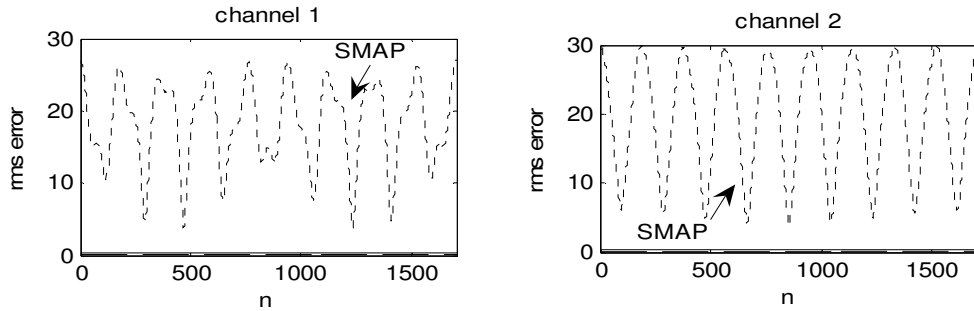Figure 5.19 SMAP-epdp channel estimator rms error versus subcarrier index (n), SNR=10 dB, DVB-T channels.
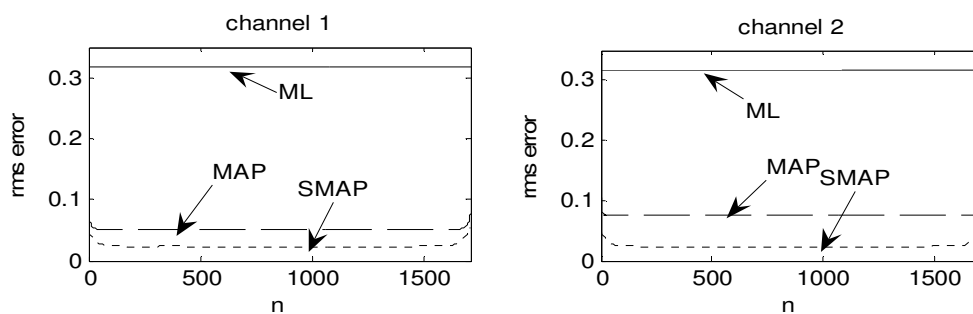
Figure 5.20 SMAP-epdp channel estimator rms error versus subcarrier index (*n*),
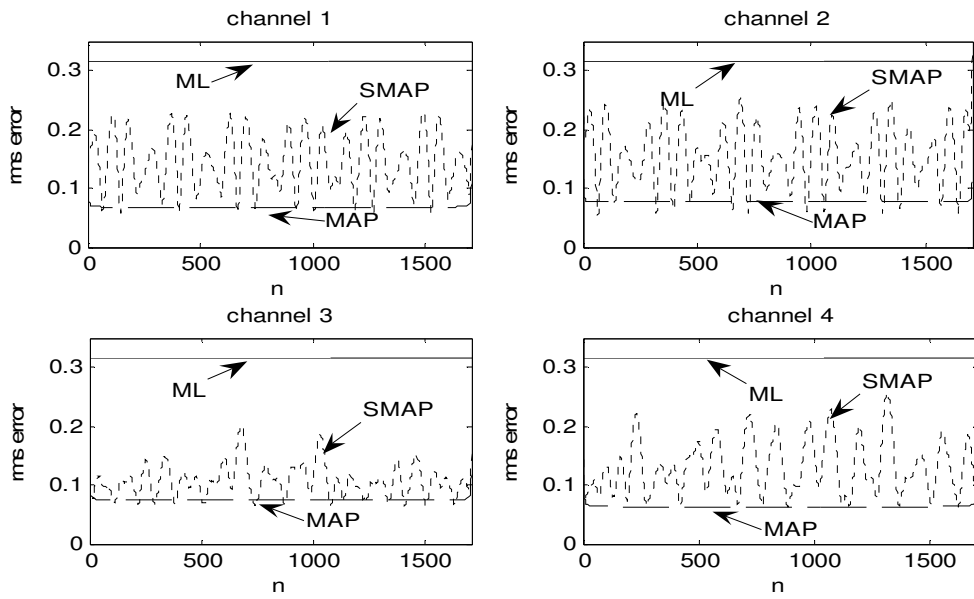SNR=10 dB, COST 207 rural area channels.
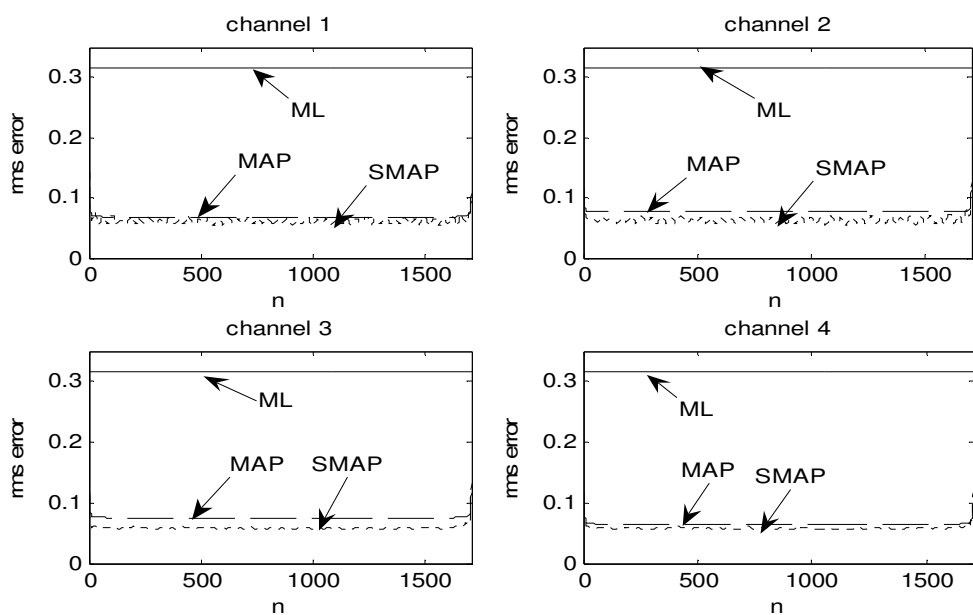
Figure 5.21 SMAP-epdp channel estimator rms error versus subcarrier index (*n*),
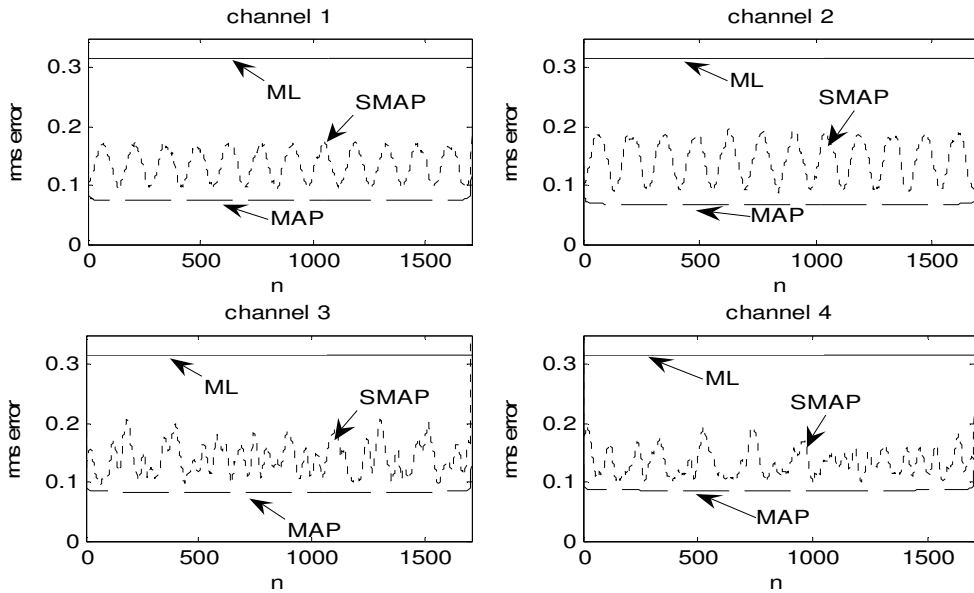SNR=10 dB, COST 207 typical urban channels.
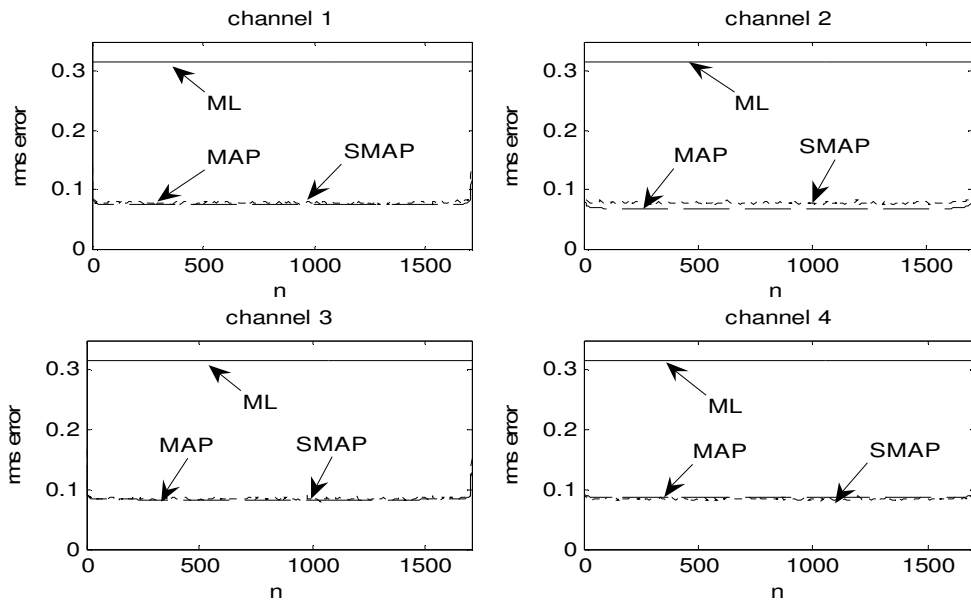
Figure 5.22 SMAP-epdp channel estimator rms error versus subcarrier index (*n*),
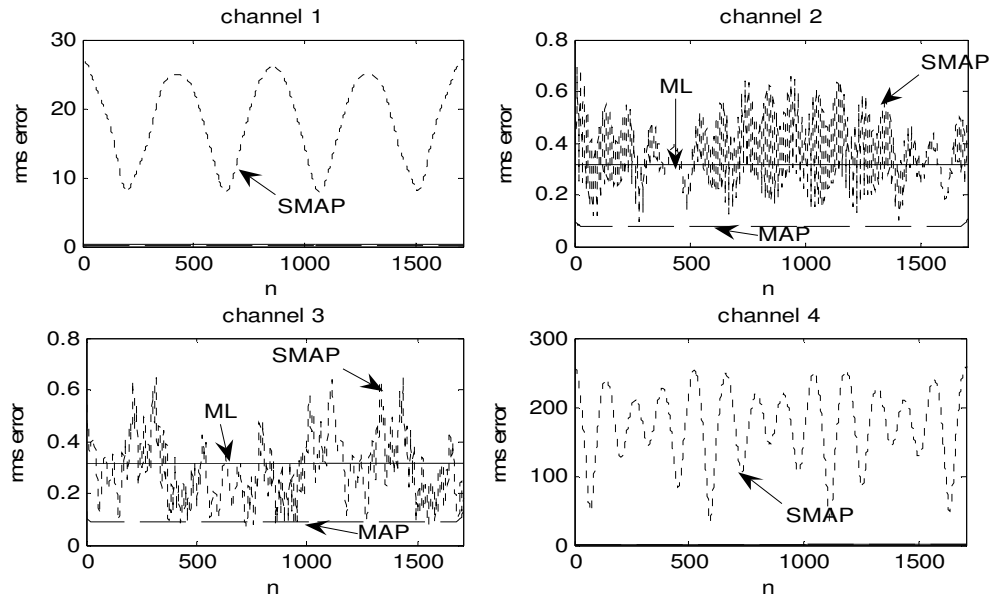SNR=10 dB, COST 207 bad urban channels.
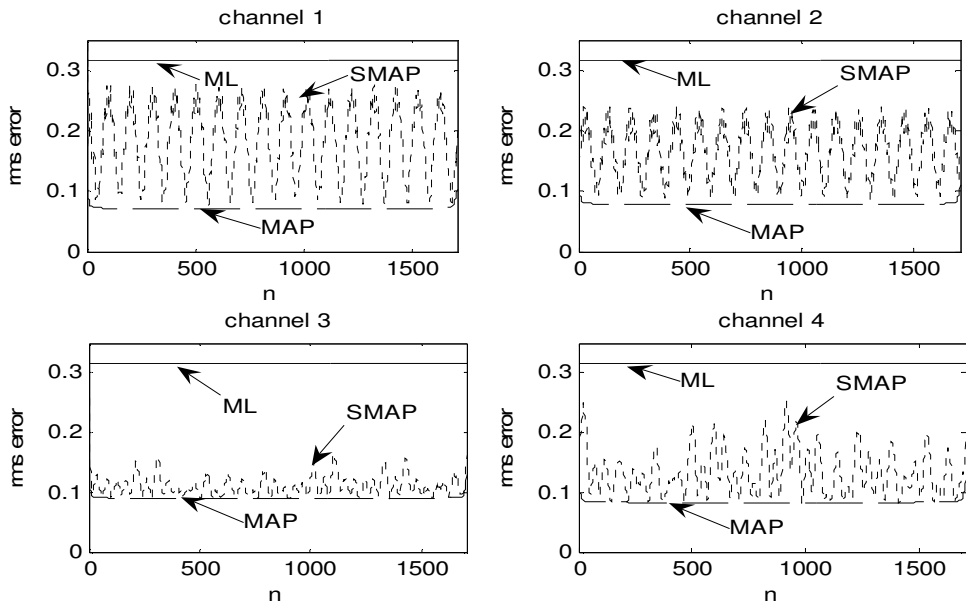
Figure 5.23 SMAP-epdp channel estimator rms error versus subcarrier index (*n*),
SNR=10 dB, COST 207 hilly terrain channels.

According to DVB-T standards [78], in addition to the transmitted data, an OFDM frame contains scattered pilot cells and continual pilot carriers. The pilots can be used for frame synchronization, frequency synchronization, time synchronization, channel estimation, transmission mode identification and can also be used to track the carrier phase noise. For the symbol of index l (ranging from 0 to 67), scattered pilots are the carriers for which index k belongs to the subset

$$\{k = K_{min} + 3*(l \bmod 4) + 12p \mid p \text{ integer}, p \geq 0, k \in [K_{min}, K_{max}]\}.$$

We have investigated the performance of the SMAP-epdp estimator using scattered pilots. Simulation results for the DVB-T channels with pilots placed according to DVB-T 2k mode are given in Figure 5.24. In the simulations, the parameters are taken to be SNR=10 dB, N=2048, K=1705, α=0.9 and 1000 runs. As seen from the figure, there are some degradations in the performances (the rms error of the estimates is higher than the full training sequence case). For DVB-T channel 2, which has a higher correlation, the performance of the proposed estimator is still much better than ML, but for channel 1 the performance degrades to ML's. Therefore, we conclude that using SMAP-epdp with pilots is profitable only for highly correlated channels.
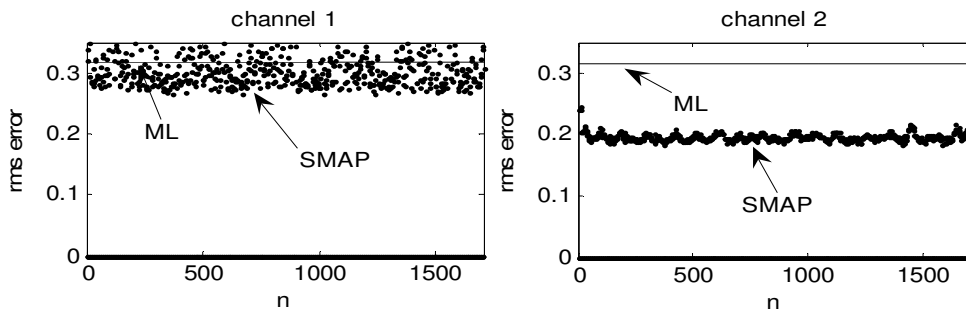
Figure 5.24 SMAP-epdp channel estimator rms error versus subcarrier index (n), SNR=10 dB, DVB-T channels, pilot aid channel estimation.

5.4.2 Approximate SMAP-epdp Simulations

The performance of Approximate SMAP-epdp estimator which uses Taylor series approximate expression (4.38) for the matrix inversion with DVB-T channel 2 data ($\tau_c = 11.34$), for SNR=10 dB, N=2048, K=1705, α=0.9 and 1000 runs, is given in Figure 5.25. In the graph, we have used 2nd degree Taylor polynomial and the center point τ_0 is selected to be 10, 50 and 100. Closed-form analytic equations for the derivative of the matrix **A** could not be found using Mathematica tool, therefore we have calculated the nth derivative of **A** at the point τ_0 numerically. The results were found to be in good agreement with those obtained by simulations, when the center point is selected well. As the center point deviates from the real value, the rms error becomes larger. However, we note that tolerance on τ_0 is quite relaxed. As an alternative approach, after estimating τ_c, the center point and matrices used can be selected to increase the performance.
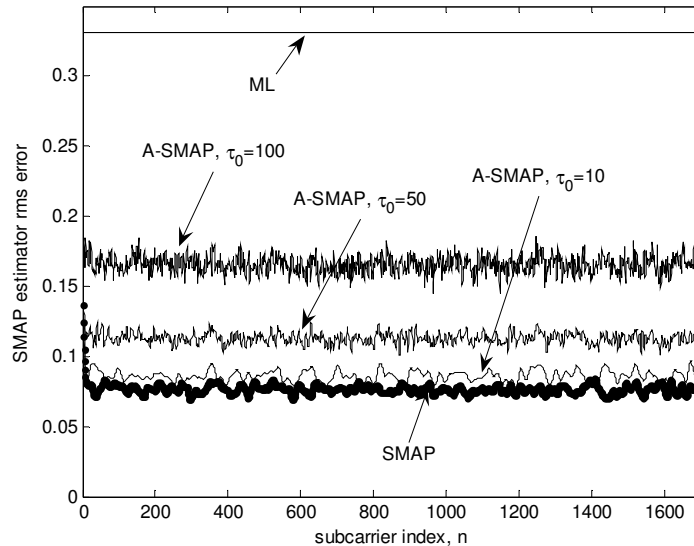
Figure 5.25 Approximate SMAP-epdp channel estimator rms error versus subcarrier index (n), DVB-T channel 2 (calculated $\tau_c = 11.34$), 2nd order Taylor, SNR=10 dB.

115

The performance of the second Approximate SMAP-epdp estimator given in (4.39) with the same DVB-T channel 2 data ($\tau_c = 11.34$) is presented in Figure 5.26. Recall that in this approximation, instead of matrix inversion for each symbol, we have suggested to keeping an array of matrices for a set of τ_c values and updating the matrix as τ_c changes significantly only. The parameters are selected to be the same as given above. In the graph, τ_0 is set to be 10, 15, 20 and 100, in order to see the performance loss due to variations in τ_0. The simulation results of approximate SMAP-epdp estimator were found to be in good agreement with those obtained for SMAP-epdp estimator, when τ_0 is selected well. As τ_0 deviates from the true value, the rms error becomes larger. However, we note that the tolerance on τ_0 is quite relaxed, even for τ_0=100 the rms error is still lower than ML estimator. Indeed, in true operation since τ_c is estimated to be about 16, τ_0=15 will occur more frequently, and τ_0=10 and τ_0=20 are rarely observed. Thus, the performance degradation will be quite tolerable.
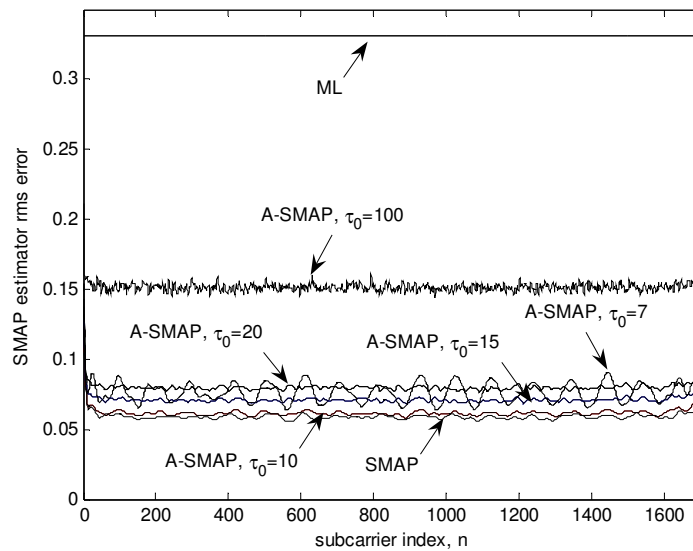
Figure 5.26 Approximate SMAP-epdp channel estimator rms error versus subcarrier index (n), DVB-T channel 2 (calculated $\tau_c = 11.34$), SNR=10 dB.

116

5.4.3 SER Performances

We have analyzed error probability performance of OFDM with QPSK modulation over Rayleigh fading channels, in the presence of channel estimation errors. Approximate SMAP-epdp, which assumes channel power delay profile is exponential, keeps an array of matrices for a set of τ_c values and updates the matrix as τ_c changes significantly only, is used for channel estimation. We have used exact BER formulas derived in Chapter 3 and simulation results, and quantified the performance loss due to channel estimation error. Channel data used in the simulations are generated randomly from channels that have exponential power delay profiles. The correctness of our analysis is verified by the fact that the system performance predicted by analysis given in section 3.4.2 (P_e is given in equation 3.55) and computer simulation (Monte Carlo simulations) yields almost the same result. The SER graphs are investigated in the cases of channel estimation with training sequence, decision feedback or pilot carriers.

5.4.3.1 Channel Estimation with Training Sequence

In this section, it is assumed that the channel is estimated periodically by a training sequence, thus the channel coefficients are estimated from all subcarriers (Details are given in section 3.3.). Figure 5.27 shows the graph of SER of Approximate SMAP-epdp estimator versus SNR for N=512, τ_c=12 and 50. The dotted lines (--) are the simulation results and the stars (*) are used for the analytical results. Approximate SMAP-epdp estimator SER expressions are calculated as $2\,P_e{}^3$, where P_e is found using (3.58) and (3.55) and by replacing $\mathbf{A}$ matrix with $\mathbf{A}(\tau_0)$. P_e is computed for each τ_0 value used, and then total P_e is found considering the percentage of τ_0 selection. For example, when histograms

---

[3] Note that it is a valid approximation for gray coded QPSK, especially when the bit error is small.

of τ_0 selection for an exponential power delay profile channel with τ_c=12 are investigated; it is observed that for low SNR over-estimation is more probable, therefore higher values of τ_0 are selected. As SNR increases, the estimation gets closer to the real value of τ_c, but still slightly over-estimation is observed. Thus, for SNR=20 dB, we have 20% of the total occurrences consisting of τ_0=10 and 80% for τ_0=15. Then, for SNR=20 dB, we computed P_e from

$$P_e = 0.2\, P_{e,\tau_0=10} + 0.8\, P_{e,\tau_0=15}. \tag{5.5}$$

We note that analytical results perfectly match the simulation results.
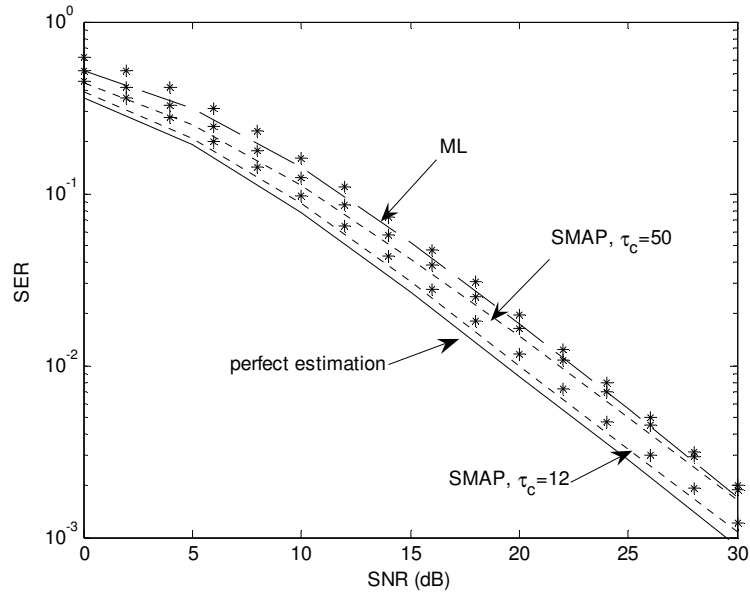
Figure 5.27 SER of Approximate SMAP-epdp estimator versus SNR, N=512, τ_c=12 and 50, using training sequence for channel estimation (--:simulation results, *:analytical results).

Figure 5.28 shows the graph of analytical SER of Approximate SMAP-epdp estimator versus SNR for N=512, τ_c =0, 12, 50 and 100. For comparison, the plots of analytic SER when there is no fading (AWGN), with perfect channel estimation and simulation result of SER when ML estimator is used are also presented in the same graph. As seen, if the channel is flat fading, the performance of the proposed estimator is essentially identical to that of the case when the channel is perfectly estimated (denoted by * in the graph). If the channel is highly correlated, the performance of the proposed estimator is very close to the case when the channel is perfectly estimated. As the correlation decreases the performance of Approximate SMAP-epdp estimator comes closer to the ML estimator performance, as expected. Note that, for low SNRs the performance improvement compared to ML estimator is more significant.
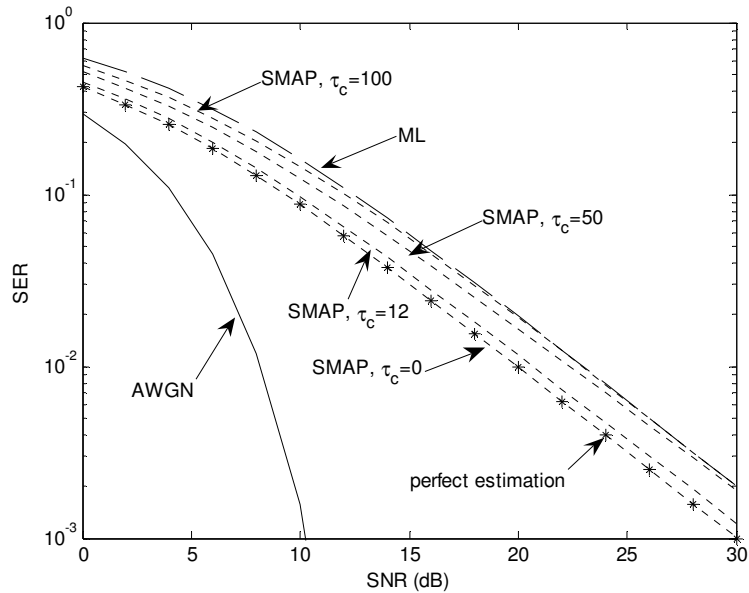
Figure 5.28 SER of Approximate SMAP-epdp estimator versus SNR, N=512, τ_c =0, 12, 50 and 100, using training sequence for channel estimation.

Finally, Figure 5.29 shows the graph of analytical SER of Approximate SMAP-epdp estimator with Taylor series expansion versus SNR for N=512, τ_c=0, 12 and 50. In the figure, stars (*) are used for SMAP-epdp estimator and circles (o) are used for Approximate SMAP-epdp obtained using 2nd order Taylor series expansion, with SNR=10 dB. For the plot, we have assumed that the center point τ_0 is selected close enough, thus we can observe the effect of estimation error in noise variance on SER performance. When we compare the performance of Approximate SMAP-epdp with SMAP-epdp estimator's, the performance is exactly the same when SNR is smaller than 20 dB. For higher SNR's, Approximate SMAP-epdp is worse, and as the correlation decreases, the degradation in the performance is more specific. Indeed, Taylor series coefficients should be updated for this value of SNR. Sensitivity graphs have shown that, when the correlation is low, and SNR is underestimated too much, the error can increase considerably.
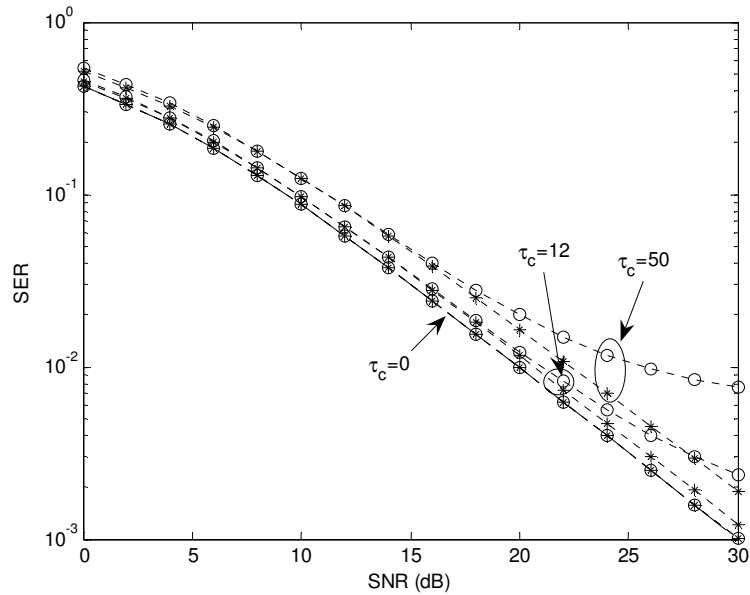
Figure 5.29 SER of Approximate SMAP-epdp estimators versus SNR, N=512, τ_c=0, 12 and 50, using training sequence for channel estimation.

120

5.4.3.2 Channel Estimation with Decision Feedback

Monte Carlo simulation results for SER performance of a QPSK modulated OFDM system where a training sequence is sent once per 50 symbols and decision directed channel estimation is performed between training symbols are given in Figure 5.30 and Figure 5.31. Other parameters are: N=1024, τ_c=12 and 50 and α=0.9. To model the time variations, the Jakes Doppler spectrum [39] is used at a Doppler frequency of f_m=40 Hz and f_m=80 Hz, respectively. The channel correlation is:

$$E\{z_{nk} \cdot z_{ml}^*\} = \frac{J_0(2\pi f_m(k-l)T_s)}{1 + j\,2\pi\tau_c(n-m)/N} \tag{5.6}$$

where n, m are subcarrier indices, k, l are symbol indices and J_0 is the Bessel function of the first kind of order zero. We conclude that SER performance of the proposed channel estimator with decision feedback is always better than the ML estimator and quite satisfactory especially for highly correlated channels.
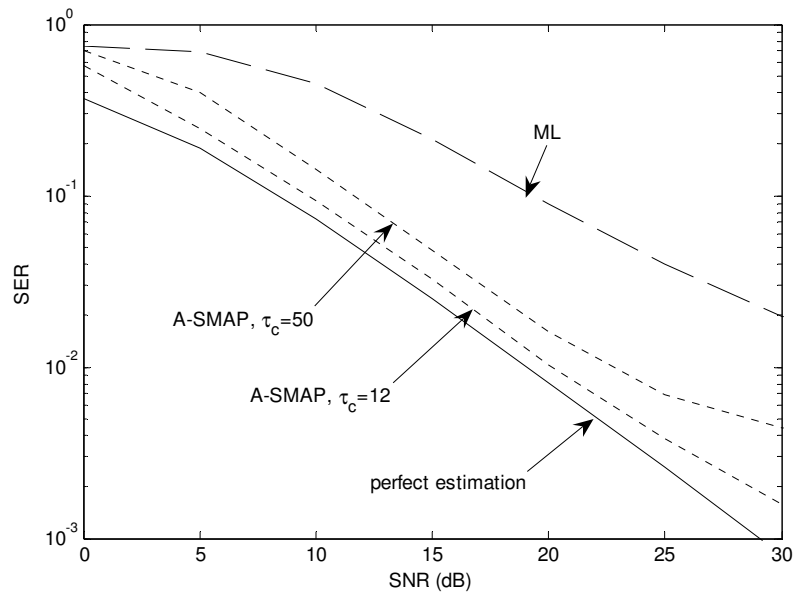
Figure 5.30 SER of Approximate SMAP-epdp estimator versus SNR, N=1024, τ_c =12 and 50, f_m=40 Hz, using training sequence and decision feedback for channel estimation, Monte Carlo simulation.
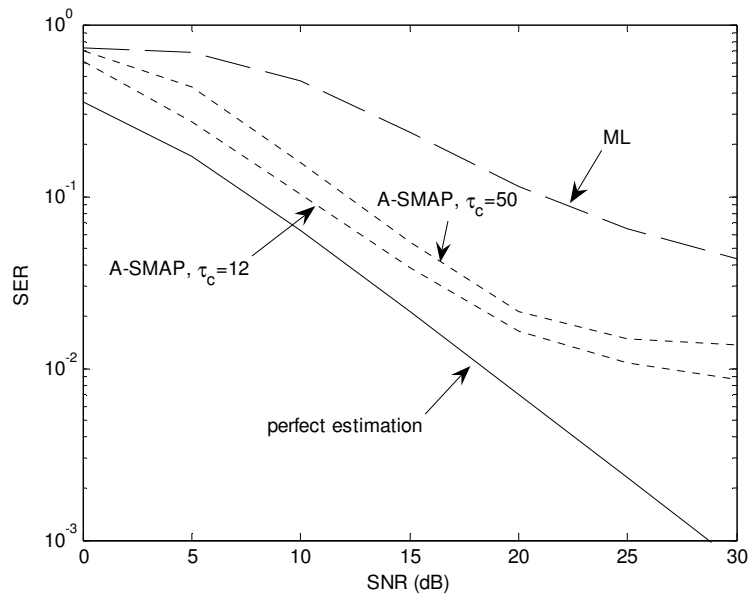
Figure 5.31 SER of Approximate SMAP-epdp estimator versus SNR, N=1024, τ_c =12 and 50, f_m=80 Hz, using training sequence and decision feedback for channel estimation, Monte Carlo simulation.

Figure 5.32 and Figure 5.33 show the SER performance of Approximate SMAP-epdp and ML channel estimation methods as a function of Doppler frequency, for SNR=10 dB and SNR=30 dB, respectively. Other parameters are the same as in the previous case. The general behavior of the graphs is that SER increases as the Doppler spread increases. When SNR is high, the degradation in the SER performance is more pronounced.
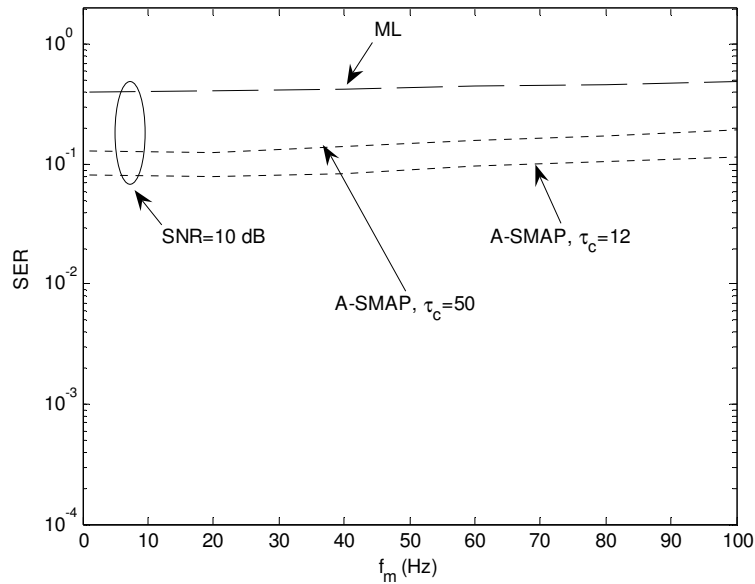
Figure 5.32 SER of Approximate SMAP-epdp estimator versus Doppler frequency (f_m), N=1024, τ_c=12 and 50, SNR=10 dB, using training sequence and decision feedback for channel estimation, Monte Carlo simulation.
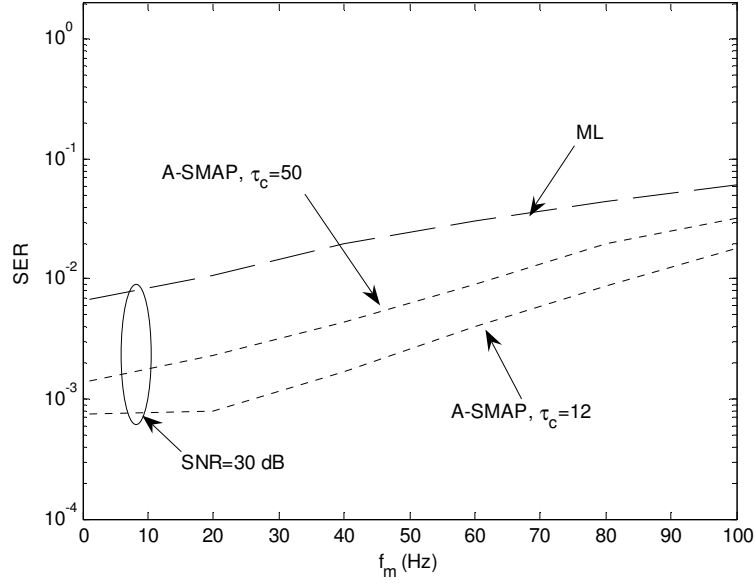
Figure 5.33 SER of Approximate SMAP-epdp estimator versus Doppler
frequency (f_m), N=1024, τ_c=12 and 50, SNR=30 dB, using training sequence and
decision feedback for channel estimation, Monte Carlo simulation.

5.4.3.3 Channel Estimation with Pilot Carriers

When pilots are used for channel estimation, although estimating the channel
responses at data locations may involve a nonlinear interpolating polynomial, the
derived data channel estimate is still linear combinations of ML or MAP
estimates. (MAP estimated channel response is also a linear function of ML
estimates, thus, the resulting estimate is a linear function of the ML estimate.) In
summary, for a general class of linear channel estimates, we can express the
channel response estimate as [32]

$$\hat{\mathbf{z}} = \mathbf{B} \cdot \mathbf{r_p} \quad \text{and} \quad \mathbf{B} = \mathbf{p_i} \mathbf{A_p}, \tag{5.7}$$

124

where $\mathbf{r_p}$ is the received signal in the pilots, $\mathbf{p_i}$ is the interpolation polynomial and $\mathbf{A_p}$ is the matrix $\mathbf{A}$ (recall that this is the MAP estimator matrix) but with pilot locations only. For ML estimation $\mathbf{A_p}$ is the identity matrix. Then, analytical SER expressions for Approximate SMAP-epdp estimator are found similarly as in the training sequence case, using (3.58), by replacing the estimator matrix $\mathbf{A}$ with $\mathbf{B}$. Similarly, P_e is computed for each τ_0 value used, and then total P_e is found considering the percentage of τ_0 selection.

Figure 5.34 shows the graph of analytical SER versus SNR graph of a QPSK modulated OFDM receiver with pilot aided channel estimation for $N=1024$, $L=8$, $\tau_c=1$ and 5. In our work, we have used a second order polynomial interpolation [4] in estimating channel responses of data tones, for its acceptable computational complexity. Then, channel estimates obtained using interpolation is given by

$$\begin{aligned}
\hat{\mathbf{z}}(k) &= \hat{\mathbf{z}}(mL+l) \\
&= c_1\hat{\mathbf{z}}_{\mathbf{p}}(m+1)+c_0\hat{\mathbf{z}}_{\mathbf{p}}(m)+c_{-1}\hat{\mathbf{z}}_{\mathbf{p}}(m-1)
\end{aligned} \tag{5.8}$$

where $\hat{\mathbf{z}}_{\mathbf{p}}$ is the estimations of pilot subchannels, $m = 0,1,\ldots, N_p\text{-}1$, $l = 0,1,\ldots,L\text{-}1$ and

$$\begin{aligned}
c_1 &= \frac{\alpha(\alpha+1)}{2} \\
c_0 &= -(\alpha-1)(\alpha+1) \quad \text{and} \quad \alpha = \frac{l}{N}. \\
c_{-1} &= \frac{\alpha(\alpha-1)}{2}
\end{aligned} \tag{5.9}$$

The dashed lines are used for the ML estimator and the dotted lines are for Approximate SMAP-epdp estimator. We conclude that, in pilot aid channel estimation, Approximate SMAP-epdp estimator provides a noteworthy advantage when the channel is highly correlated (slowly fading) at low and medium SNRs. The performance advantage of Approximate SMAP-epdp estimator decays and SER comes closer to the ML estimator's as SNR increases towards large values.
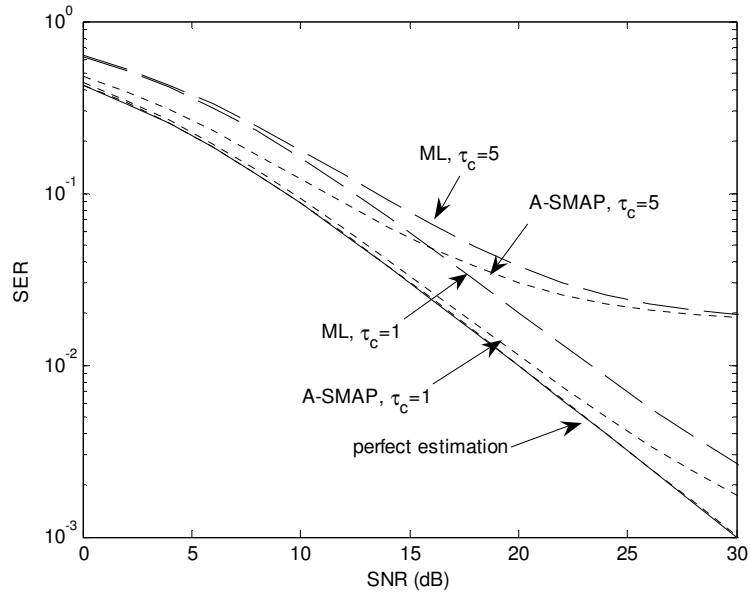
Figure 5.34 SER of Approximate SMAP-epdp estimator versus SNR, N=1024, L=8, τ_c =1 and 5, pilot aided channel estimation.

Figure 5.35 shows the graph of analytical SER of Approximate SMAP-epdp estimator versus SNR for N=1024, τ_c =1, 12, and L=4, 8. As expected, the performance of the pilot assisted channel estimation is much worse than that of the training sequence based channel estimation. As the correlation decreases, increasing L results in much higher errors. We conclude that, using pilots is acceptable when the channel is highly correlated (slowly fading).
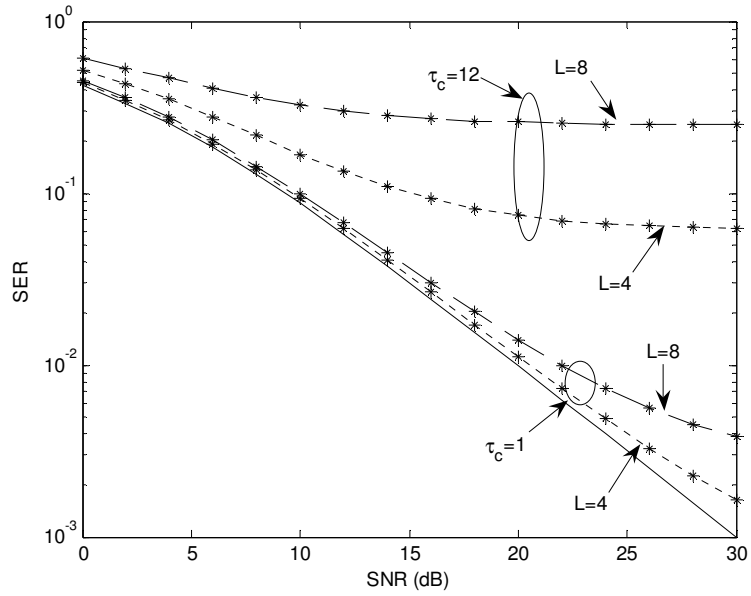
Figure 5.35 SER of Approximate SMAP-epdp estimator versus SNR, N=1024,
L=4 and 8, τ_c=1 and 12, pilot aided channel estimation.

Finally, when we compare the SER performances of training sequence, pilot assisted and decision directed channel estimation schemes, we conclude that the training sequence scheme has the lowest SER, as expected. When the channel is sufficiently slowly time varying, a training sequence with decision feedback is a good choice for estimation. For slowly fading (highly correlated) channels, using pilot carriers for channel estimation is an alternative method and the performance of the proposed estimator is shown to be advantageous especially for low to moderate SNRs.

CHAPTER 6

CONCLUSIONS

This thesis is composed of two major topics. In the first part of the thesis, we have investigated the average channel capacity of adaptively loaded OFDM systems under frequency selective slowly fading channel conditions. Using the optimum power distribution, we evaluated the average channel capacity under Rayleigh, Rician, Nakagami-m, Hoyt, Weibull and Lognormal channels, assuming that the channel state information is available at the transmitter and receiver. Following, we dealt with a lower bound for channel capacity, which assumes uniformly distributed power. It has been shown by simulations that this approach gives tight bounds for all fading channels except for lognormal channel with large variance. We have also considered the capacity under Rician fading with ideal MRC diversity at the receiver. Closed form expressions for the lower bounds with and without MRC diversity for Rician channel using series expansion have been derived. We observed that the reception always reduces to the case of AWGN regardless of the degree of fading, as the number of diversity L approaches infinity. Increasing L improves the channel capacity, especially for small values of K, Rician factor. For the high SNR case, further approximations have been derived for Rayleigh, Rician, Nakagami-m, Weibull and Lognormal channels. We conclude that these approximations are highly accurate when the average SNR is greater than 20 dB.

As a second topic, we proposed two novel channel estimation methods for OFDM systems under Rayleigh fading channels and investigated their performances

thoroughly. We have developed adaptive, simplified MAP estimators for the channel taps, to be used in OFDM systems where typically the subcarrier channel taps are highly correlated. First, we have assumed that the channel frequency correlation is exponential and proposed an estimator. We used a single parameter MAP estimator block for which the parameter is estimated by a simple procedure. We have investigated the sensitivity of the simplified MAP estimator to correlation parameter and noise variance estimation errors. It has been seen that the proposed estimator is quite insensitive to the noise variance estimation errors, if SNR and/or correlation are high. It is not sensitive to correlation estimation errors for weakly correlated channels, but dramatic errors occur for highly correlated channels. Simulations done with real channel data matched well with this result. It has been shown that this estimator works well if the channel fits the assumption and if the subchannel correlation is not high. Degradation in MSE performance is observed for highly correlated real channel estimations. Additionally, for practical use, further approximations are presented to avoid matrix inversion, which makes the implementation complicated.

Following, exponential power delay profile is assumed, which is known to be a good model for most practical channels in the literature. This model shows better performance compared to the previous one. The MSE performance of this channel estimator has been found to be very good, especially for the systems with a large number of subcarriers, when the subchannels are highly correlated. Although there is a degradation compared to the MSE performance with training, the performance of the estimator when pilots are used for channel estimation was also shown to be satisfactory especially when subchannels are highly correlated. Furthermore, the proposed channel estimator is shown to be quite insensitive to parameter estimation errors. It has been shown that the proposed estimator is also quite insensitive to the rms delay spread estimation errors, especially if the rms delay spread is over estimated. We conclude that, we do not have to estimate the rms delay spread exactly by paying the price of high complexity. We have also shown that the estimation error in noise variance is not so important, especially when SNR is high and/or the subchannels are substantially correlated. The

proposed estimator rms error increases considerably only when noise variance is over estimated significantly.

We have developed approximations to avoid the matrix inversion in the proposed simplified MAP estimator, using Taylor series expansion. The MSE performance of this approximate estimator was found to be satisfactory and this approximate estimator is quite insensitive to the selection of its initial parameters. Another approximation depending on the fact that the proposed estimator is insensitive to rms delay spread estimation errors is developed, which approximately yields MAP estimates of the channel taps with an acceptable complexity. We suggested keeping an array of matrices for a set of rms delay spread values and updating the matrix that is used in the estimator as the parameter changes significantly only. Thus, we have developed methods that can be implemented with only a limited number of computations, without the need for matrix inversion. We have computed the computational complexity of the proposed estimator: Compared to the exact MAP estimator, the Approximate SMAP estimator complexity is reduced considerably, without a noticeable degradation in the performance.

Additionally, the SER performance of the proposed Approximate SMAP estimator has been investigated for channel estimation with training sequence, decision feedback and pilot subcarriers. It is concluded that the proposed estimator always outperforms the ML estimator and the performance improvement is more significant for highly correlated channels. Thus, when the correlation is high enough, the performance of the proposed estimator is nearly equal to the case that the channel is perfectly estimated, and as the channel gets closer to independent fading, the performance of the proposed estimator comes closer to the ML estimator performance. When we compare the estimation methods, as expected, channel estimation with training sequence gives the best performance, but we pay the price of decreasing useful bit rate. If the channel is sufficiently slowly time varying, channel estimation with a training sequence and decision feedback is a good choice. For slowly fading (highly correlated) channels, using pilot aided channel estimation is an alternative method, because

the performance of the proposed estimator is shown to be advantageous for such channels especially for low to moderate SNRs.

Among the areas that seem to promise fruitful future work in the context of channel estimation for multicarrier systems are:

- The frequency selective radio channel may severely attenuate the data symbols transmitted on one or several subcarriers, leading to bit errors. Spreading the coded bits over the bandwidth of the transmitted system, an efficient coding scheme can correct the erroneous bits and thereby exploit the wideband channel's frequency diversity advantage. Therefore, the proposed estimator performance with coded OFDM can be analyzed.

- Multiple transmit and receive antennas are a strong choice to improve the capacity in OFDM systems. Channel estimation is an important issue for the MIMO-OFDM systems since computational complexity increases rapidly with the increase in the number of antennas, and any estimation error becomes crucial since the system becomes more sensitive to parameter errors. Therefore, the work done in this thesis may be extended to suit the requirements of MIMO systems.

REFERENCES

[1] B. Canpolat, Y. Tanık, "Performance of adaptively loaded OFDM under Rayleigh fading with diversity combining", *IEEE Transactions on Vehicular Technology,* vol. 53, no. 4, pp. 1105-1115, July 2004.

[2] B. Canpolat, Y. Tanık, "Performance of adaptively loaded OFDM under Rayleigh fading with diversity combining", *IEEE 54th Vehicular Technology Conference*, vol. 2, pp. 957-961, Oct. 2001.

[3] R. Prasad, *OFDM for Wireless Communications Systems,* Artech House, Inc., Boston, 2004.

[4] A. R. S. Bahai, B. R. Saltzberg, M. Ergen, *Multicarrier Digital Communications Theory and Applications of OFDM*, 2nd edition, Springer Science + Business Media, Inc., New York, 2004.

[5] X. Wang, H. V. Poor, *Wireless Communication Systems*, Prentice Hall PTR, USA, 2004.

[6] M. S. Alouini, A. J. Goldsmith, "Comparison of fading channel capacity under different CSI assumptions, *IEEE 52nd Vehicular Technology Conference*, vol. 4, pp. 1844-1849, Sept. 2000.

[7] M. S. Alouini, A. Goldsmith, "Capacity of Nakagami multipath fading channels", *IEEE 47th Vehicular Technology Conference*, vol. 1, pp. 358-362, May 1997.

[8] J. Cheng, T. Berger, "Capacity of Nakagami-q (Hoyt) fading channels with channel side information", *International Conference on Communication Technology Proceedings*, vol. 2, pp. 1915-1918, Apr. 2003.

[9] J. Cheng, T. Berger, "Capacity and performance analysis for hybrid selection / maximal-ratio combining in Nakagami fading with unequal fading parameters and branch powers", *IEEE International Conference on Communications*, vol. 5, pp. 3031-3035, May 2003.

[10] Z. Lie, Z. Yun, S. Ling, Z. Ping, "Effects of frequency-offset on the performance of OFDM systems", *Communication Technology Proceedings*, vol. 2, pp. 1029-1032, Apr. 2003.

[11] J. Jang, K. B. Lee, Y-H. Lee, "Frequency-time domain transmit power adaptation for OFDM systems in multiuser environment" *IEEE Electronics Letters,* vol. 38, no. 25, pp. 1754-1756, Dec. 2002.

[12] M. Godavarti, T. L. Marzetta, S. Shamai, "Capacity of a mobile multiple-antenna wireless link with isotropically random Rician fading", *IEEE Transactions on Information Theory*, vol. 49, no. 12, pp. 3330-3334, Dec. 2003.

[13] S. K. Jayaweera, H. V. Poor, "MIMO capacity results for Rician fading channels" *Global Telecommunications Conference,* vol. 4, pp.1806-1810, Dec. 2003.

[14] S. K. Jayaweera, H. V. Poor, "On the capacity of multi-antenna systems in the presence of Rician fading", *IEEE 56th Vehicular Technology Conference*, vol. 4, pp. 1963-1967, Sept. 2002.

[15] W. C. Y. Lee, "Estimate of channel capacity in Rayleigh fading environment", *IEEE Transactions on Vehicular Technology*, vol. 39, pp. 187-189, Aug. 1990.

[16] C. G. Gunther, "Comment on "Estimate of channel capacity in Rayleigh fading environment", *IEEE Transactions on Vehicular Technology,* vol. 45, pp. 401-403, May 1996.

[17] H. Aniktar, Y. Tanik, "New receiver structures for subcarrier synchronization in OFDM systems over frequency-selective channel", *IEEE 8th International Symposium on Computers and Communication*, vol. 1, pp. 486-491, July 2003.

[18] E. Panayirci, "A new algorithm for joint time and phase synchronization in OFDM systems", *IEEE International Symposium on Personal, Indoor and Mobile Radio Communications*, vol. 2, pp. 819-823, Sept. 2000.

[19] A. T. Hug, E. Panayirci, C. N. Georghiades, "ML NDA carrier phase recovery for OFDM systems", *IEEE International Conference on Communications*, vol. 2, pp. 786-790, June 1999.

[20] H. A. Cirpan, E. Panayirci, H. Dogan, "Nondata-aided channel estimation for OFDM systems with space-frequency transmit diversity", *IEEE Transactions on Vehicular Technology,* vol. 55, no. 2, pp. 449-457, March 2006.

[21] E. Panayirci, C. N. Georghiades, "Carrier phase synchronization of OFDM systems over frequency-selective channels via the EM algorithm", *IEEE 49th Vehicular Technology Conference*, vol. 1, pp. 675-679, May 1999.

[22] J. M. M. Ocloo, F. Alberge, P. Duhamel, "Semi-blind channel estimation for OFDM systems via an EM-MAP algorithm" *IEEE 6th Workshop on Signal Processing Advances in Wireless Communications,* pp. 605-609, June 2005.

[23] V. Srivastava, C. H. Keong, P. H. W. Fung, S. Sun; "Robust MMSE channel estimation in OFDM systems with practical timing synchronization" *IEEE Wireless Communications and Networking Conference,* vol. 2, pp. 711-716, March 2004.

[24] J. Kim, G. L. Stuber, Y. Li, "Iterative joint channel estimation and detection combined with pilot-tone symbols in convolutionally coded OFDM systems" *14th IEEE Proceedings on Personal, Indoor and Mobile Radio Communications,* vol. 1, pp. 535-539, Sept. 2003.

[25] B. Han, X. Gao, X. You, M. Weckerle, "Joint channel estimation and symbol detection for SFBC-OFDM systems via the EM algorithm", *IEEE International Conference on Communications,* vol. 6, pp. 3148-3152, June 2004.

[26] M. H. Hsieh, C. H. Wei, "Channel estimation for OFDM systems based on comb-type pilot arrangement in frequency selective fading channels" *IEEE Transactions on Consumer Electronics,* vol. 44, no. 1, pp. 217-225, Feb. 1998.

[27] O. Edfors, M. Sandell, J. J. Beek, S. K. Wilson, P. O. Borjesson, "OFDM channel estimation by singular value decomposition", *IEEE Transactions on Communications*, vol. 46, no. 7, pp. 931-939, July 1998.

[28] S. M. Çürük, Y. Tanık, "Simplified MAP Estimator for OFDM Systems under Fading", *65th Vehicular Technology Conference,* vol. 1, pp. 3165-3169, Apr. 2007.

[29] J. H. Ryu, Y. H. Lee, "Design of implementation-efficient channel estimation filter for wireless OFDM transmission" *IEEE 57th Semiannual Vehicular Technology Conference,* vol. 3, pp. 1590-1594, Apr. 2003.

[30] J. Akhtman, L. Hanzo, "Generic reduced-complexity MMSE channel estimation for OFDM and MC-CDMA" *IEEE 61st Vehicular Technology Conference*, vol. 1, pp. 528-532, June 2005.

[31] B. Yang, Z. Cao, K. B. Letaief, "Analysis of low-complexity windowed DFT-based MMSE channel estimator for OFDM systems" *IEEE Transactions on Communications,* vol. 49, no. 11, pp. 1977-1987, Nov. 2001.

[32] M. X. Chang, T. Y. Su, "Performance analysis of equalized OFDM systems in Rayleigh fading", *IEEE Transactions on Wireless Communications,* vol. 1, no. 4, pp. 721-732, Oct. 2002.

[33] S. Takaoka, H. Gacanin, F. Adachi, "Impact of imperfect channel estimation on OFDM/TDM performance" *IEEE 61st Vehicular Technology Conference*, vol. 1, pp. 442-446, May 2005.

[34] J. Chung, S. J. Park, S. C. Lee, "Effect of Channel Estimation Errors on the Performance of MIMO-OFDM Systems in Correlated Fading Channels" *Canadian Conference on Electrical and Computer Engineering,* pp. 478-481, May 2006.

[35] X. Cai, G. B. Giannakis, "Error probability minimizing pilots for OFDM with M-PSK modulation over Rayleigh-fading channels", *IEEE Transactions on Vehicular Technology,* vol. 53, no. 1, pp. 146-155, Jan. 2004.

[36] H. Cheon, D. Hong, "Effect of channel estimation error in OFDM-based WLAN" *IEEE Communications Letters,* vol. 6, no. 5, pp. 190-192, May 2002.

[37] J. Chen, Y. Tang, S. Li, Y. Li, "Effect of channel estimation error onto the BER performance of PSAM-OFDM in Rayleigh fading" *IEEE 58th Vehicular Technology Conference,* vol. 4, pp. 2444-2448, Oct. 2003.

[38] I. Gaspard, "Impact of the channel estimation onto the BER-performance of PSAM-OFDM systems in mobile radio channels", *IEEE 53rd Vehicular Technology Conference,* vol. 1, pp. 673-677, May 2001.

[39] J. G. Proakis, *Digital Communications*, 4th edition, McGraw-Hill Companies, Inc., New York, 2000.

[40] T. S. Rappaport, *Wireless Communications Principles and Practice*, 2nd Edition, Prentice Hall, Inc., 2002.

[41] M. Patzold, *Mobile Fading Channels*, John Wiley & Sons, Ltd., England, 2002.

[42] F. Babich, G. Lombardi, "Statistical analysis and characterization of the Indoor propagation channel", *IEEE Transactions on Communications*, vol. 48, no. 3, pp. 455-464, 2002.

[43] J. Sun, I. S. Reed, "Mobile radio multi-link analysis", *IEEE 52nd Vehicular Technology Conference*, vol. 3, pp. 1376-1381, Sept. 2000.

[44] J. J. Chen, L. M. A. Jalloul, "Cutoff rate analysis of pilot assisted CDMA system with power control", *IEEE 52nd Vehicular Technology Conference,* vol. 2, pp. 514-517, Sept. 2000.

[45] M. S. Patterh, T. S. Kamal, B. S. Sohi, "Performance of coherent square MQAM with L[th] order diversity in Rician fading environment", *IEEE 54th Vehicular Technology Conference*, vol. 1, pp. 141-143, 2001.

[46] S. Khatalin, J. P. Fonseka, "On the channel capacity in Rician and Hoyt fading environments with MRC diversity", *IEEE Transactions on Vehicular Technology*, vol. 55, pp. 137-141, Jan. 2006.

[47] M. S. Alouini, M. K. Simon, "Performance of generalized selection combining over Weibull fading channels**",** *IEEE 54th Vehicular Technology Conference,* vol. 3, pp. 1735-1739, Oct. 2001.

[48] N. C. Sagias, P. T. Mathiopoulos, G. S. Tombras, **"Selection diversity receivers in Weibull fading: outage probability and average signal-to-noise ratio", *IEEE Electronics Letters*, vol. 39, no. 25, pp. 1859-1860, Dec. 2003.

[49] N. C. Sagias, D. A. Zogas, G. K. Karagiannidis, G. S. Tombras, "Performance analysis of switched diversity receivers in Weibull fading", *IEEE Electronics Letters*, vol. 39, no. 20, pp. 1472-1474, Oct. 2003.

[50] G. Tzeremes, C. G. Christodoulou, "Use of Weibull distribution for describing outdoor multipath fading" *IEEE Antennas and Propagation Society International Symposium,* vol. 1, pp. 232-235, June 2002.

[51] M. S. Alouini, M. K. Simon, "Dual diversity over correlated log-normal fading channels*", IEEE Transactions on Communications*, vol. 50, no. 12, pp. 1946-1959, Dec. 2002.

[52] I. Korn, J. P. Fonseka, "M-CPM with MRC diversity in Rician-, Hoyt-, and Nakagami-fading channels", *IEEE Transactions on Vehicular Technology,* vol. 50, no. 4, pp. 1182-1189, July 2001.

[53] H. L. V. Trees, *Detection, Estimation and Modulation Theory*, John Wiley & Sons, Inc., 1968.

[54] C. W. Therrien, *Discrete Random Signals and Statistical Signal Processing*, Prentice Hall, New Jersey, 1992.

[55] T. K. Moon, W. C. Stirling, *Mathematical Methods and Algorithms for Signal Processing*, Prentice Hall, Upper Saddle River, 2000.

[56] A. Papoulis, *Probability, Random Variables, and Stochastic Processes*, 3rd ed., Mc-Graw Hill, Singapore, 1984.

[57] H.Arslan, T. Yucek, "Delay spread estimation for wireless communication systems" *Proceedings 8th IEEE International Symposium on Computers and Communication,* vol. 1, pp. 282-287, 2003.

[58] K. Witrisal, "On estimating the RMS delay spread from the frequency-domain level crossing rate" *IEEE Communications Letters*, vol. 5, no. 7, pp. 287-289, July 2001.

[59] K. Witrisal, Y. H. Kim, R. Prasad, "A new method to measure parameters of frequency-selective radio channels using power measurements" *IEEE Transactions on Communications*, vol. 49, no. 10, pp. 1788-1800, Oct. 2001.

[60] K. Witrisal, A. Bohdanowicz, "Influence of noise on a novel RMS delay spread estimation method", *11th IEEE International Symposium on Personal Indoor and Mobile Radio Communications*, vol. 1, pp. 560-566, Sept. 2000.

[61] K. Witrisal, Y. H. Kim, R. Prasad, "RMS delay spread estimation technique using non-coherent channel measurements" *IEEE Electronics Letters,* vol. 34, no. 20, pp. 1918–1919, Oct. 1998.

[62] C. R. N. Athaudage, A. D. S Jayalath, "Delay-spread estimation using cyclic-prefix in wireless OFDM systems" *IEE Proceedings-Communications*, vol. 151, no. 6, pp. 559-566, Dec. 2004.

[63] C. R. N Athaudage, A. D .S. Jayalath, "A novel RMS delay-spread estimation technique for wireless OFDM systems" *Proceedings of Joint Conference of the 4th International Conference on Information, Communications and Signal Processing*, vol. 1, pp. 626-630, Dec. 2003.

[64] Y. Huang, W. F. McColl, "Analytical Inversion of General Tridiagonal Matrices", *Journal of Physics: Mathematical and General*, vol. 30, no. 22, pp. 7919-7933, Nov. 1997.

[65] C. Fonseca, "On the eigenvalues of some tridiagonal matrices", *Pré-publicações do Departamento de Matemática da Universidade de Coimbra*, 2005.

[66] A. Monakov, "Estimation of the covariance matrix for dependent signal samples: polarization diversity systems", *IEEE Transactions on Aerospace and Electronic Systems,* vol. 30, no. 2, pp. 484-492, Apr. 1994.

[67] J. P. Burg, D. G. Luenberger, D. L. Wenger, "Estimation of structured covariance matrices" *Proceedings of the IEEE,* vol. 70, no. 9, pp. 963-974, Sept. 1982.

[68] R. L. Kirlin, W. Du, "Improvement on the estimation of covariance matrices by incorporating cross correlations", *IEE Proceedings of Radar and Signal Processing,* vol. 138, no. 5, pp. 479-482, Oct. 1991.

[69] D. B. Williams, D. H. Johnson, "Robust estimation of structured covariance matrices" *IEEE Transactions on Signal Processing,* vol. 41, no. 9, pp. 2891-2906, Sept. 1993.

[70] J. P. Hoffbeck, D. A. Landgrebe, "Covariance matrix estimation and classification with limited training data" *IEEE Transactions on Pattern Analysis and Machine Intelligence,* vol. 18, no. 7, pp. 763-767, July 1996.

[71] L. Hongbin, P. Stoica, L. Jian, "Computationally efficient maximum likelihood estimation of structured covariance matrices" *IEEE Transactions on Signal Processing,* vol. 47, no. 5, pp. 1314-1323, May 1999.

[72] S. T. Smith, "Covariance, subspace, and intrinsic Cramer-Rao bounds" *IEEE Transactions on Signal Processing,* vol. 53, no. 5, pp. 1610-1630, May 2005.

[73] K. B. Petersen, M. S. Pedersen, *The Matrix Cookbook*, 2006.

[74] D. Athanasios, G. Kalivas, **"SNR Estimation for Low Bit Rate OFDM Systems in AWGN Channel"**, *International Conference on Networking, Systems, Mobile Communications and Learning Technologies*, pp. 198-198, Apr. 2006.

[75] H. Xu, G. Wei, J. Zhu, **"A novel SNR estimation algorithm for OFDM"**, *IEEE 61st Vehicular Technology Conference*, vol. 5, pp. 3068-3071, May 2005.

[76] X. Xu, Y. Jing, X. Yu, **"Subspace-based noise variance and SNR estimation for OFDM systems"**, *IEEE Wireless Communications and Networking Conference,* vol. 1, pp. 23-26, March 2005.

[77] S. Boumard, **"Novel noise variance and SNR estimation algorithm for wireless MIMO OFDM systems"**, *IEEE Global Telecommunications Conference,* vol. 3, pp. 1330-1334, Dec. 2003.

[78] European Standard (Telecommunications series), *Digital Video Broadcasting (DVB); Framing structure, channel coding and modulation for digital terrestrial television,* Final draft ETSI EN 300 744 V1.5.1, June 2004.

APPENDIX A

FINDING PHASE PDF OF A COMPLEX RANDOM VECTOR

For a real random vector, the Gaussian density function has a form [54]:

$$p(\mathbf{x}) = \frac{1}{(2\pi)^{N/2}|\mathbf{C_x}|^{1/2}} \exp\left[-\frac{1}{2}(\mathbf{x}-\mathbf{m_x})^{\mathbf{T}}\mathbf{C_x}^{-1}(\mathbf{x}-\mathbf{m_x})\right] \tag{A.1}$$

where N is the dimension of $\mathbf{x}$. This density function is the generalization of the one-dimensional Gaussian density for real random variables and is completely characterized by the mean vector $\mathbf{m_x}$ and the covariance matrix $\mathbf{C_x}$. For a complex random vector the Gaussian density has the slightly different form [54]

$$p(\mathbf{z}) = \frac{1}{\pi^N |\mathbf{C_z}|} \exp\left[-(\mathbf{z}-\mathbf{m_z})^{\mathbf{H}}\mathbf{C_x}^{-1}(\mathbf{z}-\mathbf{m_z})\right] \tag{A.2}$$

where in this case $\mathbf{z}$ assumed to be complex random vector. Then, for a complex Gaussian vector

$$\mathbf{z} = \mathbf{x} + j\,\mathbf{y}, \tag{A.3}$$

with covariance matrix $\mathbf{C_z}$ and assuming that $E\{\mathbf{z}\,\mathbf{z^T}\} = [\mathbf{0}]$, it is known that [54]

$$\mathbf{C_x} = \mathbf{C_y} = \frac{1}{2}\mathrm{Re}\{\mathbf{C_z}\}. \tag{A.4}$$

Then, density functions of real and imaginary parts are written as

$$p(\mathbf{x}) = \frac{1}{(2\pi)^{N/2} |\mathbf{C}_\mathbf{x}|^{1/2}} \exp\left[-\frac{1}{2} (\mathbf{x} - \mathbf{m}_\mathbf{x})^\mathrm{T} \mathbf{C}_\mathbf{x}^{-1} (\mathbf{x} - \mathbf{m}_\mathbf{x}) \right]$$

$$p(\mathbf{y}) = \frac{1}{(2\pi)^{N/2} |\mathbf{C}_\mathbf{x}|^{1/2}} \exp\left[-\frac{1}{2} (\mathbf{y} - \mathbf{m}_\mathbf{y})^\mathrm{T} \mathbf{C}_\mathbf{x}^{-1} (\mathbf{y} - \mathbf{m}_\mathbf{y}) \right]$$

(A.5)

where $\mathbf{m}_\mathbf{x}$ and $\mathbf{m}_\mathbf{y}$ are the mean vectors of $\mathbf{x}$ and $\mathbf{y}$, respectively. Assuming real and imaginary parts are independent, i.e.,

$$p(\mathbf{x}, \mathbf{y}) = p(\mathbf{x}) \cdot p(\mathbf{y}). \tag{A.6}$$

Then,

$$p(\mathbf{x}, \mathbf{y}) = \frac{1}{(2\pi)^N |\mathbf{C}_\mathbf{x}|} \exp\left[-\frac{1}{2} (\mathbf{x} - \mathbf{m}_\mathbf{x})^\mathrm{T} \mathbf{C}_\mathbf{x}^{-1} (\mathbf{x} - \mathbf{m}_\mathbf{x}) - \frac{1}{2} (\mathbf{y} - \mathbf{m}_\mathbf{y})^\mathrm{T} \mathbf{C}_\mathbf{x}^{-1} (\mathbf{y} - \mathbf{m}_\mathbf{y}) \right]$$

(A.7)

Noting that

$$\begin{aligned} \mathbf{x} &= \mathbf{r} \, \mathbf{Cos}\boldsymbol{\varphi} \\ \mathbf{y} &= \mathbf{r} \, \mathbf{Sin}\boldsymbol{\varphi} \end{aligned}, \tag{A.8}$$

it is known that the polar form is [56]:

$$p(\mathbf{r}, \boldsymbol{\varphi}) = \frac{1}{|\mathbf{J}|} p_{xy} (\mathbf{r} \, \mathbf{Cos}\boldsymbol{\varphi}, \mathbf{r} \, \mathbf{Sin}\boldsymbol{\varphi}), \tag{A.9}$$

where $\mathbf{J}$ is the Jacobian of the transformation. Then

$$\mathbf{J} = \begin{vmatrix} Cos\,\varphi_1 & 0 & \cdots & 0 & -r_1 Sin\,\varphi_1 & 0 & \cdots & 0 \\ 0 & Cos\,\varphi_2 & & \vdots & 0 & -r_2 Sin\,\varphi_2 & & \vdots \\ \vdots & & \ddots & 0 & \vdots & & \ddots & 0 \\ 0 & \cdots & 0 & Cos\,\varphi_N & 0 & \cdots & 0 & -r_N Sin\,\varphi_N \\ \hline Sin\,\varphi_1 & 0 & \cdots & 0 & r_1 Cos\,\varphi_1 & 0 & \cdots & 0 \\ 0 & Sin\,\varphi_2 & & \vdots & 0 & r_2 Cos\,\varphi_2 & & \vdots \\ \vdots & & \ddots & 0 & \vdots & & \ddots & 0 \\ 0 & \cdots & 0 & Sin\,\varphi_N & 0 & \cdots & 0 & r_N Cos\,\varphi_N \end{vmatrix}^{-1}$$

(A.10)

which simplifies to

$$\mathbf{J} = \frac{1}{r_1 \cdot r_2 \cdots r_N}. \tag{A.11}$$

Then, we reach the final equation

$$p(\mathbf{r},\boldsymbol{\varphi}) = \frac{r_1 \cdot r_2 \cdots r_N}{(2\pi)^N |\mathbf{C_x}|} \exp\left[\begin{array}{c} -\dfrac{1}{2}(\mathbf{r}\,\mathbf{Cos\varphi} - \mathbf{m_x})^{\mathrm{T}} \mathbf{C_x}^{-1}(\mathbf{r}\,\mathbf{Cos\varphi} - \mathbf{m_x}) \\[2mm] -\dfrac{1}{2}(\mathbf{r}\,\mathbf{Sin\varphi} - \mathbf{m_y})^{\mathrm{T}} \mathbf{C_x}^{-1}(\mathbf{r}\,\mathbf{Sin\varphi} - \mathbf{m_y}) \end{array} \right]. \tag{A.12}$$

For a real covariance matrix $\mathbf{C_z}$, $\mathbf{C_x} = \mathbf{C_z}/2$. Then,

$$p(\mathbf{r},\boldsymbol{\varphi}) = \frac{r_1 \cdot r_2 \cdots r_N}{\pi^N |\mathbf{C_z}|} \exp\left[\begin{array}{c} -(\mathbf{r}\,\mathbf{Cos\varphi} + \mathbf{m_x})^{\mathrm{T}} \mathbf{C_z}^{-1}(\mathbf{r}\,\mathbf{Cos\varphi} + \mathbf{m_x}) \\[2mm] -(\mathbf{r}\,\mathbf{Sin\varphi} + \mathbf{m_y})^{\mathrm{T}} \mathbf{C_z}^{-1}(\mathbf{r}\,\mathbf{Sin\varphi} + \mathbf{m_y}) \end{array} \right] \tag{A.13}$$

To find the pdf of phases, we integrate (A.13) over $\mathbf{r}$, i.e.,

$$\begin{aligned} p(\boldsymbol{\varphi}) &= \int_0^\infty p(\mathbf{r},\boldsymbol{\varphi})\,\mathbf{dr} \\ &= \int_0^\infty \int_0^\infty \cdots \int_0^\infty p(\mathbf{r},\boldsymbol{\varphi})\,dr_1 dr_2 \cdots dr_N \end{aligned} \tag{A.14}$$

Then we can find pdf of each subchannel phase seperately by integrating over the other phases. i.e.,

$$p(\varphi_1) = \int\limits_{-\pi}^{\pi}\int\limits_{-\pi}^{\pi}\cdots\int\limits_{-\pi}^{\pi} p(\boldsymbol{\varphi})\, d\varphi_2 d\varphi_3 \cdots d\varphi_N . \qquad (A.15)$$

CURRICULUM VITAE

PERSONEL INFORMATION

Surname, Name	: Çürük, Selva Muratoğlu
Nationality	: Turkish (TC)
Date and Place of Birth	: 29 May 1974, Antakya
Phone	: +90-326-2274557
Email	: cselva@metu.edu.tr

EDUCATION

Degree	Institution	Year of Graduation
MS	Middle East Technical University - EEE	1999
BS	Middle East Technical University - EEE	1996
High School	Osman Ökten Anadolu Lisesi, Hatay	1992

WORK EXPERIENCE

Year	Place	Enrollment
2002-Present	Middle East Technical University - EEE	Teaching Assistant
2001-2002	Mustafa Kemal University - EEE	Teaching Assistant
1996-2001	ASELSAN Inc.	Digital Design Engineer

FOREIGN LANGUAGES

English

PUBLICATIONS

1. S. M. Çürük, Y. Tanık, "Darbe Şekillendirici Filtre Tasarımında Yeni Bir Yaklaşım", II. *İletişim Teknolojileri Ulusal Sempozyumu (ITUSEM 2005)*, December 2005.

2. S. M. Çürük, Y. Tanık, "A Novel Approach for the Design of Pulse Shaping Filter", *IEEE Communications Letters*, vol. 10, no. 6, pp. 438-440, June 2006.

3. S. M. Çürük, Y. Tanık, "Sönümlemeli Ortamda OFDM için Tasarlanan MAP Kestiricisinin Başarım Analizi", *III. URSI Ulusal Kongresi* (*URSI-TÜRKİYE 2006)*, pp. 520-522, September 2006.

4. S. M. Çürük, Y. Tanık, "Simplified MAP Estimator for OFDM Systems under Fading", 65th *Vehicular Technology Conference,* vol. 1, pp. 3165-3169, Apr. 2007.

5. S. M. Çürük, Y. Tanık, "Sönümlemeli Ortamda OFDM için Tasarlanan MAP Kestiricisi", *IEEE 15th Signal Processing and Communications Applications Cenference (SIU 2007)*, pp. 1-4, June 2007.

6. S. M. Çürük, Y. Tanık, "A Simplified MAP Channel Estimator for OFDM Systems under Rayleigh Fading", submitted.